Title
Characterization of a novel inwardly rectifying potassium channel (Kir2.6) and its role in thyrotoxic hypokalemic periodic paralysis

Permalink
https://escholarship.org/uc/item/2j13v6xn

Author
Ryan, Devon Patrick

Publication Date
2010

Peer reviewed|Thesis/dissertation

Characterization of a novel inwardly rectifying
potassium channel (Kir2.6) and its role in
thyrotoxic hypokalemic periodic paralysis

by

Devon P. Ryan

DISSERTATION

Submitted in partial satisfaction of the requirements for the degree of

DOCTOR OF PHILOSOPHY

in

Neuroscience

in the

GRADUATE DIVISION

of the

UNIVERSITY OF CALIFORNIA, SAN FRANCISCO

ACKNOWLEDGEMENTS

Finally, I would like to thank my family, without whose continued support I would not be here today. My father provided the impetus for my entry into neuroscience, through dinner-time talk about his patients and the difficulty accurately diagnosing and treating their psychiatric disorders due to a lack of there existing a firm scientific basis of understanding of their condition. My mother helped to nurture in me both a love of mathematics and computers and also, through that, a framework to think systematically about a problem solving. My parents have also provided unconditional support through the low and high points of my life. My wife, Kim, has been my biggest supporter throughout graduate school. I will never be able to express to her how much her love and companionship has meant to me.

The text of CHAPTER 1 is a reprint of the material as it appears in Chapter 49, Ion Channel Disorders, of <u>The Molecular and Genetic Basis of Neurologic and Psychiatric Disorders</u>, third edition. The coauthor in this publication directed and supervised the research that forms the basis for this chapter.

The text of CHAPTER 2 is a reprint of the material as it appears in the journal Cell (Cell, January 8, 2010; Vol140, No. 1, p. 88). The co-authors listed in the Cell paper contributed to the work as follows. Louis J. Ptáček directed and supervised the research that forms the basis for the dissertation and collected some of the patients with TPP. Tuck Wah Soong, Betrand Fontaine, Annie W.C. Kung, Wallaya Jongjaroenprasert, Mui Cheng Liang, Daphne H.C. Khoo, Jin Seng Cheah, Su Chin Ho, Rui M.B. Maciel, and Robert H. Brown Jr. provided DNA samples from individuals with TPP. Harold S. Bernstein contributed to experimental design. Matt R. Donaldson is responsible for the original discovery of *KCNJ18*. Magnus R. Dias da Silva collected and sequenced some of the TPP patient and control DNA samples and performed some of the Southern Blot analyses, probing of the genomic structure of *KCNJ18*, the multi-tissue Northern Blot, and the Luciferase assay. All other experiments were designed and carried out by Devon Ryan; this work is comparable to work for a standard thesis awarded by the University of California San Francisco.

Louis J. Ptáček

ABSTRACT OF THE DISSERTATION

Characterization of a novel inwardly rectifying

potassium channel (Kir2.6) and its role in

thyrotoxic hypokalemic periodic paralysis

by Devon P. Ryan

Doctor of Philosophy in Neuroscience

University of California, San Francisco 2010

Thyrotoxic hypokalemic periodic paralysis (TPP) is characterized by periodic bouts of paralysis or weakness concomitant with hyperthyroidism of any source. TPP is more common in men than women and in Asian than Caucasian populations. While TPP has long been believed to have genetic underpinnings, individuals with TPP typically have no family history of the disorder, complicating the discovery of its underlying mechanism. TPP is one of a family of periodic paralytic and myotonic disorders, most of which are caused by mutations in ion channels (CHAPTER 1). Screening ion channels expressed in skeletal muscle for TPP mutations revealed a novel inwardly rectifying potassium channel, Kir2.6, which is expressed specifically in skeletal muscle and transcriptionally regulated by thyroid hormones (CHAPTER 2). One mutation (I144fs) leads to a non-functional channel that presumably leads to TPP through haploinsufficiency. Other mutations lead to aberrantly large currents during times of increase PIP_2 turnover (R205H and K366R) or increased PKC activity (T354M), which occurs during hyperthyroidism. Finally, two mutations (R399X and Q407X) produce

normal currents in a cell culture system, but may have altered subcellular localization in native skeletal muscle. As Kir channels can heteromultimerize, I demonstrate (CHAPTER 3) that Kir2.6 is able to functionally heteromultimerize with at least some other Kir channels expressed in skeletal muscle, providing a mechanism for further spread of aberrant channel physiology. Finally (CHAPTER 4), computational methods are used to demonstrate that, during hyperthyroidism, Kir conductances must be kept within a regulated window, with too little conductance leading to excess potassium accumulation in the skeletal muscle T-tubule system and concomitant depolarization and spontaneous activity, and with too much conductance leading to an inability for normal stimulation to lead to action potential production. Furthermore, altered subcellular localization of these conductances can also lead to the creation of disease relevant physiology. Together, these studies describe the discovery of a novel ion channel and both the genetic and functional association of mutations in it to a periodic paralytic disorder affecting hundreds of thousands of people worldwide.

TABLE OF CONTENTS

LIST OF TABLES

LIST OF FIGURES

CHAPTER 1

Ion channel disorders

Devon Ryan and Louis Ptáček

Ion channels are a complex group of membrane spanning proteins that orchestrate the production and propagation of the electrical activity required for proper neuronal and muscular function. Along with ion transporters, ion channels aid in the maintenance of proper membrane potentials. K^+ ions have a much higher intracellular than extracellular concentration, leading to a very negative reversal potential, typically around $-90mV$. Na^+ ions, on the other hand, are far more numerous in the extracellular milieu than the cytosol, having a reversal potential around $+55mV$. Ca^{2+} and Cl^- ions are distributed similarly to Na^+ and have a very positive and a negative reversal potential, respectively. As the resting cell membrane is far more permeable to K^+ and Cl^- ions than Na^+ ions, it typically has a resting membrane potential in the range of -60 to $-90mV$. Consequently, small variations of extracellular potassium concentrations can lead to drastic changes in cellular reversal potential.

A characteristic of muscle and nerve cells is their ability to produce and conduct action potentials. Introduction of an excitatory neurotransmitter onto a small region of the cellular membrane will cause that region to depolarize slightly. This depolarization causes voltage-gated sodium channels (hereafter referred to as sodium channels) in that region to open, thereby allowing Na^+ ions to traverse the membrane down their electrochemical gradient. This process leads to further

depolarization and the opening of neighboring sodium channels. The opening of this large population of sodium channels shifts the balance of permeability in the membrane from favoring K^+ ions to favoring Na^+ ions with a concomitant depolarization of the resting membrane potential to between +20 and +30mV. Voltage-gated potassium channels also open, albeit with a slower time course. After a short delay, significant numbers of voltage-gated potassium channels open in the depolarized portion of the cell membrane. K^+ ions travel through these channels out of the cell and down their electrochemical gradient. This ionic movement, coupled with depolarization dependent inactivation of sodium channels, results in a hyperpolarization of the membrane, bringing it down to the resting membrane potential. Calcium and chloride channels also play roles in action potential formation and propagation. Calcium channels open with membrane depolarization and can contribute to membrane depolarization. In fact, some cells exhibit Ca^{2+} spikes, which can act similarly to the above describe action potentials. In some cells, chloride channels are typically in the open state and contribute to the resting membrane potential. Cl^- ions, then, counteract cation movement by traversing the membrane in parallel, thereby creating a current "shunt". Opening or closing these channels results in decreased or increased membrane excitability, respectively.

Ion channels play important roles aside from action potential generation and propagation in neurons and muscle cells. Calcium channels couple neuronal excitation with synaptic transmission by increasing the intracellular Ca^{2+} concentration. This increased Ca^{2+} concentration allows for the proper function of

the synaptic machinery. In muscle cells, opening of calcium channels in the T-tubule system results in the activation of sarcoplasmic reticulum calcium-activated calcium channels. These channels then allow large amounts of Ca^{2+} to exit from intracellular stores, leading to muscle contraction.

Ion channels are regulated through many mechanisms. As mentioned earlier, many ion channels are activated by voltage. Other classes of ion channels are opened or closed by interacting with intra- or extracellular ligands. Still other types of ion channels are activated, or "gated", by stretching of the cell membrane. The likelihood of a channel opening or closing is also dependent on its post-transcriptional modifications, such as phosphorylation and glycosylation.

As discussed later, alteration of ion channel properties or levels can lead to malfunction of any of the processes discussed above, resulting in human pathology. Much insight has been gained into the role played by mutant ion channels in human disorders in the past 15 years. This rapid progress can be attributed to advances both in molecular biology, allowing for the cloning and eventual expression of these genes, and biophysics, which has allowed for detailed electrophysiological characterization of both wild-type and disease-associated mutant single channels and cells expressing them.

STRUCTURE AND FUNCTION OF ION CHANNELS

Sodium channels

The Na^+ reversal potential is created through the activity of ion pumps, such as the Na^+/K^+-ATPase. This pump transports intracellular Na^+ outside of the cell, establishing a positive electrochemical gradient across the cell membrane.

3

As the resting membrane potential (RMP) of muscles and nerves is far more negative than the reversal potential of sodium channels, open sodium channels in the membrane will conduct Na^+ ions into the cell, thereby leading to depolarization. At the resting membrane potential, however, these channels are in the closed (non-conducting) state, opening with subsequent depolarization. This Na^+ influx leads to rapid depolarization and further sodium channel opening. 1 to 2 ms after opening, sodium channels undergo fast inactivation. In this process, a small region of the domain 3-4 linker (D3-4) projects into the channels pore and occludes ion passage. Sodium channels also undergo slow inactivation, which occurs over a much longer timescale (seconds to minutes) and involves all four domains. Repolarization is required for removal of the inactivation gate and entrance of the channel into the deactivated, i.e. activateable, state. The time course of this process results in a refractory period for sodium channel activation and, thereby, action potential formation.(Catterall, 2000; Yu and Catterall, 2003)

Sodium channels were first described by Hodgkin and Huxley, who demonstrated their voltage-dependence of activation, rapid inactivation, and ion selectivity.(Hodgkin and Huxley, 1952) It was found that these channels consist of a large 260 kDa α-subunit with or without auxiliary subunits (β_1- β_4). There are currently nine known α-subunits (Na_V1.1-1.9) with a tenth related α-protein of uncertain function (Na_X). Analysis of the sequence of these α–subunits indicates that they fold into four similarly structured domains (1-4). Each domain is constructed of six membrane spanning α-helical segments (S1-6) with a reentrant loop between S5 and S6. The N- and C-termini are intracellular and the

intracellular domain linker regions D1-2 and D2-3 are large while that of D3-4 is comparatively small (Figure 1). The S4 segment of each domain contains positively charged amino acids at every third position. These residues imbue the S4 segments with voltage sensitivity, causing it to move toward the cytosol during hyperpolarization and partially into the extracellular milieu during membrane depolarization. This movement of the S4 segment during depolarization conveys the channels voltage-sensitivity and induces a conformational change resulting in channel opening. The reentrant loop in each of the domains forms the external most portion of the ion-conducting pore and provides the location for the ion selectivity filter. This filter sequence, DEKA, is conserved across sodium channels and its mutation to EEEE, the calcium channel selectivity sequence, produces channels selective for Ca^{2+} ions with otherwise normal properties. The small D3-4 intracellular loop is the site of the fast inactivation gate. This structure is poised to enter the intracellular portion of the ion-conducting pore and obstruct ion passage (inactivation). Proteolytic removal of this domain or the expression of separated D1-3 and D4 produces sodium channels with slowed inactivation. Fast inactivation can be restored by the expression of proteins containing this region.(Catterall, 2000; Yu and Catterall, 2003)

Figure 1. Schematic structure of voltage-gated sodium and calcium channel subunits.

A. The sodium channel α-subunit (left) is comprised of four domains, labeled I through IV. Each domain consists of six membrane-spanning helices (S1 through S6) with a reentrant pore-forming loop between the fifth and sixth of these segments. The S4 segment of each domain contains a series of positively charged residues (+ symbols) at every third residue. The β-subunit (right) is composed of a single transmembrane helix with an extracellular N-terminus and intracellular C-terminus. The N-terminus bears homology to immunoglobulin-like folds, for which and immunoglobulin-like crystal structure is shown. **B.** The calcium channel α_1-subunit (left) is schematically identical to that of the sodium channel α-subunit. The α_2-δ-subunit is comprised of two segments joined by a disulfide bond. The α_2-segment is extracellular and composed of two α-helices. The δ-segment forms a membrane-spanning α-helix with an intracellular C-terminus and an extracellular N-terminus. It is the N-terminus that forms a disulfide bond with the C-terminus of the α_2-segment. Its intracellular β-subunit (bottom) is formed by four α-helices and interacts with the D1-2 linker region of the α_1-subunit. Palmitoylization of this subunit can lead to membrane anchoring. The γ-subunit (right) is comprised of four membrane-spanning helices, numbered S1 through S4 with an intracellular N- and C-terminus.

A

Na$_V\alpha$

I II III IV Na$_V\beta$

B

α_1

I II III IV $\alpha_2-\delta$

γ

β
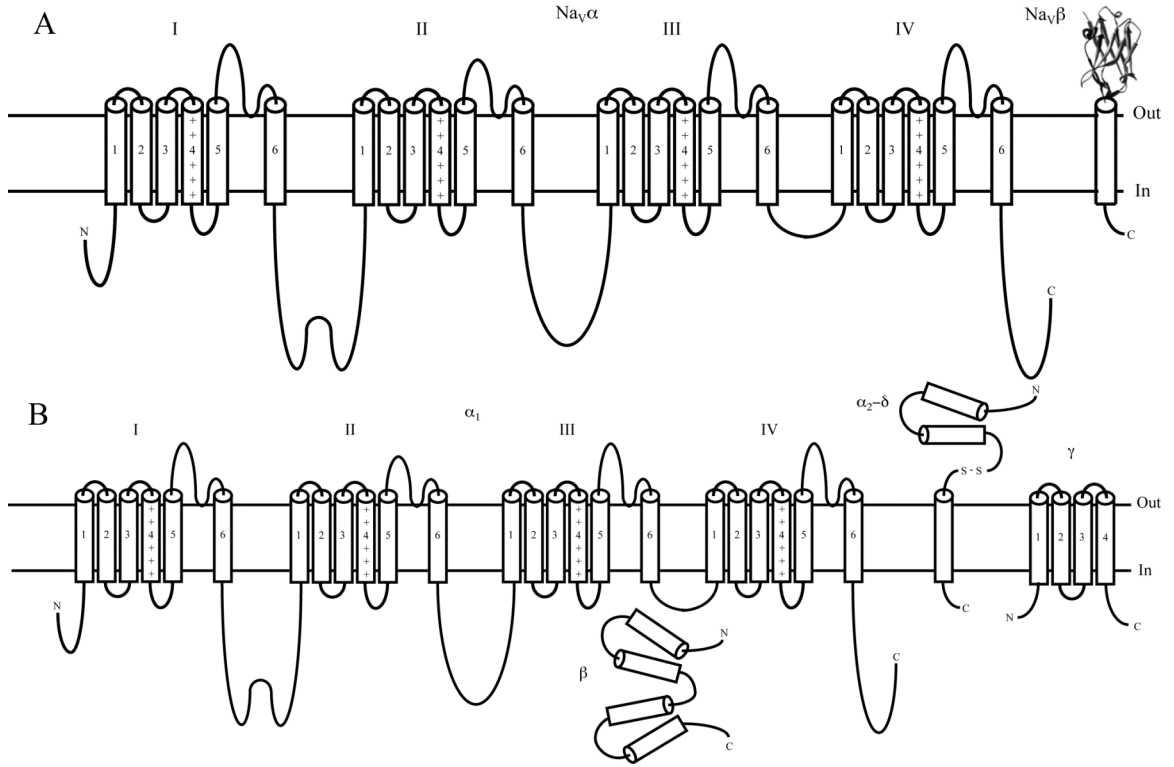
Incorporation of β-subunits results in channels with altered properties and is important for proper function *in vivo*. There are four known β-subunits (β_1- β_4), which bear no similarity to other ion channel auxiliary subunits. Instead, they resemble proteins containing immunoglobulin-like folds. The transmembrane segment of β-subunits appears to be physiologically unimportant as attachment of the extracellular N-terminus to other membrane-spanning proteins or to membrane-anchored sequences affect sodium channel function in the same manner. The loop connecting the D4 pore with the D4S6 segment has been shown to be important for this interaction. These β-subunits alter the kinetics of channel activation and fast-inactivation through an unknown mechanism. Some β-subunits are also able to bind to extracellular matrix proteins, which may be important in the formation of nodes of Ranvier.

Calcium channels

Calcium channels are vital for maintaining proper neuronal and muscular excitation, activation of calcium-dependent enzymes, gene expression, and neurotransmission. There are at least ten calcium channels, all with differing kinetics, cellular expression, and sub-cellular localization. Calcium channels are broadly divided into high voltage-activated (HVA) channels and low voltage-activated (LVA) channels. LVA channels (also known as the T-type channels $Ca_V3.1$ through $Ca_V3.3$) activate in response to small membrane depolarizations. This property enables them to play a large role in action potential generation. HVA channels, in contrast, open due to larger depolarization of the cell membrane potential. This class is further subdivided according to their

physiological properties and pharmacological reactivity into L-, N-, P-, Q-, and R-types. L-type channels (Ca$_V$1.1 through Ca$_V$1.4) both activate and inactivate slowly and are pharmacologically characterized by sensitivity to dihydropyridines. N-type channels (Ca$_V$2.2) produce more rapidly inactivating currents and are blocked by the ω-conotoxins GVIA and MVIIA. This channel is important for inhibitory neurotransmitter release. The P- and Q-type channels (Ca$_V$2.1) are produced by alternative splicing from the same gene and differ according to their sensitivity to the ω-agatoxin IVA. These channels are localized in presynaptic terminals where they play a role in synaptic release, more often excitatory than inhibitory. R-type channels where originally characterized due to their resistance to blockade by the previously mentioned antagonists. These channels inactivate rapidly and activate at more hyperpolarized potentials than other HVA channels. Their function in neurons is poorly understood.(Khosravani and Zamponi, 2006)

All calcium channels contain a large α$_1$-subunit genetically and evolutionarily related to the α-subunit found in sodium channels. In addition, HVA channels have associated α$_2$-δ-, β-, and γ-subunits with which they form heteromultimers. As referenced above, the α$_1$-subunit consists of four homologous domains each containing six membrane-spanning helices and a pore-forming reentrant loop (Figure 1). Like the equivalent sodium channel subunit, the calcium channel α$_1$-subunit pore-regions contain a signature sequence, EEEE, responsible for discrimination of divalent over monovalent cations. The S4 segments of each domain contain positively charged residues at every third position that allow the channel to sense and respond to voltage

changes. Like other voltage-gated channels, calcium channels undergo voltage-dependent inactivation. In these channels, physical blockade of the channel pore by the D1-2 linker seems to be pivotal. The S6 segments of each domain are also involved in this process, likely through the formation of a binding pocket for the inactivation gate. Unlike other voltage-gated channels, calcium channels inactivate with increasing intracellular Ca^{2+} levels, likely to prevent Ca^{2+} induced apoptosis. The C-terminus contains the region responsible for this property.(Khosravani and Zamponi, 2006)

Association of calcium channel α_1-subunits with α_2-δ-, β-, and γ-subunits is known to result in altered channel kinetics and expression. The α_2-δ-subunit is the product of a single gene that is cleaved and then rejoined via a disulfide bond. The δ portion forms a membrane-spanning α-helix while the α_2-portion forms an extracellular peptide. When co-expressed with α_1-subunits, the α_2-δ-subunit produces channels with faster activation and inactivation kinetics as well as a hyperpolarizing shift in voltage-dependent inactivation (i.e., it inactivates at a more negative potential). Importantly, this also leads to increased α_1-subunit expression. There are four β-subunits (β_1 through β_4) and these are all located in the cytosol, with the exception of β_{2a}, which can be palmitoylated to become membrane anchored. This subunit is similar to membrane-associated guanylate kinase homologs and binds to the D1-2 linker region. The functional result of co-expression of α_1- and β-subunits is a channel with increased expression and altered kinetics. The final auxiliary subtype is the γ-subunit. This family consists of eight members (γ_1 through γ_8) each containing four membrane spanning

helices and intracellular N- and C-termini. This subunit can associate with only some of the α_1 subtypes to produce functional consequences, such as kinetics. The regions involved in this interaction are unknown.(Khosravani and Zamponi, 2006)

Potassium channels

Potassium channels are a large and incredibly diverse family of proteins found ubiquitously. These channels are involved in regulating potassium flow, maintaining cell volume, setting the resting membrane potential, and action potential formation and regulation. Potassium channels are regulated by a variety of mechanisms, including membrane potential, redox state, and second messengers. There are two primary categories of potassium channels: voltage-gated and inwardly rectifying.

Voltage-gated potassium channels

The voltage-gated family of potassium channels is comprised of more than 30 members divided into 12 subfamilies according to homology and function. Voltage-gated potassium channels are constructed of four α-subunits, each having a structure reminiscent of a sodium or calcium channel domain. These subunits consist of six membrane-spanning α-helices with an outer pore-forming reentrant loop between the fifth and sixth segments (Figure 2). Homomeric or heteromeric assembly of these subunits is sufficient to produce functional channels. These assemblies are, however, often associated with auxiliary $K_V\beta$-subunits or MiRPs, which results in altered gating properties and trafficking. Recently, the crystal structure of a mammalian voltage-gated potassium channel

in complex with a β-subunit in the open conformation has been solved.(Long et al., 2005) Analysis of this and other structures indicates that during rest (deactivation), the ion permeation pathway is blocked due to constriction of its intracellular mouth by the S6 segments. During activation, these helices bend outward to create an ~4Å opening. As in other voltage-gated channels, the voltage-sensitive S4 segment of K_V channels has charged residues at every third position. This segment moves in the membrane in response to voltage, leading to the conformational changes involved in channel opening. Upon opening, K^+ ions can permeate through the pore created by S6 and the S5-6 reentrant loop (the P-loop). The P-loop is the site of the ion selectivity filter, which consists of a conserved G(Y/F)G motif.(Jan and Jan, 1997; Grottesi et al., 2005; Long et al., 2005)

Figure 2. Structure of voltage gated and inwardly rectifying potassium channels.

Left: The KV channel α-subunit is structured similarly to that of the sodium and calcium channel. It consists of six membrane-spanning α-helices (S1 through S6) with a reentrant loop between S5 and S6. As with other voltage-gated channel, the S4 segment contains positively charged residues at every third residue (+ symbols). The α-subunit associates with both the minK/MiRP family (middle) and β-subunits (bottom). MiRP subunits are constructed from a single membrane-spanning helix. The crystal structure of the KVβ2-subunit is also shown (bottom). The inwardly rectifying potassium channel (right) is constructed of two membrane-spanning helices, M1 and M2. The crystal structure of the bacterial KCSA protein is shown. The pore is in the center, formed by the P-loop and the M2 helix. The N- and C-termini are not shown but are both intracellular.

K$_V\alpha$

MiRP

K$_{ir}$

N

1 2 3 4 5 6

+
+
+
+
+
+

N

K$_V\beta$

C

N

C

Out

In

C
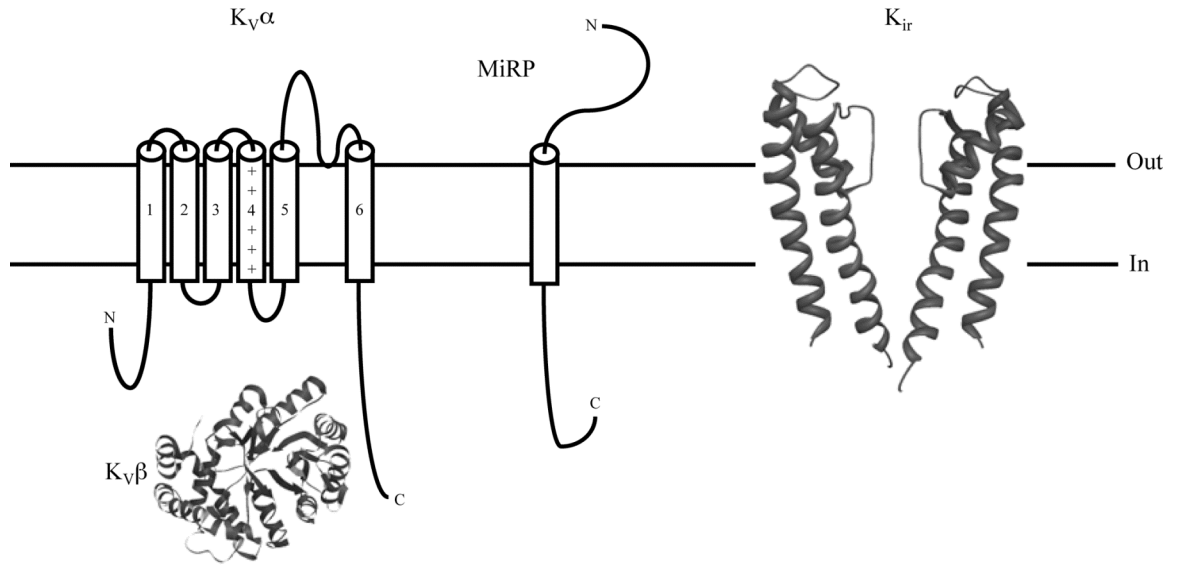
After activating, the channel can inactivate in one of two ways: N-type or C-type inactivation. N-type inactivation requires an N-terminal structural element that forms a "ball and chain". This structure is positively charged and stabilized by interaction with PIP_2. Depolarization leads to destabilization of this interaction and the structure's occlusion of the channel pore. Not all K_V channels contain this N-terminal structure and those lacking it are unable to undergo N-type inactivation. All K_V channels are able to undergo C-type inactivation, which involves regions toward the C-terminus of the channel. It is believed that the cause of this inactivation is destabilization or collapse of the outer ion-conducting pore. This process seems to depend on the occupancy state of the outer pore by K^+ ions.(Jan and Jan, 1997)

$K_V\beta$-subunits interact with the cytosolic portion of $K_V\alpha$-subunits, primarily of the K_V1 family. These β-subunits are clustered into three families, $K_V\beta1$-3, and have a highly conserved C-terminus and a variable N-terminus. The N-terminus of $K_V\beta1$-subunits contains an "α-ball" like structure similar to that required for N-type inactivation. In fact, incorporation of some of these β-subunits into channels that do not display N-type inactivation results in channels that can display N-type inactivation. For channels that already display N-type inactivation, incorporation of some of these β-subunits hastens the inactivation time course. Other $K_V\beta$-subunits induce a hyperpolarizing shift of the voltage dependence of activation. These subunits can also accelerate the kinetics involved in channel activation. A general property of $K_V\beta$-subunits is that they lead to increased surface expression of K_V channels. β-subunit activity can be modulated by

phosphorylation by a host of kinases and the subunit is also directly responsive to cytosolic redox state.(Li et al., 2006)

A second important class of auxiliary proteins is that encoded by the *KCNE* genes. These genes encode small type-1 integral membrane proteins (Figure 2) named *minK* and *MiRP2* through *MiRP5*, where MiRP stands for *minK*-related protein, which was originally believed to be the minimal channel forming subunit. These auxiliary subunits were subsequently shown to associate with $K_V10.1$ and result in increased surface expression, increased current, decreased current, altered kinetics, and altered sensitivity to pharmacological modulation, depending on the MiRP used. Since then, these auxiliary proteins have been shown to interact with most $K_V\alpha$-subunits tested, the exception being *MiRP1* and *MiRP3* interaction with $K_V1.4$. The specific sites involved in the interaction between MiRPs and α-subunits are unknown. The C-terminus of these *KCNE*-encoded proteins has been shown to be important for enabling control of channel activation. The specificity of this interaction, however, seems to be conveyed through interaction between α-subunits and the MiRP transmembrane segment. It is also unknown how many of these auxiliary subunits assemble in each channel, estimated at between 2 and 14 per channel.(Li et al., 2006)

Inwardly rectifying potassium channels

There are seven families of inwardly rectifying potassium channels denoted $K_{ir}1$ through $K_{ir}7$. These families differ in genetic sequence and biophysical characteristics. Some of the families are weakly rectifying ($K_{ir}1$, $K_{ir}4$, and $K_{ir}5$), some notable for being modulated by intracellular ATP ($K_{ir}1$, $K_{ir}3$, and

$K_{ir}6$) or G-proteins ($K_{ir}3$), while others have small single channel conductance ($K_{ir}7$) or strong rectification ($K_{ir}2$).(Nichols and Lopatin, 1997; Krapivinsky et al., 1998)

Like voltage-gated potassium channels, inwardly rectifying potassium channels are comprised of four homomeric or heteromeric subunits. Here, however, each subunit consists of two membrane-spanning α-helices (M1 and M2) homologous to the S5 and S6 membrane-spanning units of voltage-gated potassium channels (Figure 2). The area between these membrane-spanning groups is the outer-pore forming loop (P-loop) containing the G(Y/F)G selectivity filter. This motif is conserved across all known potassium channels, where it provides transient binding sites for potassium ions. The M1 and M2 portions of each subunit pack around the P-loop, which forms the inner-pore. The inner-pore extends into the cytoplasm by the C-terminus. The C-terminus contains motifs required for ER-export as well as G-protein interaction ($K_{ir}3$ family), ATP binding ($K_{ir}1$, 3 and 6 families), and a PSD95-discs large-Zonula occludens (PDZ) ligand domain ($K_{ir}2$ family).(Ma et al., 2001; Stockklausner et al., 2001) Only the $K_{ir}2$ family is known to contain members involved in relevant human neurological disorders, so it will be described further.

$K_{ir}2$ channels are gated primarily in two ways: rectification and phosphatidylinositol 4,5-bisphosphate (PIP_2) interaction. Inward rectification, due to binding by intracellular polyamines and Mg^{2+}, is an asymmetric current voltage relationship where the channel is able to pass more inward than outward current. Polyamines bind to residues on the C-terminus and M2 region of the channel

subunits and block potassium ions from traversing the channel.(Lu, 2004) As ions such as Mg^{2+}, Ba^{2+} and Rb^+ and polyamines are cations, their interaction with ion channels is voltage dependent. Potential gradients across the cell membrane keep these interactions low during hyperpolarization but allow these cations to follow potassium ions outward through the channel during depolarization. This asymmetric current-voltage relationship is important for setting the resting potential of cells while not leading to current shunting during depolarization. PIP_2 mediated gating is due to the interaction with numerous residues throughout the N- and C-termini of the channel. The binding of these residues likely causes a change of structure of the channel, increasing the diameter of the inner-pore (specifically the G-loop).(Soom et al., 2001; Lopes et al., 2002; Du et al., 2004)

Chloride channels

Chloride channels comprise the final major group of ion channels. Activity in these channels is associated with fluid excretion in epithelial tissue and the acidification of intracellular organelles. In muscle, these channels aid in setting the resting membrane potential. These channels also alter threshold for action potential generation by providing a current shunt, as mentioned earlier. All 9 of these channels in humans are members of the same ClC family of proteins. These proteins are expressed ubiquitously. A recent complication in the study of these channels was the discovery that some of them are, in fact, Cl^-/H^+ exchange-transporters.

ClC proteins have a structure completely dissimilar to cation channels, a fact which has led to much difficulty in their study. Understanding of these proteins has been aided recently by the crystallization of a number of bacterial Cl^-/H^+ transporters of this family (Figure 3). Although these proteins form ion pumps, their high homology to ClC ion channels and some of their other characteristics suggest that these pumps and channels likely share structural similarity as well. Functional transporters and channels of this family are comprised of two-fold symmetric homodimers. This two-fold symmetry results in two sets of transport machinery, for transporters, and two ion-conducting pores, for channels. Each subunit has intracellular N- and C-terminal sections with 18 membrane-embedded helices (including membrane-embedded helices) in between. Part of these subunits appears to be an inverted repeat of the other, which has important structural consequences, especially for members of the transporter subfamily. The C-terminus of mammalian ClC proteins seems to be involved in ATP binding, likely through their cystathionine β-synthetase (CBS) motifs. The ClC members crystallized to date all lack obvious ion conducting pore sequences; although, this is unsurprising as they function as transporters. These crystal structures have revealed that the transporters contain three sites of Cl^- interaction: an internal site situated near the cytosolic interface and bound to Cl^- in crystal structures, an internal site near the middle of the membrane-spanning portion of the protein that is also bound to Cl^- in crystal structures, and an external site located near the interface with the external environment that interacts with a glutamate residue carboxylate group (Glu_{ex}), a residue conserved across all ClC transporters but

not channels. Glu_{ex} seems to function by providing an obstruction to Cl^- passage through the subunit. Interestingly, substitution of this residue with glutamine, which lacks the carboxylate group, results in a conformational change creating a pathway leading to the external milieu. Furthermore, this is one of two glutamates proposed to be involved in interacting with H^+ ions, suggesting that protonation may lead to a similar alteration.(Dutzler, 2006; Miller, 2006)

Figure 3. Crystal structure of the ClC chloride channel from E. coli.

A. Side view of the two halves (gray and black) with the cytosol on the bottom and extracellular space on the top. **B.** Top down view of this same channel complex.

A

B
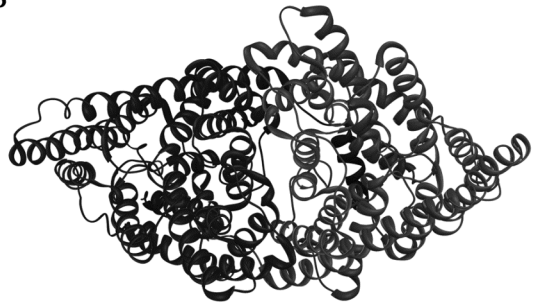
ClC channel physiology is very different from that of cation channels, due to the presence of two pores in each channel. These channels undergo two forms of gating. Fast gating involves the closure of one subunit pore on a millisecond timescale. Common gating leads to the closure of both pores simultaneously. Three properties affect fast gating: pH, Cl^- concentration, and voltage. Interestingly, activation by intracellular, but not extracellular, H^+ ions is voltage dependent. The location of the fast gate appears to be Glu_{ex}, the same residue whose protonation leads to conformational change of ClC transporters. This site has also been mutated in ClC channels, leading to nearly complete opening of the channel. Low external pH produces a similar effect. This suggests that protonation leads to removal of fast gating and channel opening. ClC voltage sensitivity occurs through a method different from that of cation channels. Here, intracellular H^+ ions sense the membrane voltage and protonate Glu_{ex} in a voltage-dependent manner. Removal of extracellular Cl^- leads to complete loss of voltage dependence. The mechanism underlying this Cl^- dependent activation is currently not understood.(Dutzler, 2006; Miller, 2006)

Clinical manifestation and molecular pathogenesis of ion channel disorders

There are many known ion channel disorders; those of particular neurological interest include a group of muscle diseases including periodic paralyses and non-dystrophic myotonias. A second group contains two disorders leading to either an increase or decrease in pain perception and a third that

directly causes pain perception in the form of migraine. These disorders are broadly called pain-associated disorders. A third grouping of disorders is distinguished by the presence of either progressive or episodic ataxia. The final group is a broad categorization of the known ion channel mutation associated epilepsies.

Periodic paralyses, non-dystrophic myotonias and myasthenic syndrome

There are a number of ion channel mutations that lead to primary muscle disorders, as opposed to malfunction of nerve input to muscle cells. These disorders span a spectrum from muscle hyperexcitability to hypoexcitability. After onset of muscle contraction, hyperexcitable muscle displays prolonged depolarization and muscle tone, leading to myotonia. In hypoexcitable muscle, however, normal levels of excitation are unable to cause muscle contraction, leading to weakness and paralysis in patients. Myotonia congenita and potassium-aggravated myotonia reside at one end of this excitability spectrum, being caused by hyperexcitability. Andersen-Tawil syndrome and hypokalemic periodic paralysis are at the other end of the spectrum. Thyrotoxic hypokalemic periodic paralysis may also reside at this end. In the middle are paramyotonia congenita and hyperkalemic periodic paralysis. There is considerable phenotypic overlap between these disorders. A clinically and genetically related disorder that also results in paralysis is myasthenic syndrome. Like other paralytic disorders, myasthenic syndrome results from decreased muscle excitability.

Myotonia congenita

Myotonia congenita is characterized by muscle stiffness upon movement initiation that is relieved with further movement. This process of movement-induced diminution of symptoms is termed "warm-up". Fainting goat and mouse models of myotonia congenita have shown that there is a drastic reduction in the whole-cell chloride conductance.(Adrian and Bryant, 1974; Adrian and Marshall, 1976) There are two forms of myotonia congenita: a dominant form, termed Thomsen's disease, and a recessive form, termed Becker generalized myotonia. The dominant form first manifests by age two, while the recessive form manifests later in life, between ages 4 and 9. In patients with the dominant form, there is neither progression to muscle weakness nor initial leg stiffness, hypertrophy or transient weakness, while this is not the case for the recessive form. Permanent weakness can occur in Becker's disease patients, while this is not the case for Thomsen's disease patients. Becker's disease is far more prevalent, estimated at 1-2:50,000. Interestingly, both of these forms are caused by mutations in the same gene, the skeletal-muscle chloride channel, *CLCN1*.

There are many mutations in *CLCN1* associated with either MC form. These mutations are distributed throughout the channel, with no obvious aggregation in specific channel regions. These mutations disrupt the channel in a variety of ways. The Thomsen's mutation, I290M, for example, has altered activation voltage sensitivity. Wild-type channels reach half maximal opening ($V_{1/2}$) around -20mV and are 15-20% open at the resting membrane potential. I290M mutant channels, however, have a $V_{1/2}$ of +55mV and are not open at the

resting membrane potential. When coexpressed with wild-type channels, the resulting currents have intermediate voltage sensitivity, with a $V_{1/2}$ of around +25mV. The I290M is unable to fully open, even during an action potential, meaning that it cannot contribute to the action potential repolarization phase, thereby prolonging depolarization and producing myotonia. A mutation in the neighboring residue has also been found, though it, E291K, is associated with Becker's instead of Thomsen's MC. This mutant channel produces no current and, when coexpressed with wild-type, results in a 50% current decrease. This is consistent with many other recessive mutations and implies that such mutations do not interact with wild-type channels.(Pusch et al., 1995)

Since both types of mutations lead to loss of current, why are there two forms of inheritance? Early in the study of myotonia congenita, it was recognized that deficit in chloride channel function is important to its pathogenesis. Studies with reversible chloride channel blockers have found that up to 90% of channels must be blocked to cause myotonia.(Furman and Barchi, 1978) Consequently, it follows that Thomsen's MC mutant channels, such as I290M, produce a dominant negative loss of function, while recessive mutants, such the E291K, often lead to haploinsufficiency. Thus, there must be at least two Becker's MC mutations to result in sufficient disruption to lead to myotonia.

Potassium-aggravated myotonia

Another disorder similar to myotonia congenita has been described, due to mutations of the sodium channel gene *SCN4A*. A general aspect of this disorder is myotonia of the abdomen, limbs, and extraocular muscles that worsens with

potassium administration, thereby leading to the term potassium-aggravated myotonia (PAM). Symptoms include myotonia that may be induced by cold and is often relieved by exposing the affected area to warmth. Exercise and rest following exercise are also known to induce attacks. Some patients experience pain during these myotonic attacks. Others have long lasting attacks or attacks of fluctuating severity. Many patients respond to treatment with acetazolamide.(Lehmann-Horn et al., 1993)

PAM is caused by mutations in the voltage-gated sodium channel α-subunit $Na_V1.4$. There are seven known mutations leading to PAM in five residues. Three different mutations, G1306A/E/V, occur at the same residue in the linker region between domains 3 and 4. Other mutations are located in the S5 through S6 segments of the channel. A general feature of PAM mutations is slowed inactivation. At least some of these mutations also leading to depolarized shifts in the voltage sensitivity of inactivation.(Hayward et al., 1996) This prolongs action potential duration and provides more channels able to contribute to these prolonged action potentials.

Paramyotonia congenita

Paramyotonia congenita (PMC) is similar to PAM, being associated with "paradoxical" myotonia because it worsens with exercise instead of improving, as is the case with the "warming-up phenomenon" in myotonia congenita.(von Eulenberg, 1886) Muscle stiffness in afflicted individuals can progress to focal weakness. Affected regions tend to include the face, neck and proximal upper extremities. The most distinguishing characteristic of PMC is that myotonic

attacks and subsequent weakness can be induced by muscle cooling. Other patients find that exercise provokes attacks, particularly during repetitive movements such as squatting and fist clenching. Technically, to make this diagnosis, one must demonstrate a decrease in the compound muscle action potential amplitude after muscle cooling.

As with PAM, PMC is caused by mutations in $Na_V1.4$. There are at least 13 mutations reported to cause PMC and they are located throughout the channel with no apparent aggregation in specific channel regions. In general, these mutations lead to slowing of and expedited recovery from inactivation, though this is not the case for all mutants. The mutations occurring at the R1448 position in D4S4 are good examples of this. These result in a 4, 1.8 and 3-fold increase in the time required for fast inactivation for R1448C, R1448P, and R1448S, respectively.(Ji et al., 1996) R1448P also recovers more slowly from inactivation, while R1448S deactivates approximately 6-fold more slowly and recovers from inactivation more quickly than wild-type.(Lerche et al., 1996; Bendahhou et al., 1999) Another common feature of PMC mutations is that they incompletely inactivate, producing small sustained-currents even with long duration depolarizations. An important caveat is that there is not uniformly rigorous clinical characterization of phenotype for PMC-causing SCN4A mutations in the literature. Hence, some patients with myotonia congenita or hyperkalemic periodic paralysis are misdiagnosed as having PMC since they report 'worsening' with muscle cooling in the absence of decreased CMAP amplitudes after muscle cooling.

Taken together, PMC alterations are expected to lead to myotonia in much the same way as potassium-aggravated myotonia mutations. The primary difference between these disease mutations is the presence of significant sustained non-inactivating currents in PMC mutants. The addition of this current slowly adds to the decrease in the membrane potential between action potentials. As this progresses toward more positive potentials, an ever decreasing number of sodium channels are able to recover from inactivation, until eventually the membrane potential is so depolarized that action potentials cannot be generated and weakness ensues.

Hyperkalemic periodic paralysis

While some muscle disorders result purely in muscle stiffness, others result in muscle stiffness and weakness. Hyperkalemic periodic paralysis (HyperKPP) is one such disorder. It is characterized by recurrent bouts of muscle weakness lasting for hours to days. These can occur multiple times per day and first manifest between infancy and early childhood. HyperKPP is typified by bouts provoked through potassium administration, reminiscent of PAM. In many patients, rest following exercise and fasting can evoke attacks. The name suggests that HyperKPP patients have elevated serum potassium levels. In fact, many patients have normal potassium levels during attacks. Potassium administration uniformly provokes attacks in these patients. Thus, precipitation of attacks by potassium administration as a diagnostic test or reports of attacks induced by eating high potassium foods is helpful (required) in making the diagnosis unless there is documented hyperkalemia during an attack.

As with PMC, HyperKPP is caused by mutations the gene encoding the voltage-gated sodium channel α-subunit $Na_V1.4$ and was the first of the channelopathies to be characterized genetically (Ptacek et al., 1991; Rojas et al., 1991). There are only five mutations in this gene associated with "pure" HyperKPP, i.e. only weakness, (L689I, I693T, A1156T, I1495F, and the double mutant F1490L+M1493I), six others being associated with both weakness and stiffness. These pure HyperKPP mutations tend to result in channels that activate at more hyperpolarized potentials than wild-type. They also commonly produce non-inactivating currents. Instead of simply prolonging action potential duration and slowly depolarizing the cell membrane, this non-inactivating current leads to more rapid depolarization and prevents action potential initiation. This is compounded by many HyperKPP mutations more slowly entering slow inactivation. An important caveat is that there is not uniformly rigorous clinical characterization of phenotype for hyperKPP-causing SCN4A mutations reported in the literature.

A potassium- and temperature-sensitive phenotype

There are rare families that have a hybrid phenotype of hyperKPP/PMC (de Silva et al., 1990). However, to make this diagnosis accurately, one must have clear evidence of both. This could include a documented high serum potassium level during an attack or precipitation of attacks by potassium administration or high potassium foods in conjunction with documented CMAP decrement after muscle cooling. HyperKPP patients are not infrequently misdiagnosed as having both

because their muscles 'don't work as well' when they are cold. But this is the case for everyone including healthy people without periodic paralysis!

Hypokalemic periodic paralysis

Another periodic muscle disorder that is also characterized by muscle weakness, but occurs in the presence of decreased serum potassium, is hypokalemic periodic paralysis (HypoKPP). Attacks typically affect the limbs, occur between multiple times per day and only sporadically throughout life, and first manifest in the second decade of life. Progressive interictal weakness is also common in HypoKPP. Attacks are provoked by conditions causing rapid K^+ flux into cells, such as rest following exercise, insulin usage, and high carbohydrate consumption. In contrast to normal muscle, excised HypoKPP muscle depolarizes and becomes inexcitable due to increases in serum K^+ concentrations.(Rudel et al., 1984) This depolarization and loss of force are further exacerbated by the addition of insulin or adrenaline. Action potentials in such muscle rise more slowly and to a more shallow amplitude than wild-type.(Jurkat-Rott et al., 2000) Such alteration in action potential characteristics should lead to decreased conduction velocity. While myotonia is known to occur in HyperKPP patients, this is not the case for those with HypoKPP. Interestingly, HypoKPP shows complete penetrance in men but incomplete penetrance in women. There are at least two loci for HypoKPP, all in different ion channel genes.

HypoKPP1

The first, and most prevalent, type of hypokalemic periodic paralysis, HypoKPP1, is caused by mutations in the L-type voltage-gated calcium channel α_1-subunit $Ca_V1.1$ and tends to manifest upon waking. This channel is expressed at T-tubules in skeletal muscle where it couples excitation with contraction. There are three known mutations in this gene associated with HypoKPP, all affecting positively charged residues on the voltage-sensitive S4 segments. These mutations have not been thoroughly characterized, but the data available indicates that they lead to decreased current. The R1239H mutation, for instance, leads to a 66% decrease in current.(Jurkat-Rott et al., 2000) This explains the inability of depolarization to result in proper contraction and weakness. How decreased serum K^+ levels in mutant expressing muscles leads to weakness remains unknown.

HypoKPP2

A rare cause of HypoKPP is mutation of $Na_V1.4$, which is also involved in PAM, PC, and HyperKPP. This channel is involved in creating the rising-phase of the action potential in muscle cells. All of the mutations in this channel that lead to HypoKPP are located in the voltage-sensitive S4 segment of domain 2. These mutations seem to lead to altered inactivation properties. The R672G mutation, for instance, activates more slowly, inactivates more slowly, and recovers at a delayed rate from inactivation. The R672H mutation, conversely, activates more quickly and recovers more slowly from inactivation.(Jurkat-Rott et al., 2000) Both of these mutations should result in more slowly rising and smaller action

potentials. Recently, it has been shown that at least some HypoKPP2 mutations lead to the introduction of a gating-pore current. This current is mediated by passage of sodium ions through the pore created by the movement of the voltage sensor S4 segment.(Sokolov et al., 2007) A proposed model for HypoKPP2 from these mutations, then, is that intracellular sodium levels gradually increase in muscle cells that are unable to clear using sodium-potassium ATPases due to hypokalemia (extracellular K^+ ions being required for this mechanism). This buildup of intracellular Na^+ leads to a gradual depolarization of the membrane and a shift of voltage-gated channels from deactivated to inactivated states. It is likely that other HypoKPP mutations in both associated loci lead to weakness by this method.

Andersen-Tawil syndrome

Andersen-Tawil syndrome (ATS) is an unusual disorder involving periodic paralysis, cardiac arrhythmia, and developmental defects. Episodes of paralysis first manifest by adulthood and occur 1 to 8 times per month, lasting for hours to days. In some patients, movement during these episodes is accompanied by a painful stabbing sensation. Cardiac arrhythmia first manifests between infancy and early adulthood, often in the form of palpitations but can be asymptomatic. ATS patients have a number of notable developmental defects: toe clinodactyly and syndactyly, small hands and feet, broad forehead, high arched or cleft palate, mild facial asymmetry, microcephaly, and missing teeth or persistant primary dentition.(Yoon et al., 2006a) ATS patients also have impaired executive function and abstract reasoning.(Yoon et al., 2006b) In about ~70% of cases,

ATS is caused by mutation in *KCNJ2*, which encodes the strong inward-rectifier potassium channel $K_{ir}2.1$.(Plaster et al., 2001; Donaldson et al., 2003) Early on, the importance of proper $K_{ir}2.1$ function in cardiac function and skeletal development was demonstrated by knockout of this gene in mice, leading to cardiac abnormalities.(Zaritsky et al., 2001)

There are numerous mutations located throughout $K_{ir}2.1$, all seeming to lead to dominant-negative loss of $K_{ir}2.1$ current. Some mutations are at sites directly (R312C) or indirectly (V302M) interacting with membrane PIP_2. PIP_2 binding is required for channel opening, so it is unsurprising that these mutant channels with decreased PIP_2 affinity show decreased current.(Lopes et al., 2002) Instead of directly interacting with PIP_2, V302M is involved in coupling PIP_2 interaction with other residues to movement of the G-loop and, thereby, channel opening.(Ma et al., 2006) Another common change caused by ATS mutations is altered trafficking. Two such mutations, 95_98del and 314_315del, are translated but do not traffic to the surface, decreasing whole-cell current by 94%.(Bendahhou et al., 2003) Regardless of the underlying mechanism, these mutations lead to membrane depolarization in a dominant negative manner and an inability of voltage-gated channels to recovery from inactivation. While this explains cardiac and skeletal muscle abnormalities, it is unclear how ATS mutations lead to skeletal deformations.

Thyrotoxic hypokalemic periodic paralysis

Thyrotoxic hypokalemic periodic paralysis, TPP, is the most prevalent of the sporadic periodic paralyses and has a non-uniform gender and ethnic

34

distribution. TPP is a rapid-onset weakness disorder associated with hypokalemia but only in the setting of thyrotoxicosis. Bouts of weakness are similar to those seen in ATS and are prevented by treating the underlying thyrotoxicosis. There are more men with TPP than women, though thyrotoxicosis is more prevalent among women. TPP is found in all parts of the world and is most common in Asians, followed by Latinos, Caucasians, and Africans (in that order). While up to 10% of Chinese men who are thyrotoxic have TPP, only 0.1% of Caucasian Americans with thyrotoxicosis also have TPP.(Kelley et al., 1989; Dias Da Silva et al., 2002) The underlying genetic basis of TPP remains to be elucidated.

Myasthenic syndrome

A final paralytic disorder, myasthenic syndrome, is also caused by muscle hypoexcitability. There are many causes of myasthenic syndrome, but the one of interest here is mutation of $Na_V1.4$, which is also mutated in HyperKPP, HypoKPP, PMC, and PAM. Myasthenic syndrome is characterized by bouts of bulbar paralysis, first manifesting in infancy. These bouts last from 3 to 30 minutes and are infrequent, occurring between 1 and 3 times per month. The known patient with an $Na_V1.4$ mutation also has delayed motor development, upper body weakness, weakness of the ocular muscles and is mentally retarded. She has increased frequency dependent rundown of elicited compound muscle action potential. There are two *SCN4A* mutations associated with myasthenic syndrome, S246L in the D1 S2-S3 linker and V1442E in the D4 S3-S4 linker. Given the presence of S246L in unaffected individuals, it is assumed that this

mutation is in fact not disease causing. The V1442E mutation results in a hyperpolarized shift in the voltage-sensitivity of inactivation. Consequently, 98% of mutant versus only 13% of wild-type channels are inactivated at rest, leading to sever hypoexcitability and paralysis. It is unclear how this leads to mental retardation.(Tsujino et al., 2003)

Pain-associated disorders

There are three ion channel disorders associated with pain. One of these disorders increases the perception of pain. A second decreases pain sensitivity to dangerous levels. A third does not alter the perception of external stimuli, instead leading to a rare familial migraine disorder.

Primary erythermalgia

Primary erythermalgia, also termed primary or familial erythromelalgia, is a rare autosomal dominant chronic pain disorder with onset between infancy and early adolescence. Individuals with this disorder experience severe episodes of burning pain in the hands and feet, along with redness and warmth in these areas. Some patients experience these symptoms in other areas as well, including the face, ears, elbows and knees (63% in one study) and sometimes even extending to vaginal areas.(Dib-Hajj et al., 2005) These symptoms can be elicited by standing, exercise, or exposure of prone areas to heat. These symptoms occur with a frequency ranging from several times per month to multiple times per day and this frequency may progress with age. There is no proven pharmacological treatment for erythermalgia, though many patients find relief with pain medication and/or exposure of the affected area to cold-

temperature. It was hypothesized that erythermalgia is caused by sensitized C-fibers.(Layzer, 2001)

Recent genetic studies have found that primary erythermalgia is caused by mutations in *SCN9A*, the gene encoding the voltage-gated sodium channel α-subunit $Na_V1.7$. These channels are primarily expressed in nociceptive dorsal root ganglion (DRG) neurons and sympathetic ganglia neurons, where they seem to be important in bringing the membrane potential to threshold for action potential initiation. Its expression in DRG neurons is particularly important given their role in the conductance of pain perception. To date, nine mutations in eight amino acids have been found associated with erythermalgia. The first two mutations, I848T and L858H, are in the S4-S5 linker region in D2.(Yang et al., 2004) Expressed in cell-culture systems, these mutations lead to channels with a number of altered properties, the most important being a hyperpolarizing shift in $V_{1/2}$, the midpoint voltage for activation. These mutations also lead to a slowing in the transition from the open to closed (deactivated) state. This implies that these channels will produce increased current due to sub-threshold input and, thereby, cause hyperexcitability. This belief is bolstered by the observation that the application of a slowly increasing ramp depolarization induces significantly larger currents from mutant compared to wild-type channels. This effect is especially pronounced between –40 and –70mV, below normal action potential threshold but not far above the resting membrane potential.(Cummins et al., 2004) Other known mutations lead to similar changes in excitability, though by different mechanisms. Some other mutations lead to activation at more hyperpolarized

potentials and brisker recovery.(Dib-Hajj et al., 2005; Han et al., 2006) A few other mutations have been found, primarily in the pore region, but their affects on channel kinetics have not been studied.(Drenth et al., 2005; Michiels et al., 2005)

Channelopathy-associated insensitivity to pain

Pain perception is vital to the proper survival of all complex organisms and, as such, the prevalence of humans and other organisms lacking this ability is extremely low. Recently, a new disorder has been described that is characterized by the absence of pain perception and termed channelopathy-associated insensitivity to pain (CAIP). Clinically, this disorder is characterized by lack of pain sensation without accompanying neuropathy. Normally, this would yield a diagnosis of congenital indifference to pain. However, these patients do not fit its criterion of sensing pain while being indifferent to its presence and, therefore, are also similar to patients with congenital insensitivity to pain. Individuals with any of these disorders often have injuries to their lips and tongue due to biting them frequently at an early age. They also frequently suffer from bruises, cuts, and fractured bones. All other sensation is normal. Patients with these disorders have a prevalence to be employed as "human oddities" in street theater. The first patient diagnosed with CAIP, for instance, regularly performed shows in which he placed knives through his arms and walked on hot coals. Thus, CAIP represents an overlap of aspects of the two previously described disorders.(Cox et al., 2006)

CAIP is caused by mutations in *SCN9A*, which encodes the voltage-gated sodium channel α-subunit $Na_V1.7$ and is responsible for the pain hypersensitivity

seen in primary erythermalgia. This suggests that instead of a gain-of-function mutation, CAIP-associated mutations are likely loss-of-function. Na$_V$1.7 knock-out mice have been created and found to have a decreased response to noxious stimuli. Null mice are also completely unresponsive to inflammatory pain induced by formalin injection.(Nassar et al., 2004) There are three known mutations in *SCN9A* associated with CAIP: W897X, located in the P-loop of D2; a single base deletion leading to I767X, located in the S2 segment of D2; and S459X, located in the D1-2 linker region. These mutant channels have been expressed with β1 and β2 subunits in cell-culture systems and produce currents much less than wild-type and no different from background. This suggests that DRG neurons in patients with CAIP have decreased Na$_V$1.7 function and, thus, are less able to reach threshold for action potential initiation due to excitatory input. This finding also suggests that *SCN9A* polymorphisms may contribute to differences in pain perception within the normal population.(Cox et al., 2006)

Familial hemiplegic migraine

Migraine is a common neurological disorder, estimated to affect 12-28% of the population.(Stovner et al., 2006) Cortical spreading depression (CSD) is believed to be the systems-level basis for the aura component of migraine. It is clear that there are strong genetic components to migraine although they are complex. However, one type of migraine with a simple autosomal dominant mode of inheritance is familial hemiplegic migraine (FHM). This form of migraine is characterized by migraine with aura associated with hemiparesis and, in some forms, cerebellar degeneration. Aura symptoms, such as numbness and blurred

vision, last between 30 and 60 minutes. Other symptoms of FHM include altered consciousness, gaze-evoked nystagmus, coma, nausea, phonophobia and photophobia. FHM can also present as benign familial infantile convulsions or alternating hemiplegia of childhood. Symptoms of FHM typically first manifest in childhood or adolescence. There are multiple subtypes of FHM, with cerebellar degeneration possible in FHM1 but absent in other forms. Three of the subtypes, FHM1-3, have known causative genes while FHM4 has only been mapped to chromosome 1q31.("Classification and diagnostic criteria for headache disorders, cranial neuralgias and facial pain. Headache Classification Committee of the International Headache Society," 1988; Lance and Olesen, 2004) Two of the known loci are ion channel genes while the third, FHM2, is the Na^+/K^+-ATPase *ATP1A2*.

<center>*FHM1*</center>

FHM1 is caused by mutations in the *CACNA1A* gene, which encodes the P/Q-type voltage-gated calcium channel α_1-subunit $Ca_V2.1$. This channel is expressed throughout the brain, where it couples excitation to neurotransmission. In the cerebellum, mutation of this gene is associated with episodic ataxia and spinocerebellar ataxia. There are 17 known mutations in this gene associated with FHM1, almost exclusively residing in the voltage-sensitive S4 segment or the pore-forming S5 and S6 segments. These mutations account for approximately 50% of FHM cases. Many of these mutations have been characterized electrophysiologically, producing a series of contradicting findings that has complicated the understanding of this disorder.

One of the more thoroughly studied mutations, R192Q, is located in the S4 segment of D1, where it alters a residue thought to be important for G-protein coupled receptor inhibition of the channel.(Ophoff et al., 1996) This inhibition is important for dopamine modulation of neurons. Studies utilizing the recombinant human channel expressed in mammalian cells demonstrate a hyperpolarizing shift in the voltage for half-maximal activation, $V_{1/2}$.(Hans et al., 1999) This shift is typical of FHM1 mutations and should lead to increased opening due to sub-threshold activation and, thus, aberrantly increased neurotransmitter release. R192Q mutant channels also have increased surface expression and are less sensitive to inhibition by G-protein coupled receptors, further compounding the shift in $V_{1/2}$.(Melliti et al., 2003) Knock-in mice have confirmed these predictions, showing a decreased threshold for CSD.(van den Maagdenberg et al., 2004) Recent studies with $Ca_V2.1$ knock-out mouse neurons transfected with R192Q mutant channels, however, have contradicted these findings.(Cao and Tsien, 2005) In these studies, mutant channels actually produce less whole-cell current and result in decreased synaptic transmission. While the majority of these findings are supportive of FHM1 mutations causing increased neuronal excitability and a decreased threshold for CSD, more work must be done to reconcile all findings.

FHM3

The final subtype of FHM associated with a mutated ion channel is FHM3, which is due to mutations in a gene (*SCN1A*) encoding a voltage-gated sodium channel α-subunit $Na_V1.1$. This channel is expressed throughout the central

nervous system. There has only been one study on FHM3 mutations, which found that they account for 15% of FHM cases. The one known FHM3 mutation, Q1489K, is located in the D3-4 linker region. Electrophysiological study has indicated that it causes faster recovery from inactivation than wild-type channels. As these channels likely underlie action potential generation and frequency regulation, such a change is expected to lead to neuronal hyperexcitability. Presumably, then, patients with this mutation have a lower threshold for CSD.(Dichgans et al., 2005)

Progressive and episodic ataxias

Many cases of ataxia are acquired due damage of the cerebellum or its output tracts. Some cases, however, are inherited. These can include both episodic and progressive forms. A general feature of both of these is that they are related to cerebellar dysfunction.

Episodic ataxia

Episodic ataxia (EA) is a rare autosomal dominant disorder primarily affecting cerebellar motor coordination. There are multiple forms of EA, differentiated by their attack duration, genetic cause and the presence of myokymia. Ataxic bouts can be induced by stress, startle, or heavy exertion such as exercise and first appear in infancy. Patients with some forms of EA have symptoms overlapping with familial hemiplegic migraine and spinocerebellar ataxia, all of which are allelic to FHM1. Other symptoms can include nystagmus, vertigo, tinnitus, diplopia, and seizures. Ataxia in these patients appears to be caused by misfiring of Purkinje cells in the cerebellum. Associated seizures seem

to be related to altered hippocampal firing. There are at least six genetic loci for episodic ataxia (EA1-6), of which four contain known causative genes (EA1-2 and EA5-6). Of these genes, three are ion channels, while the third, EA6, is the excitatory amino-acid transporters, *EAAT1*.

EA1

The first subtype of episodic ataxia, EA1, is also known as episodic ataxia with myokymia and hereditary paroxysmal ataxia with neuromyotonia. This subtype first manifests in childhood to early adolescence as stress inducible bouts of ataxia with interictal myokymia. Ataxic bouts are short-lived, lasting from seconds to minutes. Mutations in *KCNA1*, which encodes the voltage-gated potassium channel α-subunit $K_V1.1$, underlie EA1. There are at least 17 mutations known to be associated with EA1. These mutations are spread throughout the channel with no clear aggregation in specific channel regions.

Most of these mutations have received some electrophysiological study. The consensus of these experiments is that EA1 mutations result in channels with decreased whole-cell currents. This seems to be due in large part to slowed activation kinetics and a depolarized shift of $V_{1/2}$. The altered $V_{1/2}$ alone results in channels that begin to open later during action potentials than wild-type, this being compounded by the slower rate of activation in mutants. Some mutations also produce increases or decreases of depolarization kinetics. Many other mutation-specific alterations underlie EA1 pathophysiology. The I177N mutation, for instance, decreases single channel conductance.(Imbrici et al., 2003) Five mutations lead to decreased membrane expression of the channel either through

improper trafficking (R239S and F249I), impaired translation or protein stability (E325D), misfolding and the formation of membranous aggregates (R417X), or a currently unknown mechanism (F184C).(Zerr et al., 1998b; Zerr et al., 1998a; Bretschneider et al., 1999; D'Adamo et al., 1999; Manganas et al., 2001)

KCNA1 is expressed in interneurons and basket cells in the cerebellum. These cells form inhibitory synapses onto Purkinje cells and are important for regulating Purkinje cells, and by extension, cerebellar output. As with other K_V channels, $K_V1.1$ channels are involved in repolarizing the membrane potential following the action potential rising phase. As EA1 mutations lead to a decreased ability of these channels to fulfill such a role, it is expected that neurons expressing them will display prolonged action potentials and synaptic release. This will cause increased inhibitory input into Purkinje cells and altered cerebellar output. In support of this hypothesis, mice with the EA1 associated mutation V408A have more frequent and higher amplitude inhibitory postsynaptic currents.(Herson et al., 2003)

EA2

The second type of episodic ataxia, EA2, is differentiated by the presence of progressive cerebellar atrophy, vertigo, visual disturbances, migraines, absence seizures and dysarthria. Aside from physical and emotional stress, attacks in these individuals may also be elicited by coffee or alcohol. EA2 is further differentiated from EA1 by attacks lasting from hours to days. EA2 is caused by mutations in $Ca_V2.1$, a voltage-gated calcium channel $α_1$-subunit encoded by *CACNA1A*. This gene is also responsible for FHM1 and type-6

spinocerebellar ataxia (SCA6), which form a spectrum of symptoms with pure FHM1 at one end, EA2 in the middle, and SCA6 at the other end.

There are numerous mutations associated with EA2, with a slight preponderance for location in the S5 to S6 segments of each domain. Few of these mutations have been characterized. Of the characterized mutations, C271Y and G293R decrease protein stability while F1490K does not yield measurable currents.(Guida et al., 2001; Wan et al., 2005) The consensus from these mutations is that EA2 is caused by decreased $Ca_V2.1$ activity. Supporting this idea, many of the other known EA2 mutations result in truncated proteins, which are presumably non-functional. In the cerebellum, $Ca_V2.1$ is expressed highly in Purkinje cells, which provide the cerebellar output pathway. Here, these channels connect excitation with neurotransmitter release. As many of the known EA2 mutations are expected to result in decreased $Ca_V2.1$ function, Purkinje cells in affected humans should have decreased output with unaltered activity. This model of EA2 pathophysiology is supported by $Ca_V2.1$ knock-out mice, which display ataxia, absence seizures, and cerebellar degeneration.(Jun et al., 1999)

EA5

EA5 is an infrequently occurring type of episodic ataxia, differentiated by the presence of both ataxia and juvenile myoclonic epilepsy in many patients. Patients with EA5 also present with vertigo during attacks and interictal nystagmus and vertigo. These attacks are responsive to acetazolamide treatment. EA5 is caused by a single known mutation in the calcium channel β_4-

subunit encoding gene, *CACNB4*. Mutations in this gene also cause juvenile myoclonic epilepsy (discussed below). The β_4-subunit is expressed in the cerebellum, where it produces currents with slowed inactivation. The one known EA5 mutation, C104F, results in currents 30% greater than wild-type. Presumably, this leads to either neuronal hyperexcitability or increased transmitter release upon excitation, though this has yet to be demonstrated.(Escayg et al., 2000)

Spinocerebellar ataxia

Spinocerebellar ataxia (SCA) is a large grouping of disorders broadly characterized by the presence of slowly progressive ataxia often concomitant with cerebellar atrophy. These disorders are differentiated by their age of onset, duration, and symptomology. There are at least 25 types of SCA, of which, SCA6 and SCA13 are caused by mutations in ion channels.

SCA6

SCA6 is typified by cerebellar dysfunction (namely ataxia, dysarthria, and nystagmus) and degeneration. Other signs include loss of vibratory and proprioceptive sensitivity, with onset between ages 5 and 65. These symptoms last between 20 and 30 years, before leading to death. Interestingly, some patients present without progressive ataxia but with either episodic ataxia or migraine, indicative of EA2 and FHM1, respectively. Such patients can occur within the same family as those with typical SCA6 characteristics. As EA2, FHM1, and SCA6 are allelic, it appears that the pathophysiology is partly conserved across these diverse disorders and that genetic background and

46

environmental factors contribute to disease manifestations.(Zhuchenko et al., 1997)

There is a correlation, however, between the severity of *CACNA1A* mutations and disease state. Many FHM1 mutations lead to channels with altered kinetics, while those of EA2 tend to lead to loss of function. SCA6 mutations, however, seem to lead to both loss of normal function and toxic gain of function. As with other SCA types, most cases of SCA6 are caused by polyglutamine expansion, in SCA6 this expansion is of greater than 18 repeats. Such mutant channels form intracellular inclusions, which seem to lead to apoptosis.(Ishikawa et al., 1999) As with similar expansion diseases, increased expansion length is correlated with earlier onset. Interestingly, recording of mutant channels that are able to traffic to the membrane indicates that these have hyperpolarized inactivation voltage-sensitivity.(Toru et al., 2000) As these channels connect excitation to neurotransmitter release, such an effect will yield decreased neuronal output, as is also the case with lack of membrane trafficking.

Aside from polyglutamine expansions, there are also a number of missense mutations associated with SCA6. These mutations are present in patients with phenotypes overlapping either SCA6 and EA2 or SCA6 and FHM1. Two such mutations, C287Y and G293R, form intracellular inclusions similar to polyglutamine expansion mutants.(Wan et al., 2005) Consequently, it seems that a common underlying pathophysiology of SCA6 is decreased $Ca_V2.1$ current, concomitant with intracellular inclusions.

SCA13

Type-13 spinocerebellar ataxia (SCA13) is typified by the common SCA symptoms (dysarthria, nystagmus and ataxia) with the addition of epilepsy, an inability to run, and increased reflexes. The accompanying ataxia is mildly progressive and can be accompanied by mental retardation. Symptom onset varies with the causative mutation.(Waters et al., 2005) SCA13 is caused by mutations in the *KCNC3* gene, which encodes the voltage-gated potassium channel α-subunit $K_V3.3$. Two *KCNC3* mutations are known to be associated with SCA13. The first of these, R420H, is located in the voltage-sensing S4 segment and leads to dominant negative non-conducting channels. The second mutation, F448L, results in channels with hyperpolarized shifts of $V_{1/2}$. In addition, this mutation leads to slowed entry into deactivation.(Waters et al., 2006)

The function of $K_V3.3$ in the cerebellum is well understood. It is expressed in cerebellar granule cells, Purkinje cells, and deep cerebellar neurons. This channel aids in the repolarization phase of action potentials and is required for high-frequency firing with little frequency adaptation. These channels typically deactivate very rapidly, allowing for shortened after-hyperpolarizations. As R420H will lead to a drastic decrease in K_V3 mediated currents, neurons expressing it are expected to have difficulty maintaining high-frequency firing rates. F448L, on the other hand, likely prolongs after-hyperpolarizations, thereby leading to decreased maximal firing rates.

Epilepsy and convulsive disorders

Epilepsy is a common neurological disorder with a 3% lifetime prevalence. While a variety of brain lesions are known to lead to epilepsy, approximately 33% of cases are not due to brain trauma or structural disturbance. In these cases, the cause seems to be genetic, usually via complex inheritance. In a few cases, however, epilepsy is inherited in a simple Mendelian manner, often a result of ion channel mutations. These disorders are clinically related in that they affect both genders and manifest with absence seizures, generalized tonic-clonic seizures and myotonic jerks either separately or in combination. These disorders are typically chronic and may show progression.

Generalized epilepsy with febrile seizures + and related disorders

One epilepsy syndrome is generalized epilepsy with febrile seizures + (GEFS+). GEFS+ is clinically and genetically related to a number of other disorders, including severe myoclonic epilepsy of infancy (SMEI) and intractable epilepsy in childhood (IEC). GEFS+ is characterized by febrile seizures, often persisting beyond 6 years of age. These seizures may appear as afebrile tonic-clonic, myoclonic or absence in type. Patients with related disorders have more severe phenotypes. SMEI is characterized by tonic-clonic seizures, impaired psychomotor development, myoclonic seizures and ataxia. IEC is intermediate between SMEI and GEFS+, presenting with all of the symptoms of SMEI, except myoclonic seizures.(Gardiner, 2005) It has been suggested that these disorders are part of a larger extended phenotype.(Singh et al., 2001) There are at least

five subtypes of GEFS+, separated according to causative genes. Of these, three are ion channels with type 3 and 5 caused by mutant GABA receptor subunits.

Type 1

The first subtype of GEFS+ is caused by mutations in *SCN1B*, which encodes a voltage-gated sodium channel β-subunit. Unlike other causative genes, mutations in *SCN1B* are not known to lead to SMEI or IEC. This β-subunit is required for proper channel inactivation. There are two mutations in *SCN1B* known to lead to GEFS+: a missense mutation, C121W, and a mutation in a splice acceptor site leading to a small in-frame deletion, I70_E74del.(Wallace et al., 1998; Audenaert et al., 2003) Both of these mutations are located on the extracellular N-terminus of the channel. The in-frame deletion mutant, I70_E74del has not been characterized. The C121W mutation causes the loss of a disulfide bridge and is likely malformed. This mutation shows a decrease in frequency dependent rundown, leading to the neuronal hyperexcitability thought to underlie many forms of epilepsy.(Meadows et al., 2002)

Type 2

Another subtype of GEFS+, which is associated with IEC and SMEI, is caused by mutations in the voltage-gated sodium channel α-subunit $Na_V1.1$. Interestingly, other $Na_V1.1$ mutations lead to either juvenile myoclonic epilepsy, discussed below, or familial hemiplegic migraine, discussed above. There are approximately 90 mutations in *SCN1A* associated with GEFS+ type 2 and associated disorders. These mutations are located throughout the channel and can result hyperexcitability. An important channel property that prevents

50

hyperexcitability is delayed recovery from inactivation. Wild-type $Na_V1.1$ channels, for example, rundown 30% during 10Hz stimulation. GEFS+ mutant D188V channels, however, only rundown 10% during this same stimulation, due to expedited recovery from inactivation.(Cossette et al., 2003) Other mutations lead to hyperexcitability through other mechanisms, such as delayed entry into slow inactivation.

While some GEFS+ mutations cause membrane hyperexcitability, others, such as R859C, lead to hypoexcitability. This is a result of $V_{1/2}$ being shifted to more depolarized potentials in the mutant. Interestingly, this mutation also recovers more slowly from inactivation than wild-type. Consequently, neurons expressing these mutant channels have a higher threshold for action potential initiation and also increased frequency dependent rundown.(Barela et al., 2006) There are also a number of non-sense and otherwise non-functional mutations that seem to lead to membrane hypoexcitability. How this membrane hypoexcitability leads to a GEFS+ type phenotype is unclear.

Type 4

The final channel associated with GEFS+ and a related disorder is the voltage-gated sodium channel $Na_V2.1$, encoded by *SCN2A*. There are two mutations in *SCN2A* leading to GEFS+ related phenotypes: R102X and R187W. The R102X truncation mutation is located in the intracellular N-terminus and results in nonfunctional channels. As R102X does contain the N-terminal inactivation ball, it associates with wild-type channels and shifts their inactivation voltage-sensitivity to more hyperpolarized potentials.(Kamiya et al., 2004) This

leads to membrane hypoexcitability and causes seizures through an unknown mechanism. R187W is located on the intracellular loop connecting S2 and S3 in D1. The end result of this mutation on membrane excitability is unclear. Electrophysiological experiments have shown that R187W mutants have delayed inactivation, suggesting neuronal hyperexcitability. Yet, this channel also inactivates at more hyperpolarized potentials, suggesting neuronal hypoexcitability.(Sugawara et al., 2001) Which altered channel property predominates in patients is unknown.

Childhood absence epilepsy

Childhood absence epilepsy (CAE) is another common neurological disorder, affecting 1 in 1000 people. This disorder is characterized by absence seizures presenting as the first seizure type between the ages of 3 and 12. These seizures are often quite frequent, occurring multiple times daily, and are associated with bilateral 3Hz spike-and-wave discharges. While the majority of CAE cases are polygenic, 10% seem to be caused by ion channel mutations. Of these, many are caused by mutations in the T-type calcium channel *CACNA1H*, while a few other cases are due to mutations in the GABA$_A$ receptor γ-subunit *GABRG2* or the chloride channel *CLCN2. CLCN2* mutations also cause a phenotype overlapping with juvenile myoclonic epilepsy and will be discussed there.

There are at least 20 mutations in *CACNA1H* associated with CAE. Interestingly, these mutations are mostly localized in the intracellular loop between domains 1 and 2. While many ion channel mutations seem to lead

inevitably to disease, *CACNA1H* mutations seem to only convey a high susceptibility to seizure phenotype acquisition. These mutations lead to a variety of kinetic alterations, such as a positive or negative shift of $V_{1/2}$ or slowed or hastened inactivation. Overall, these mutations can lead to either hypoexcitability or hyperexcitability. While it is unclear how hypoexcitability might lead to CAE, the mechanism underlying hyperexcitability is clearer, as *CACNA1H* is expressed heavily in the thalamus, which is the origin for many absence seizures.(Chen et al., 2003)

Juvenile myoclonic epilepsy

Also known as Janz syndrome, juvenile myoclonic epilepsy (JME) is a common form of epilepsy characterized by myoclonus occurring early in the morning, causing patients to drop objects. Aside from bouts of myoclonia, JME patients may have tonic-clonic and absence seizures. In fact, there is some phenotypic overlap between CAE and JME, due to the presence of absence seizures in both. The onset of these seizures is between ages 12 and 18. There are a number of known genetic loci for JME. Two of these loci are ion channels, *CLCN2* and *CACNB4*, with the other two a GABA receptor subunit and the poorly understood gene *EFHC1*.

CACNB4 mutations

The first type of JME is caused by mutations in *CACNB4*, which encodes the voltage-gated calcium channel β_4-subunit. This subunit is expressed heavily in the cerebellum and mice lacking it have a "lethargic" phenotype similar to JME. Two mutations in the β_4-subunit are known to be involved in JME: C104F and

R482X. The C104F leads to a phenotype overlapping with episodic ataxia (EA5) and is discussed above. The R482X mutation decreases the time constant for entry into fast inactivation. This is expected to lead to hypoexcitability rather than hyperexcitability. Consequently, it is unclear how this mutation result in JME.(Escayg et al., 2000)

<center>*CLCN2*</center>

For inhibitory GABAergic input to be effective, the chloride reversal potential must be appropriate. Chloride channels play a large role in setting this value. Not surprisingly then, there are three known mutations in the chloride channel *CLCN2* associated with epilepsy. Each of these mutations results in a slightly different phenotype in patients. The first mutation, M200fsX231, results in patients having either typical JME or waking grand mal seizures. This truncation removes much of the channel, including regions involved in ion conduction. Not surprisingly then, this mutant is not found to be functional. The second *CLCN2* mutation, 74_117del, results in either CAE or grand mal seizures on awakening. Like the M200fsX231 mutation, this mutant is non-functional. As these two mutants result in a loss of function, there will be a slow accumulation of Cl⁻ in neurons. Overtime, this will alter the Cl⁻ reversal potential and negate the affect of GABAergic input. The third *CLCN2* mutation, G715E, does produce functional channels. These channels, however, have an altered voltage-sensitivity of activation, likely resulting in hyperexcitability.(Haug et al., 2003)

<center>54</center>

Generalized epilepsy with paroxysmal dyskinesia

Most cases of epilepsy and paroxysmal dyskinesia occur separately and are caused by different underlying pathophysiology. In some cases, however, these two disorders do cosegregate in patients. Generalized epilepsy with paroxysmal dyskinesia, GEPD, is characterized by absence and/or generalized tonic-clonic seizures first manifesting in infancy or early childhood. These same patients also manifest with signs of paroxysmal dyskinesia in childhood or adolescence. EEG recordings of these patients show interictal spike-wave complexes. There is one known mutation associated with GEPD, D434G, in the voltage and calcium-gated potassium channel gene *KCNMA1*.(Du et al., 2005) This gene encodes a large-conductance BK channel similar in structure to the K_V channels, with an added membrane-spanning segment (S0) that results in an extracellular N-terminus. BK channels also have a C-terminal RCK domain that seems to be involved in ligand interaction. Like K_V channels, BK channels open with depolarization and aid the repolarization phase of action potentials. Unlike K_V channels, however, BK channels also activate with increasing calcium concentrations.

Electrophysiological experiments have demonstrated that mutant BK channels produce greater whole-cell currents, activate at more hyperpolarized potentials, and are 3-5 fold more sensitive to calcium than wild-type channels. In fact, the ability of mutant channels to activate at more negative potentials seems to be an effect of their increased calcium sensitivity. In neurons, these changes should lead to an increased rate of repolarization following action potential

initiation. While this may result in an increase in the current required to initiate an action potential, it will also greatly decrease the refractory period between them. This may then lead to neuronal hyperexcitability. Such an occurrence in the thalamus, a location where *KCNMA1* is expressed, could lead to epilepsy in the same manner as CAE mutations. Paroxysmal dyskinesia in these patients, however, is likely a result of this neuronal hyperexcitability occurring in the basal ganglia.(Du et al., 2005)

CONCLUSION AND FUTURE DIRECTIONS

There has been tremendous progress in understanding the contribution of ion channels to human disease in the past 15 years. Much of this progress is due to the nature of ion channels, i.e., their relative ease of study, and the years of research beginning with Hodgkin and Huxley on the squid giant axon. These pre-Human Genome Project experiments described the key conductances in both neurons and muscle and how they contributed to proper function. The advent of the modern patch-clamp apparatus allowed for the characterization of single ion channels before their genetic underpinnings were understood. During this time, the kinetic details of channel gating and its role in excitation began to be understood. It was only a matter of time before the revolution in molecular biology provided the tools to clone and recombinantly express the underlying channels for these conductances, thereby providing a DNA-level perspective on function. As the toolbox for characterizing the bevy of ion channel mutations at the molecular and electrophysiological level were largely already in existence, it is unsurprising then that there has been rapid progress in characterizing

channelopathies. While this process will always be an essential component to understanding ion channel disorders, the next 15 years will show a gradual migration of interest away from single molecule or cell-oriented experimentation toward tissue and organism level experimentation. With the creation of knock-in and knock-out mice, this process has already begun.

There are some conclusions that we can draw from what is currently known of ion channel disorders. Firstly, with few exceptions, they are inherited in simple Mendelian fashion. These disorders are almost always autosomal dominant and have a high penetrance. When mutations occur in a channel composed of multiple α-subunits, the mutations tend to affect channel properties in a dominant-negative manner. While few ion channel disorders are persistent or progressive, their complications, such as muscle weakness, may be. Clinically similar phenotypes can have disparate genetic underpinnings and, conversely, different mutations in the same channel can lead to disparate phenotypes, even when the mutations are neighboring. Consequently, gaining a more complete understanding of the molecular-underpinning of ion channel disorders will provide us with the basis to better determine how they lead to dysfunction at the tissue and organism level.

CHAPTER 2

Mutations in a potassium channel (Kir2.6) causes susceptibility to thyrotoxic hypokalemic periodic paralysis

Devon P. Ryan[1,2,16], Magnus R. Dias da Silva[2,14,16], Tuck Wah Soong[3,7], Bertrand Fontaine[4], Matt R. Donaldson[2,15], Annie W. C. Kung[5], Wallaya Jongjaroenprasert[6], Mui Cheng Liang[7], Daphne HC Khoo[8], Jin Seng Cheah[9], Su Chin Ho[8], Harold S. Bernstein[10], Rui M. B. Maciel[11], Robert H. Brown Jr.[12], Louis J. Ptáček[1,2,13,*]

1. Neuroscience Graduate Program, University of California, San Francisco, San Francisco, California, 94158, USA.

2. Department of Neurology, University of California, San Francisco, San Francisco, California, 94158, USA.

3. Ion Channel & Transporter Laboratory, National Neuroscience Institute, Singapore, 308433.

4. INSERM, Université Pierre et Marie Curie-UPMC, UMRS 546, and Assistance Publique-Hôpitaux de Paris, Centre de Référence des Canalopathies Musculaires, Groupe Hospitalier Pitié-Salpêtrière, Paris, France.

5. Department of Medicine, University of Hong Kong, Queen Mary Hospital, Hong Kong SAR, China.

---

[14] Current address: Department of Biochemistry, Universidade Federal de São Paulo, São Paulo 04044-020, Brazil.

[15] Current address: Department of Dermatology, Texas Tech University, Lubbock, Texas 79409, USA.

[16] Authors contributed equally

6. Department of Medicine, Ramathibodi Hospital, Mahidol University, Bangkok, Thailand.

7. Department of Physiology, Yong Loo Lin School of Medicine, National University of Singapore, Singapore, 308433.

8. Department of Clinical Research, Singapore General Hospital, Singapore.

9. Department of Medicine, Yong Loo Lin School of Medicine, National University of Singapore, Singapore, 308433.

10. Cardiovascular Research Institute, University of California, San Francisco, CA 94143-0130, USA.

11. Department of Medicine, Division of Endocrinology, Universidade Federal de São Paulo, São Paulo 04039-032, Brazil.

12. Massachusetts General Hospital, 16th Street, Navy Yard, Charlestown, MA 02129, USA.

13. Howard Hughes Medical Institute, University of California San Francisco, San Francisco, CA, 94158, USA.

* Correspondence: ljp@ucsf.edu

Summary

Thyrotoxic hypokalemic periodic paralysis (TPP) is characterized by acute attacks of weakness, hypokalemia, and thyrotoxicosis of various etiologies. These transient attacks resemble those of patients with familial hypokalemic periodic paralysis (hypoKPP) and resolve with treatment of the underlying hyperthyroidism. Because of the phenotypic similarity of these conditions, we

hypothesized that TPP might also be a channelopathy. While sequencing candidate genes, we identified a previously unreported gene (not present in human sequence databases) that encodes an inwardly rectifying potassium (Kir) channel, Kir2.6. This channel, highly identical to Kir2.2, is expressed in skeletal muscle and is transcriptionally regulated by thyroid hormone. Expression of Kir2.6 in mammalian cells revealed normal Kir currents in whole-cell and single channel recordings. Kir2.6 mutations were present in up to 33% of the unrelated TPP patients in our collection. Some of these mutations clearly alter a variety of Kir2.6 properties, all altering muscle membrane excitability leading to paralysis.

Introduction

The periodic paralyses and non-dystrophic myotonias comprise a group of muscle disorders characterized by abnormal muscle relaxation (myotonia) and/or paroxysmal muscle weakness. These disorders are subdivided based on the presence of myotonia with weakness, response to potassium, temperature sensitivity, association with cardiac arrhythmia and facial dysmorphology, and induction by thyrotoxicosis. Many of these entities are now known to result from ion channel mutations, termed channelopathies (Ryan and Ptácek, 2008).

TPP is a sporadic muscle disorder characterized by episodic attacks of weakness and hypokalemia in some thyrotoxic individuals. Patients are normal between attacks, which resolve with treatment of thyrotoxicosis. Episodic weakness in TPP is clinically similar to the known channelopathies familial hypoKPP and Andersen-Tawil syndrome (ATS) (Ptacek et al., 1994; Bulman et al., 1999; Plaster et al., 2001) and is the most common form of periodic paralysis,

being most prevalent in young Asian and Latin American men (Silva et al., 2004; Kung, 2006). In these populations, up to 10% of thyrotoxic male individuals develop episodic weakness. In Caucasians, this number is less than 0.1% (Kelley et al., 1989). Although thyrotoxicosis is more common in women, most individuals with TPP are men.

Aside from similarity to the familial periodic paralyses, several observations indicate that TPP may be a genetically conditioned disorder unmasked by thyrotoxicosis. Although weakness is a common symptom of thyrotoxicosis, episodic flaccid paralysis arises in only some thyrotoxic patients. TPP recurs in patients with recurring hyperthyroidism, such as relapses of Graves Disease (Kung, 2002) and, as with other channelopathies, a similar phenotype is seen across species (Nemzek et al., 1994).

While screening skeletal muscle ion channel candidate genes in TPP patients, we serendipitously identified a previously unreported gene—here named *KCNJ18*, encoding an inwardly rectifying potassium channel, Kir2.6. This subfamily, which includes Kir2.1 through Kir2.4 and Kir2.2v/Kir2.5, is one of seven subfamilies (Kir1.x to Kir7.x). Kir subunits have two membrane-spanning domains, are selective for potassium, stabilize the resting membrane potential near the potassium equilibrium potential, and tetramerize to form functional, inwardly rectifying channels (Nichols and Lopatin, 1997; Krapivinsky et al., 1998).

The structural and functional homology of these channels suggests they arose through gene duplication with subsequent diversification. This process plays a crucial role in evolution, allowing redundant gene variants to acquire

novel characteristics and functions, with a likely role in expanding protein diversity. Kir channels have assumed specific functions in excitable tissues and mutations in these channels can cause human disease. Kir channelopathies include the episodic muscle and developmental features of ATS (Kir2.1), the renal tubular secretion defects seen with Barter syndrome type III (Kir1.1), and defective insulin secretion in persistent hyperinsulinemic hyperglycemia of infancy (Kir6.2) (Abraham et al., 1999; Plaster et al., 2001).

Kir2.6 shares 99% identity with Kir2.2 and was considered an excellent candidate for TPP because it is primarily expressed in skeletal muscle and likely contributes to cell membrane excitability. Furthermore, *KCNJ18* has a thyroid hormone response *cis*-element (TRE) within its promoter, which might drive increased expression of Kir2.6 to protect against membrane potential instability.

Genetic analysis revealed mutations in Kir2.6 in multiple TPP patients. Electrophysiological analysis indicates that some of these mutations have large effects on Kir2.6 currents either inherently or via thyroid hormone inducible mechanisms. As such, mutations may cause predisposition for the episodic weakness seen only during thyrotoxicosis.

Results

Screening candidate genes and genomic characterization of *KCNJ18*

Since ion channel mutations cause familial periodic paralysis, we screened ion channels known to be expressed in skeletal muscle with putative thyroid response elements (TREs) of the DR-4 motif in their promoter regions, for mutations (Table 1). While screening *KCNJ12*, we noted a number of

polymorphisms that violated Hardy-Weinberg equilibrium, suggesting the existence of another gene. By changing PCR methods and primers we specifically amplified a highly homologous sequence that we have submitted under NCBI accession number FJ434338 as *KCNJ18*.

Sequencing ten clones from low stringency PCR yielded the known genes *KCNJ12* (Kir2.2) and *KCNJN1*/*KCNJ17* (Kir2.2v/Kir2.5). In addition, a previously unreported paralog *KCNJ18* (Kir2.6, Figure 4) was seen, which shares 98-99% identity in the coding region (96-99% at the amino acid level, depending on the SNPs present in *KCNJ18*) with *KCNJ12* (Table 2 and Table 3), >95% identity with *KCNJ17* (data not shown), and is only one amino acid different from *KCNJ12X* (AB181299).

Table 1. Genes screened for mutations associated with TPP.

Gene	Protein	Promoter region sequenced?
Calcium Channels		
CACNA1S	Ca$_V$1.1	Yes
Sodium Channels		
SCN4A	Na$_V$1.4	Yes
Endosulfine		
ENSA	α-Endosulfine	No
Inwardly rectifying potassium channels		
KCNJ2	Kir2.1	No
KCNJ4	Kir2.3	No
KCNJ8	Kir6.1	No
KCNJ11	Kir6.2	Yes
KCNJ12	Kir2.2	Yes
KCNJ14	Kir2.4	No
KCNJN1/KCNJ17	Kir2.2v/Kir2.5	Yes
Voltage-gated potassium channels β-subunits		
KCNE1	minK	No
KCNE2	MiRP1	No
KCNE3	MiRP2	Yes
KCNE4	MiRP3	No
KCNE5	KCNE5	No
G-protein coupled receptors		
TAAR9	Trace amine associated receptor 9	No
Inwardly rectifying potassium channel auxiliary subunits		
ABCC9	SUR2	No
Chloride channels		
CLCN4	ClC-4	No

Table 2. Non-synonymous and synonymous variation that distinguish Kir2.2 from Kir2.6.

Amino Acid Residue	Alleles	Residues	
		Kir2.2	Kir2.6
15	C/T	Ser	Leu
81	G/C	Arg	Arg
216	T/C	Gly	Gly
273	G/A	Glu	Glu
377	C/T	Tyr	Tyr
402	C/T	Asp	Asp
430	A/G	Glu	Gly

Table 3. Single nucleotide polymorphisms (SNPs) in *KCNJ18* and their prevalence across ethnicities.

Residue Change		Prevalence (% chromosomes)			
Nucleotide	Amino Acid	Caucasian	Chinese	Mexican	African American
c.17G>A	p.Arg6Gln	36.4	24.4	6.2	36.7
c.78G>A	p.Ser26Ser	0	1.2	0	0
c.87C>A	p.Asn29Lys	0	0	0	2.2
c.116A>G	p.Gln39Arg	43.2	18.6	44.8	40
c.119A>G	p.His40Arg	43.2	17.4	44.8	40
c.167C>A	p.Asp56Glu	40.9	17.4	41.7	30
c.264G>A	p.Ser88Ser	0	0	0	1.1
c.298G>A	p.Val100Ile	4.6	0	2.1	0
c.327C>T	p.His109His	0	0	2.1	8.9
c.353_354delinsGG	p.His118Arg	0	0	0	1.1
c.467T>C	p.Lys156Pro	0	0	0	1.1
c.576C>G	p.His192Gln	2.3	0	0	1.1
c.735G>A	p.Pro245Pro	0	1.2	0	0
c.745G>A	p.Val249Ile	43.2	18.6	40.6	31.1
c.837G>A	p.Pro279Pro	0	0	0	2.2
c.843C>G	p.Phe281Leu	0	0	1.0	0
c.996C>T	p.Phe332Phe	0	0	0	3.3
c.1013A>T	p.Tyr338Phe	0	1.2	0	0
c.1024T>C	p.Tyr342His	2.3	0	0	0
c.1113T>C	p.Ser371Ser	0	0	2.1	6.7

Figure 4. Structure and sequence of *KCNJ18* (Kir2.6).

A. *KCNJ18* shares a high degree of identity with *KCNJ12* in both exons (boxes) and introns (lines). The coding region of both *KCNJ18* and *KCNJ12* is contained within exon 3 (black region). The first intron of *KCNJ12* is longer than that of *KCNJ18* causing 0% identity in this non-overlapping region (dotted line). **B.** *KCNJ18* sequence-exon boundaries are noted with a caret (^). Coding sequence is capitalized with the corresponding amino acid above. Underlined nucleotides denote differences between *KCNJ18* and *KCNJ12*, with non-synonymous differences having a gray background. **C.** Diagram of Kir2.6 with the relative locations of TPP associated mutations.

To verify that *KCNJ18* is a paralogous locus, a human BAC DNA library was screened for *KCNJ18* and *KCNJ12* by PCR with gene-specific primers. Two non-overlapping BAC clones contained either *KCNJ18* (RP11-437N10) or *KCNJ12* (RP11-728e14). A Southern blot performed on BamHI digested RP11-437N10 yielded a 2.6-Kb fragment (Figure 5B). Furthermore, we are unable to specifically amplify *KCNJ12* from RP11-437N10, but are able to do so from RP11-728e14, as confirmed by sequencing the PCR product. The reverse is true for specifically amplifying *KCNJ18* (Figure 5C). It appears that during the analysis and alignment of genome sequences, the high identity between *KCNJ12* and *KCNJ18* resulted in non-homologous end joining of non-overlapping BACs and, therefore, exclusion of *KCNJ18*. Based on sequencing of both ends of RP11-437N10, we locate this BAC centromeric to *KCNJ12* in the same chromosomal segment, where there is a currently gap (Figure 5D). Taken together, these data suggest that the two homologs arose through duplication of this region (Figure 6).

Figure 5. Genomic characterization of *KCNJ18*

A. Both *KCNJ12* and *KCNJ18* have three recognized exons (hatched regions). Probes constructed from exon 1 (A1, unique for each gene) were used for Northern blot and genome-walking to determine exon 1 boundaries. **B.** Radiolabeled A2 primers from exon 3 were used as a probe for Southern blot upon BamH1-digested *KCNJ18* containing BAC DNA, **C.** *KCNJ12* specific primers were able to yield PCR products from control human genomic (hG) DNA and BAC RP11-728E14 (containing *KCNJ12*) but not RP11-437N10 (containing *KCNJ18*). **D.** From this BAC end sequencing, we place *KCNJ18* centromeric to *KCNJ12* on chromosome 17 in a previously identified sequencing gap and not overlapping with *KCNJ12*.

A
A1-Used for PCR exon1 boundaries
A2-Used as probe for Southern blot
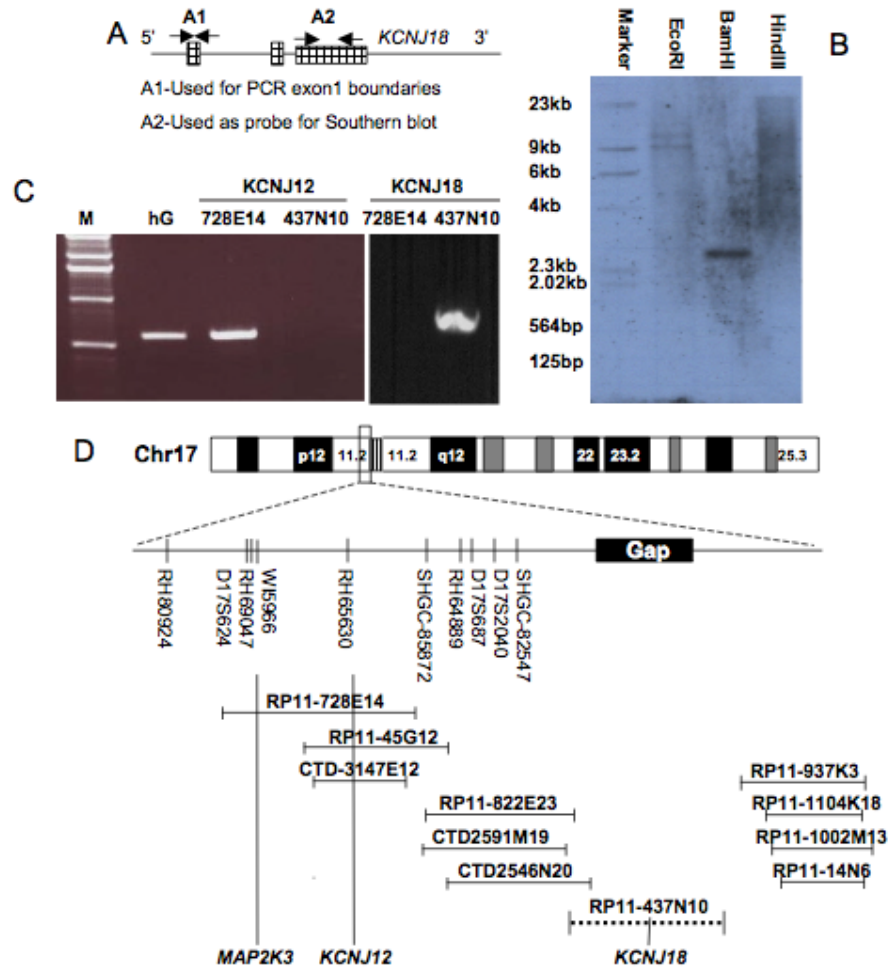
Figure 6. KCNJ18 and KCNJ12 are unique.

Alignment of the BACs containing *KCNJ12* (RP11-728E14) and *KCNJ18* (RP11-437N10) suggests that *KCNJ18* is largely a duplication of *KCNJ12* (A, diagram as in Figure 4 where dashed lines indicate duplication boundaries and arrows primer position). The duplication/unique region boundary can be specifically amplified from each BAC using a specific forward primer (111F: CCCAATCAAGCAGAAACACA or 112F: CCTGCTAGATCCCAGCTCAG) and a non-specific reverse primer (111R; GGAGAAACCGGAGAAACACA), indicating that the BACs are unique (B). Both primer pairs are also able to produce different PCR products from human genomic DNA (hG). Alignment of the sequence of both BAC and human genomic PCR products indicates that the amplicons from an individual primer pair match between BAC and human genomic DNA, but not between primer pairs except in the duplicated region (C). A portion of the sequence is shown for both genomic DNA (111_Genomic or 112_Genomic for amplicon from 111F or 112F primer, respectively) and BAC DNA is shown. N indicates the presence of a polymorphism. Cons shows the conservation between all four sequences with a "*" indicating 100% conservation and a ":" indicating at least partial conservation, due to a polymorphism. The boundary of the unique and duplicated region is indicated. PCR from genomic DNA was performed with the same method used to screen for TPP mutations. BAC PCR was performed using Phusion DNA polymerase (Finnzymes, MA) according to the manufacturers instructions. Digested BAC DNA was probed with biotinylated

synthetic probe targeted against either the unique exon 1 (CTGTTGGGAAGCCTGTTTC/ GTCACGAGGGTAAGCCAAGC, D top) or the conserved exon 3 (CAACCCCTACAGCATCGTGTC/TCCACACAGGTGGTGAACAT, D bottom). Both BACs were digested with BamHI or HindIII for 16 hours prior to fractionation. BAC RP11-728E14 was (digested as indicated) was run on lanes 1 and 3 while BAC Rp11-437N10 was run on lanes 2 and 4. Blots were performed simultaneously from the same digested DNA and gel. Expected sizes, according to reference BAC sequence, were: 0bp, D top 1; 7174bp, D top 2; 0bp, D top 3; 8408bp, D top 4; 6589bp, D bottom 1; 6572bp, D bottom 2; 2583bp, D bottom 3; 2583bp, D bottom 4.

A

Unique Region Duplicated Region *RP11-728E14*

RP11-437N10

D

| *HindIII* | | *BamHI* | |
| 1 | 2 | 3 | 4 |

9Kb —
7Kb ═
5Kb —
4Kb —

| *HindIII* | | *BamHI* | |
| 1 | 2 | 3 | 4 |

9Kb ═
7Kb ═
5Kb —
4Kb —
3Kb —
2Kb —

B

	hG		437N10		728E14	
111F	+		+		+	
112F		+	+			+

1000bp —

C

```
111_Genomic  AGANGGATCTCCAGGAAGTGTCTCCCTGACNGACTGGGAAGTCATCTTTATTGAAGACATTTGGCCAGAGNGAGAGGCAT
112_Genomic  TCACAGCACCAATTAGCTGCCACCCAAAGGAATGGGAGAGAGGCAGGCAAGAGCCACATAGTCAGGGAAGGCTTCCTGGAG
RP11-437N10  AGACGGATCTCCAGGAAGTGTCTCCCTGACGGACTGGGAAGTCATCTTTATTGAAGACATTTGGCCAGAGTGAGAGGCAT
RP11-728E14  TCACAGCACCAATTAGCTGCCACCAAAGGAATGGGAGAGAGGCAGGCAAGAGCCACATAGTCAGGGAAGGCTTCCTGGAG
Cons           *: * *        *    *      *  ** **          * * * * *  * *  * *   *   * *

111_Genomic  CCAGGCCCCTGAGAAACAGGGGAGGCAGAGCAAGAGGGAGGACAGAGCAGAGGCCAGAGCCCANGCAGGATACAGCATCG
112_Genomic  GAGGTGGTCCAAGCCAGACTTGGAGTGACTGTGGTGTCTCCTAGAGACACCAGGGCCAACGTGCGTGGTCAAATCCTAGG
RP11-437N10  CCAGGCCCCTGAGAAACAGGGGAGGCAGAGCAAGAGGGAGGACAGAGCAGAGGCCAGAGCCCACGCAGGATACAGCATCG
RP11-728E14  GAGGTGGTCCAAGCCAGACTTGGAGTGACTGTGGTGTCTCCTAGAGACACCAGGGCCAACGTGCGTGGTCAAATCCTAGG
Cons              *   *    *  **    *      * **   *   **   :   *    *    *    *

                                          Unique ←┬→ Duplicated

111_Genomic  TGCCACTGCCACNGGCATAAGGGGCGGTGAATTTCTATCCCAGCTTTGCCATGGACTGGCTGCNTTTCCCTAGGCACGGC
112_Genomic  TCTCTATTTCCACAGCCCTGGAAGTCCTGAATTTCTATCCCAGCTTTGCCATGGACTGGCTGCGTGTCCCTAGGCACAGC
RP11-437N10  TGCCACTGCCACAGGCATAAGGGGCGGTGAATTTCTATCCCAGCTTTGCCATGGACTGGCTGCGCATTTCCCTAGGCACGGC
RP11-728E14  TCTCTATTTCCACAGCCCTGGAAGTCCTGAATTTCTATCCCAGCTTTGCCATGGACTGGCTGCGTGTCCCTAGGCACAGC
Cons           *     *   *   **    *  *  *********************************:* ********** **

111_Genomic  ACTCATCCTAACTGATCCCCAGTTTCTTGCCTCTATCAAAAGAAACTAATGTGAATGGAAATGGCATGTGTCACAGTGAT
112_Genomic  ACTCATCCTATCCGAGCCCCAGTTTCTTGCCTCTATCAAAAGAAACTGGTGTGAATGGAAGTGGCATGTGTCACAGTGAC
RP11-437N10  ACTCATCCTAACTGATCCCCAGTTTCTTGCCTCTATCAAAAGAAACTAATGTGAATGGAAATGGCATGTGTCACAGTGAT
RP11-728E14  ACTCATCCTATCCGAGCCCCAGTTTCTTGCCTCTATCAAAAGAAACTGGTGTGAATGGAAGTGGCATGTGTCACAGTGAC
Cons         **********  * ** *************************** ********** ******************

111_Genomic  GAGTGTTCCTGATGCACAGCAGTTGCGCACTTCCAGTTTACTGGGGTTGGAAAGCGTGTGTGGCAGTAAGAGGTCCGTGC
112_Genomic  GAGTGTTCCTGACGCACAGCAGTTGCGCAGTCCCAGTTTACTGGGGTTGGAAAGCGTGTGTGGCAGTAAGAGGTCCGTGC
RP11-437N10  GAGTGTTCCTGATGCACAGCAGTTGCGCACTTCCAGTTTACTGGGGTTGGAAAGCGTGTGTGGCAGTAAGAGGTCCGTGC
RP11-728E14  GAGTGTTCCTGACGCACAGCAGTTGCGCAGTCCCAGTTTACTGGGGTTGGAAAGCGTGTGTGGCAGTAAGAGGTCCGTGC
Cons         ************ ***************** * ********************************************

111_Genomic  AAGGNGGTATGGGGTCAGAACAGCCTCTGTGGGGCCCCGCTCGCNACCNTCTAGCTATGGAGAGCCTGAGTCTCCTCACT
112_Genomic  AAAGCGGTATGGGGTCAGAACAGCCTCTGTGGGGCCCCGCTCGCTACCGTCTAGCTGTGGGGTGCCTGAGTCTCCTCACT
RP11-437N10  AAGGCGGTATGGGGTCAGAACAGCCTCTGTGGGGCCCCGCTCGCTACCGTCTAGCTATGGAGAGCCTGAGTCTCCTCACT
RP11-728E14  AAAGCGGTATGGGGTCAGAACAGCCTCTGTGGGGCCCCGCTCGCTACCGTCTAGCTGTGGGGTGCCTGAGTCTCCTCACT
Cons         ** *:*****************************************:***:****** *** *  ****************
```

The flanking 5' and 3' UTR regions of *KCNJ12* and *KCNJ18* were characterized by Rapid Amplification of cDNA Ends (RACE), using the unique nucleotides at the 3'-end of the primers from the coding sequence as the gene specific primers. Despite the high homology, unique upstream sequences were noted in RACE clones in the 5' UTR. Sequencing of the BACs revealed a unique exon 1 for each gene. We obtained the Kir2.6 cDNA from a human testis cDNA pool using specific outer primers designed from the RACE clone sequences. The forward primer was taken from the unique exon 1 sequence and the reverse from the 3' UTR. Each of the DNA sequence variants found in the *KCNJ18* BAC clone that differ from *KCNJ12* are also present in the full-length *KCNJ18* cDNA, establishing it as an independent transcript. This transcript was also amplified from pooled human brain and skeletal muscle cDNA. For both genes, exon 3 contains the entire coding region, (Figure 4A).

Probes for the unique exon 1 of *KCNJ12* and *KCNJ18* were used for northern blot analysis. Both transcripts are highly expressed in skeletal muscle (Figure 7A-C) and the transcript sizes differ (~2.2 Kb for *KCNJ12*, ~6 Kb for *KCNJ18*).

Figure 7. Expression pattern and transcriptional regulation of KCNJ18.

The A1 probe set (Figure 5A) was used to specifically probe multiple tissue Northern blot membranes for **A.** *KCNJ18* and **B.** *KCNJ12* mRNAs, which are found specifically in skeletal muscle. **C.** β-Actin was used as a loading control. **D.** The *KCNJ18* regulatory region can function as an enhancer for luciferase expression in HEK293T and either proliferating or differentiated C2C12 cells. A DR4 positive control, an empty vector control, and a mutated *KCNJ18* TRE control were also tested. Luciferase expression by the WT *KCNJ18* is enhanced in a T3-dose dependent manner from 0nM T3 (hypothyroid) through 200nM (hyperthyroid) T3 after compensating for the internal renilla control.
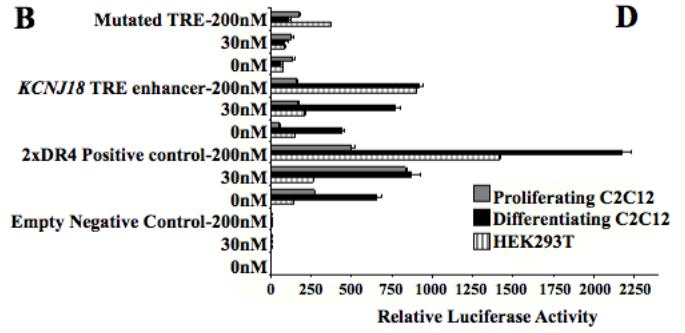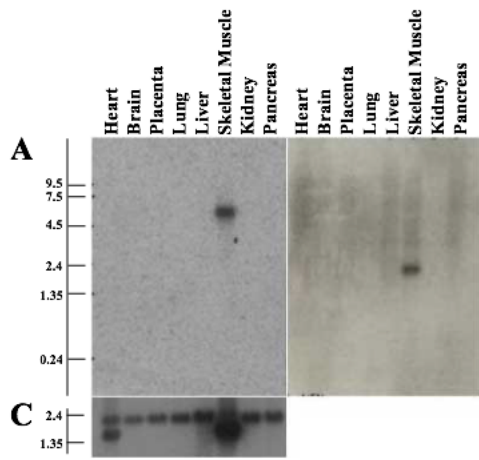
Triiodothyronine (T3) enhances *KCNJ18* transcription

We tested whether *KCNJ18* transcription is regulated by T3 since there is a putative TRE (in reverse strand) between nucleotides -265 and -249 (5'-TGACCTGGCCTcACCTCAGGG-3'), which differs from the consensus TRE by only 1 base pair (c). This is a direct motif repeat with a 4-nucleotide link (DR4). A luciferase assay in mammalian cells over-expressing thyroid hormone (TR) and retinoid X receptors (RXR) was used to determine if this TRE motif is functional. Mouse skeletal muscle myoblasts (C2C12) or human embryonic kidney cells (293T) were transfected with reporter constructs containing the *KCNJ18*/TRE-pGL3 wild-type (WT), negative controls consisting of mutant (Mut) or empty pGL3 vector (Emp), and positive control (2xDR4-pGL3). The WT construct produced high luciferase activity compared to controls and responded in a dose-dependent fashion to T3. However, the truncated Mut construct produced only 25% and 7% as much luciferase activity as WT in 293T and C2C12 cells, respectively (Figure 7D). These results corroborate our data from an electrophoretic mobility shift assay with nuclear extracts from a pool of TR-transfected 293T cells (data not shown).

Mutational analysis of *KCNJ18* in TPP patients

The *KCNJ18* coding region was specifically amplified and sequenced in 30 TPP patients collected from U.S., Brazil, and France. Five mutations were found. Two C-to-T transitions, c.C1195T (R399X) and c.C1219T (Q407X), were identified in 1 and 5 affected individuals, respectively. Missense mutations

78

c.C1061T (T354M) and c.A1097G (K366R) were identified in a single patient each. Two further patients, both from France, presented with both a T140M mutation and a single nucleotide deletion (c.428delC) leading to a frame-shift with a stop codon at position 151 (I144fs). The T140M mutation appears alongside the I144fs mutation, which is the likely causative change. These mutated residues are well conserved in Kir2 channels (Figure 8). None were found in 281 healthy controls (137 Caucasians, 48 Mexicans, 45 African Americans, 43 Chinese, and 8 Japanese-Brazilians). Since TPP is highly prevalent in Asian thyrotoxic patients, we sequenced *KCNJ18* in TPP patients from Hong Kong, Thailand, and Singapore. One of 83 TPP subjects from Hong Kong harbored a mutation (R205H), none of 31 Thai subjects harbored mutations, and 7 of 27 Singaporean subjects harbor mutations (all R399X). R399X was found in 1 of 76 Singaporean control samples, as expected from the prevalence of TPP among thyrotoxic individuals. No mutations were found in 98 Hong Kong thyrotoxic controls not manifesting TPP. Results are summarized in Table 4 and the mutation positions within Kir2.6 are indicated in Figure 4C.

Figure 8. Kir 2.6 mutations found in our TPP cohort and their conservation across species.

A total of six mutations were found in our cohort of TPP patients. Chromatograms from mutations with R205H, T354M, K366R, R399X, Q407X, and I144fs (versus wild-type) are shown. The missense mutations (R205H, T354M, and K366R) are at residues that are well conserved both among human Kir2 family members as well as across other species (position of the mutation is underlined).

	R205H	T354M	K366R
Mutant			
Kir2.6 Human	VALRDGK	VPSTPRC	VENKFLL
Kir2.2 Human	VALRDGK	VPSTPRC	VENKFLL
Kir2.1 Human	IAMRDGK	VPNTPLC	AEKKYIL
Kir2.3 Human	ISVRDGK	VAGTPCC	QESKITV
Kir2.4 Human	VALRDHR	VPGTPVC	---KSSF
Kir2.2 Cavia	VALRDGK	VPSTPRC	VENKFLL
Kir2.2 Mus	VALRDGK	VPSTPRC	VENKFLL
Kir2.2 Bos	VALRDGK	VPSTPRC	VENKFLL
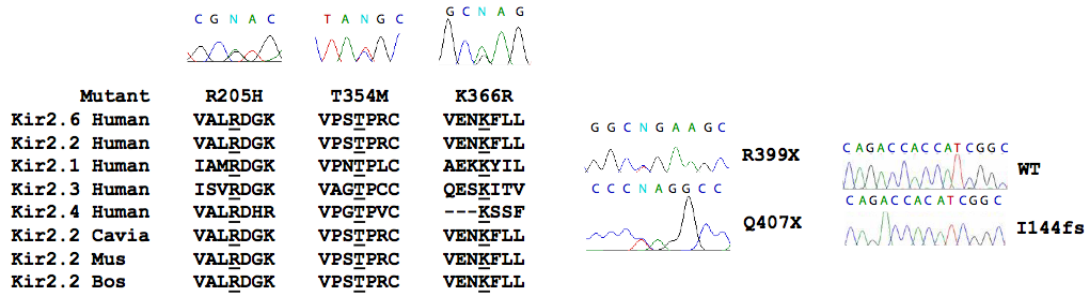
Table 4. Summary of TPP patients with or without associated KCNJ18 mutation.

	Caucasian/ Brazilian	Singapore	Hong Kong	Thailand
Mutation (+)	10[*]	7[*]	1	0
No Mutation (-)	20	20	82	31
Total	30	27	83	31
Percent	33.3%	25.9%	1.2%	0%

* p < 0.05, Fisher's exact test versus matched ethnic controls

Electrophysiology of WT and mutant Kir2.6

Kir2.6 channels were fused to EGFP (N-terminal for mutant and both C-terminal and N-terminal for WT) and expressed in 293T cells. Whole-cell recordings of WT expressing cells indicate that Kir2.6 produces typical inwardly rectifying currents (Figure 9A). This inward rectification is vital for the proper function of skeletal muscle as it allows potassium current around the resting membrane potential but not during action potentials. Normalizing currents to that produced at -60mV allows comparison of rectification, which is unaffected by any of the TPP mutations (Figure 9B). Some of the mutations alter current density (Figure 9C-D). The I144fs mutation results in a complete loss of current while the T354M mutation causes a small decrease in current density. Cotransfection of the I144fs mutation with WT channels (fused to the C-terminus of EYFP) indicates that I144fs does not exert a dominant negative effect (Figure 10).

Kir2.2 has a single channel conductance of 30-34pS and a high open probability (P_o) (Takahashi et al., 1994; Preisig-Muller et al., 2002). Kir2.6 has identical single channel characteristics, with a conductance of approximately 34pS and a P_o of ~80% (Figure 11A-C).

Figure 9. KCNJ18 encodes an inwardly rectifying potassium channel whose conductance properties are altered by some TPP mutations.

A. When expressed in 293T cells, Kir2.6 produces stereotypical Kir currents. Voltage steps were performed from the resting membrane potential (0mV driving force) to between -60 and +60mV in increments of 10mV. **B.** Normalization of these values to maximal current allows for comparison of rectification between WT and mutant channels. TPP mutations do not lead to altered rectification. **C.** Current density can instead be measured by normalizing currents to cellular capacitance. **D.** Both the I144fs and T354M mutation lead to decreased current density, most easily seen at -60mV. P-values calculated with a T-test versus EGFP-Kir2.6 WT. 5-12 cells per data point.

A

Current (nA)

Time (ms)

B

Driving Force (mV)

Normalized Current

- ▼ EGFP-Kir 2.6
- ● Kir 2.6 WT-EGFP
- ✴ EGFP-Kir 2.6 R205H
- ✕ EGFP-Kir 2.6 T354M
- ■ EGFP-Kir 2.6 K366R
- ▲ EGFP-Kir 2.6 R399X
- ⋈ EGFP-Kir 2.6 Q407X

C

Driving Force (mV)

Current Density (pA/pF)

- ▼ EGFP-Kir 2.6
- ● Kir 2.6 WT-EGFP
- ♦ EGFP-Kir2.6 I144fs
- ✴ EGFP-Kir2.6 R205H
- ✕ EGFP-Kir2.6 T354M
- ■ EGFP-Kir2.6 K366R
- ▲ EGFP-Kir2.6 R399X
- ⋈ EGFP-Kir2.6 Q407X
- ○ Untransfected

D

EGFP-Kir 2.6 WT
Kir 2.6 WT-EGFP
EGFP-Kir 2.6 I144fs   ***
EGFP-Kir 2.6 R205H
EGFP-Kir 2.6 T354M   *
EGFP-Kir 2.6 K366R
EGFP-Kir 2.6 R399X
EGFP-Kir 2.6 Q407X
Untransfected   ***

pA/pF

Figure 10. The I144fs mutation does not act in a dominant negative manner.

Wild-type (black squares) channels were expressed in HEK293 cells at half their normal levels with or without an equivalent amount of I144fs mutant (red circles for WT + I144fs). Voltage steps indicate that the wild-type current is unaffected by coexpression of the I144fs (wild-type=-471.074±123.65pA/pF and cotransfected=-402.898±62.69pA/pF at -60mV).

EYFP-Kir2.6 WT
EYFP-Kir2.6 WT + EGFP-Kir2.6 I144fs
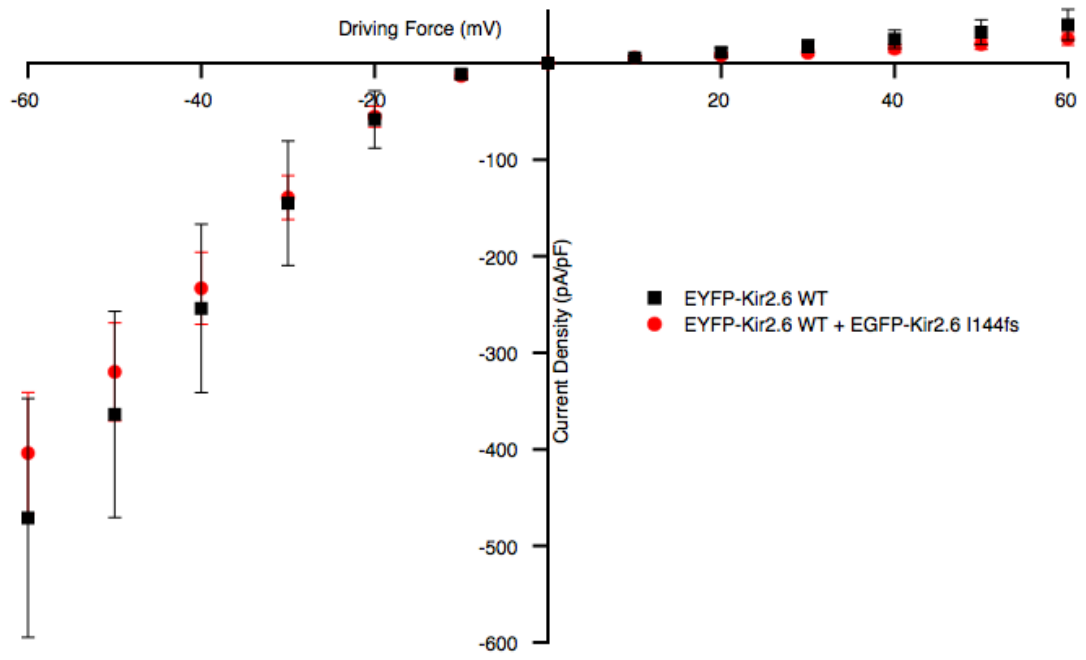
Figure 11. TPP mutations in Kir2.6 alter single channel response to PKC.

A. Kir2.6 produces stereotypical single channel currents. Scale bars: 200ms by 2pA. Openings (O) are down and closings (C) are up. **B.** Wild-type and mutant single channel conductance is unaltered by PKC activation or mimicking constitutive phosphorylation at T354 (T354E). **C.** Open probability, however, is decreased in WT but not T354M mutant channels by the activation of PKC or T354E. P-values using a T-test versus EGFP-Kir2.6 WT. 5-9 patches per data point, each with 1-3 (typically 2 or 3) channels.

A

C

O

B

Driving Force (mV)

-120   -100   -80   -60   -40   -20

Single Channel Conductance (pA)

-1

-2

-3

-4

● EGFP-Kir 2.6
■ EGFP-Kir 2.6 T354M
▲ EGFP-Kir 2.6 T354E
▼ EGFP-Kir 2.6 T354M + PMA
⋈ EGFP-Kir 2.6 + PMA

C

1.0

0.8

0.6

Open Channel Probability

0.4

0.2

0.0

● Kir 2.6 WT
■ Kir 2.6 T354M
▲ Kir 2.6 T354E
▼ Kir 2.6 T354M + PMA
⋈ Kir 2.6 WT + PMA

***   ***   ***   ***   ***

-120   -100   -80   -60   -40   -20

Driving Force (mV)
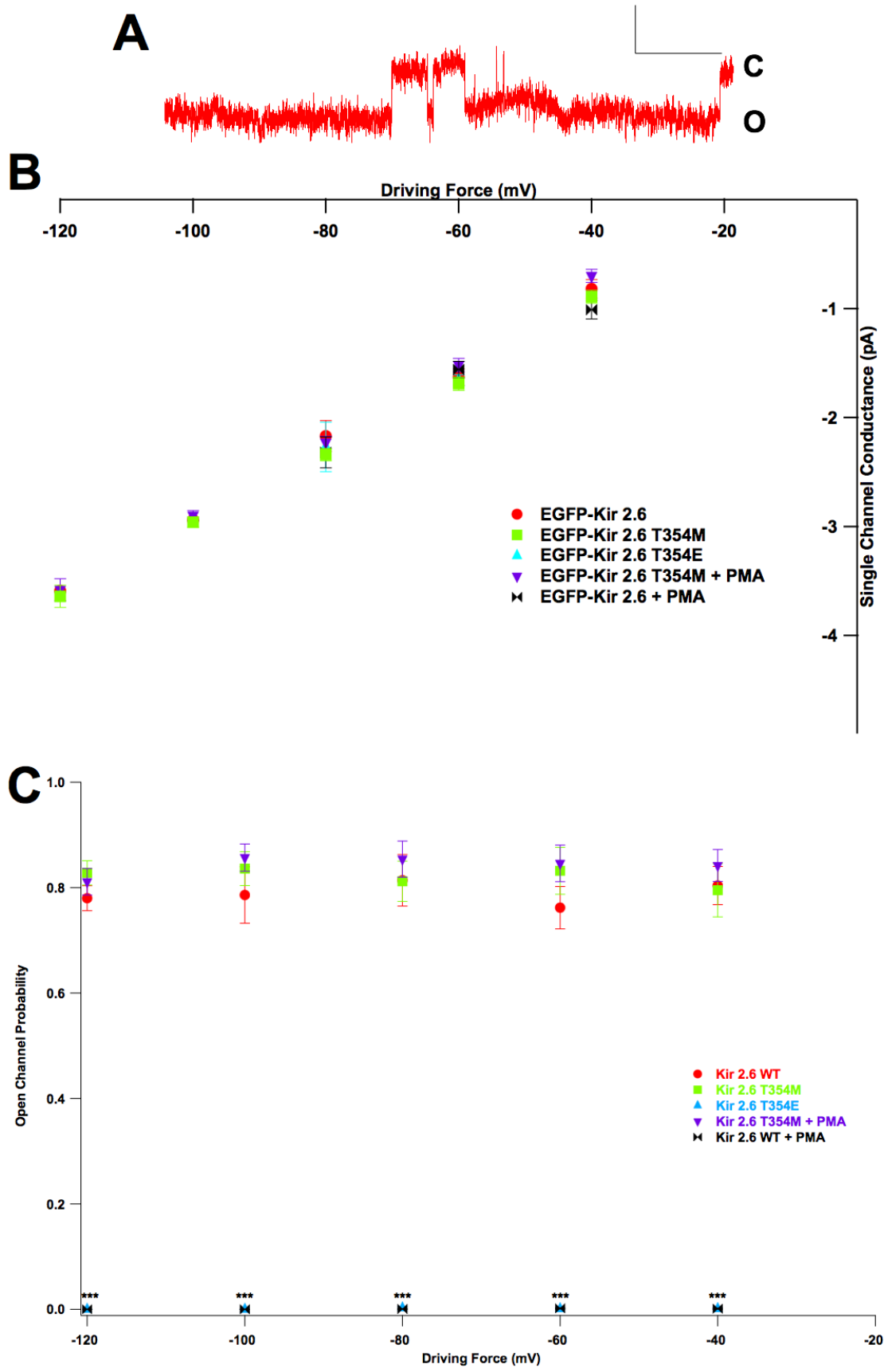
PKC activation, which is increased during thyrotoxicosis, results in decreased Kir2.2 whole-cell currents, and threonine 354 is involved in this process (Karle et al., 2002). As the equivalent Kir2.6 residue is mutated in one TPP patient, we tested whether phosphorylation of this residue alters single channel characteristics and if the T354M mutation abrogates these alterations. The single channel conductance and P_o of the T354M mutant are identical to WT Kir2.6 channels (Figure 11B-C). Activating PKC with phorbol 12-myristate 13-acetate (PMA) does not seem to alter the single channel conductance of either the mutant T354M (35.7±0.85pS with PMA vs. 33.8±0.89pS without) or WT channels (32.8±3.0pS with PMA vs. 34.2±0.9pS without, Figure 11B). However, while PKC activation does not alter the P_o of mutant channels, it nearly abolishes that of WT channels (WT: 78.9±0.9%, WT + PMA: 0.00069±0.00033%, T354M: 82.1±0.8%, T354M + PMA: 84.2±0.8% average across voltages, Figure 11C). Similarly, mimicking pseudo-constitutive phosphorylation of this residue (T354E) results in unaltered single channel conductance (30.5±0.17pS) and a decreased P_o (0.00093±0.00048%).

Kir channel interactions with phosphatidylinositol-(4,5) bisphosphate (PIP_2) occur via positively charged residues in the C-termini and are required for the opening of mammalian Kir channels. Mutation of such residues in Kir2.1 leads to ATS (Donaldson et al., 2003). PIP_2 turnover is increased during thyrotoxicosis and we hypothesized that the R205H and K366R mutations may alter interactions with PIP_2 (Kavok et al., 2001). We artificially decreased the availability of membrane PIP_2 with polylysine and measured the time for channel

openings to decrease, as measured by the T_{50} time constant. Both the R205H

and K366R mutations cause an ~1.5-fold increase in T_{50}, (WT: T_{50} 38.98±0.016s,

base 0.85±5.08e-4, A 7.82±1.68e-3; R205H: T_{50} 55.34±0.016s, base 0±3.78e-4,

A 6.0±7.88e-4; K366R: T_{50} 58.47±0.024s, base 1.02±8.13e-4, A 8.92±1.56e-3;

Figure 12A-D, p<0.001 according to Figure 13). This increase in T_{50} indicates

that mutant channels may produce more current than WT channels during

thyrotoxicosis when PIP_2 turnover is increased.

Figure 12. Kir2.6-PIP2 interactions are altered by TPP mutations.

Inside-out patches were perfused with isotonic solution for 40 seconds prior to perfusion with polylysine. **A.** Wild-type, **B.** R205H, and **C.** K366R openings decreased following polylysine perfusion. **D.** Curve fits of idealized channel openings (smooth black curves in A-C), were used to derive the T_{50} value. Both the R205H and the K366R mutant channels have an altered interaction with PIP_2 and take significantly longer to reach half-maximal opening than WT channels. 5-10 cells and 9-20 total channels per channel type. P<<0.001 in accordance to a statistical model, Figure 13.
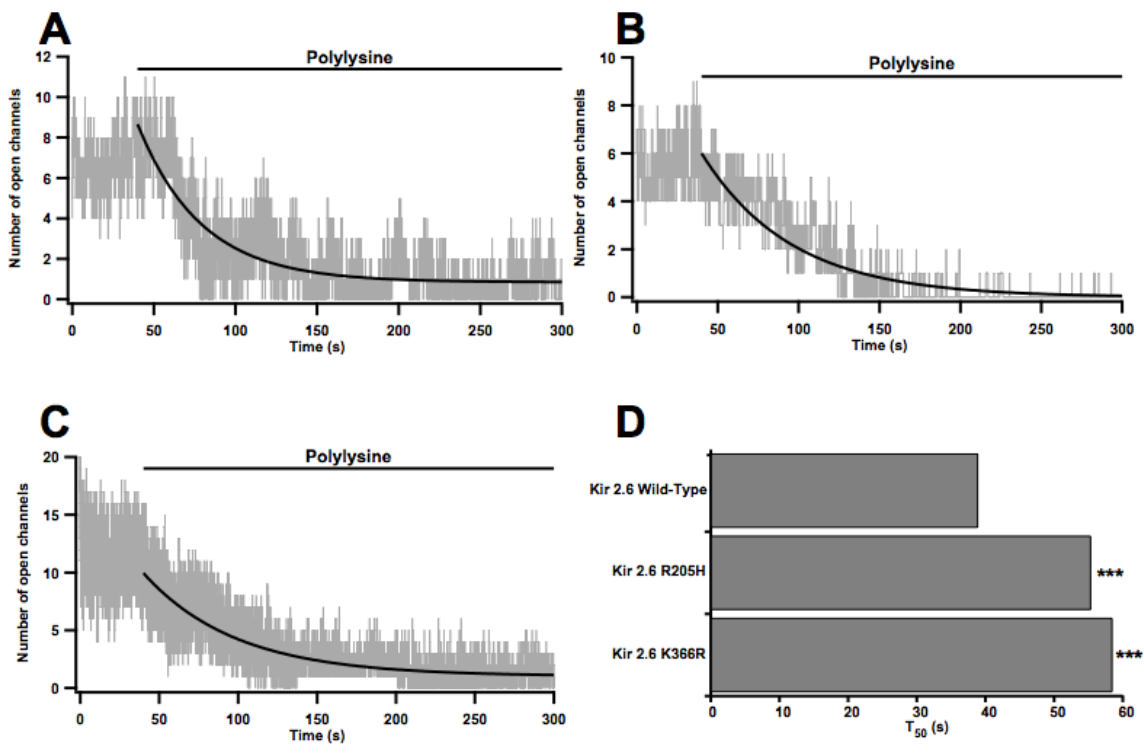
Figure 13. Statistical modeling of ion channel PIP2 interactions indicates robustness of T50 estimations.

Individual idealized ion channel open and closed states were simulated in accordance to fit parameters from Figure 12. Open state dwell times were randomly selected from an exponential distribution with mean 220ms. Closed state dwell times were randomly selected from a similar distribution whose mean was altered over time such that the mean open probability would follow the curve fit from Figure 12. Initial open probability for each channel type was also taken from Figure 12 (0.65 for wild-type, 0.55 for R205H mutant, or 0.49 for K366R mutant). For each run, 11 (wild-type, A), 9 (R205H mutant, B) or 19 (K366R mutant, C), idealized openings were summed and fit with an exponential function as in Figure 12. Simulations were sampled at either 1kHz or 50kHz and the values derived from their fit stored and displayed as a histogram (D, light bars are 1kHz simulations and dark bars are 50kHz simulations). 1000 (1kHz sampling) or 100 (50kHz sampling) runs of each simulation were performed for each channel. The resulting T_{50} values have means 39.82±0.07s or 39.65±0.20s (Wild-type sampling 1kHz or 50kHz, respectively), 55.96±0.13s or 55.58±0.34s (R205H mutant 1kHz or 50kHz sampling, respectively), and 59.67±0.11s or 58.63±0.40s (K366R mutant 1kHz or 50kHz sampling, respectively). Simulations were run in Igor Pro (Wavemetrics). Similar results are seen if dwell times are chosen from Gaussian or gamma distributions (not shown).
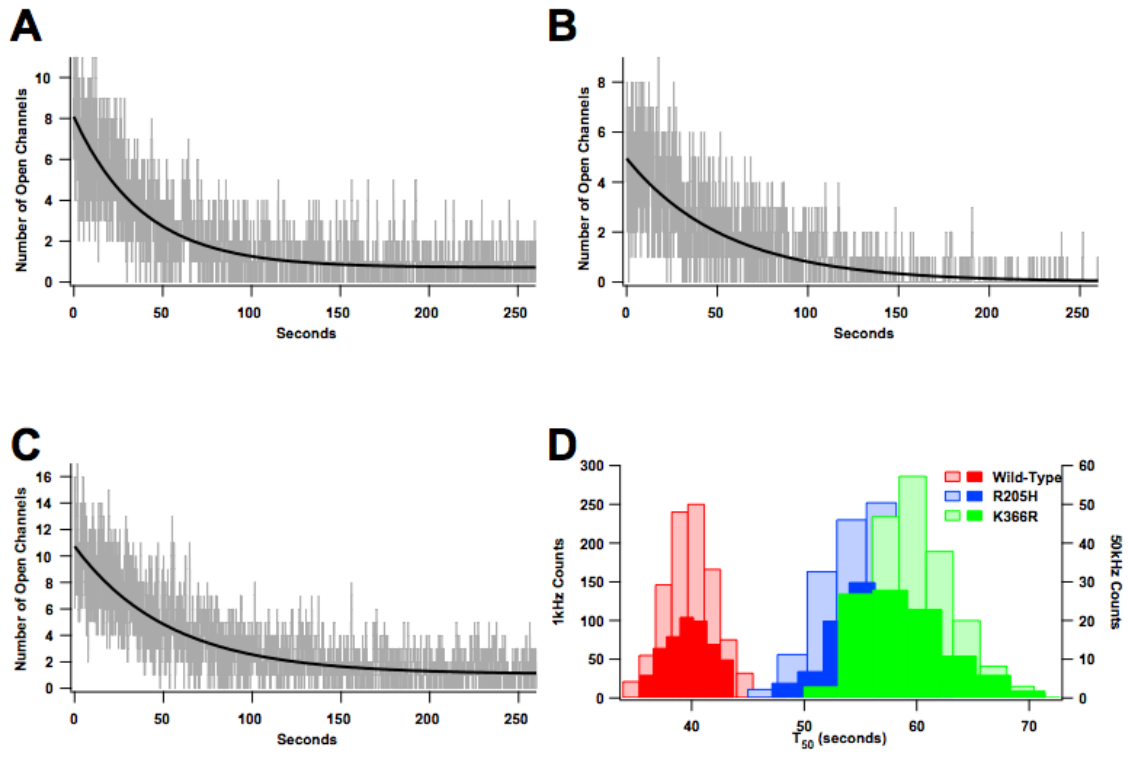
Discussion

Genomic context of *KCNJ18*

We have identified *KCNJ18* as a paralog of *KCNJ12* sharing up to 99% identity in coding sequence and having largely similar UTR and intron sequences. Because of this remarkable similarity, amplification of *KCNJ12* for sequencing inadvertently amplified *KCNJ18*; sequence differences were previously interpreted as heterozygosity for polymorphic alleles for a single gene (*KCNJ12*), though we now present evidence for two unique genes. Duplicated regions are enriched in or around sequence gaps, such as that containing *KCNJ18*, and are known to be difficult to recognize (Bailey et al., 2001; Eichler et al., 2004). It has been estimated that over 5% of the human genome is composed of duplicons, large regions (1 to over 100 Kb) of duplicated sequence sharing high (>90%) identity (Bailey et al., 2001). Such regions are thought to result from inter- or intra-chromosomal segmental duplication, with the latter involving DNA flanking pericentromeric regions.

KCNJ18 is not the first paralog of *KCNJ12* to be reported. *KCNJ17* (Kir2.5) has 95% identity to *KCNJ12* but the GYG selectivity filter is changed to SYG, rendering it non-functional (Namba et al., 1996). We verified that *KCNJ17* is a third paralog using gene-specific primers to amplify it from control and patient DNA along with *KCNJ12* and *KCNJ18*.

The exact positions of *KCNJ18* and *KCNJ17* remain unclear. Although a BAC containing *KCNJ17* has not been found, both RP11-437N10 (containing

KCNJ18) and RP11-728e14 (containing *KCNJ12*) have been mapped to 17p11.1-2. *KCNJ12* and *KCNJ17* were originally localized to 17p11.1 by FISH (Hugnot et al., 1997; Namba et al., 1997). According to the BAC sequences, we localize *KCNJ12* and *KCNJ18* to this pericentromeric region. Although pericentromeric duplications are thought to contain heterochromatic DNA and have fewer expressed genes, we have presented several lines of evidence suggesting that *KCNJ18* is transcribed and functional and that the BAC containing it is distinct.

Regulation of Kir2.6 expression

Protein regulation by thyroid hormones is complex, occurring both by transcriptional and post-translational events (Bassett et al., 2003). Transcriptional regulation is particularly important in skeletal muscle, where both decreased (hypothyroidism) and increased (thyrotoxicosis) T3 has a profound effect on muscle performance. Some channels, such as Kv1.5 and Kv4.2, are known to be transcriptionally regulated by T3, while T3 regulation of Kir transcription has received little attention (Le Bouter et al., 2003). To determine the feasibility of T3 altered transcription, we searched for putative thyroid response elements (TRE) in the regulatory region of these genes using the publicly available TESS-TRANSFAC v6.0 software (http://www.cbil.upenn.edu/tess). Based on 2-Kb of sequence 5'-upstream of *KCNJ18*, we identified four putative TREs with Lq scores of 0.9 to 1 (best is 1), with mismatch allowance of 10%. Of these, only a single predicted TRE of the DR4 variety had a high score. A similar search of the regulatory region of *KCNJ12* identified no putative TREs.

To add credence to these predictions, we found that TRβ-T3 complexes bind to these TRE-*KCNJ18* sequences. Luciferase assay results show that the regulatory region of *KCNJ18* confers dose-dependent T3 transcriptional modulation (Figure 7) in HEK293 and differentiated C2C12 cells.

Possible role of Kir2.6

Multiple tissue northern blotting revealed a skeletal muscle-specific pattern of both Kir2.2 and Kir2.6 expression. To prevent nonspecific detection of similar transcripts, we performed these blots by probing against the unique exon 1. Earlier expression studies in human (heart only) and mouse (multiple tissues) suggest that Kir2.2 is expressed abundantly in many tissues including heart, skeletal muscle, and neurons (Takahashi et al., 1994; Wible et al., 1995). However, the probes used in these experiments were designed against the coding region of Kir2.2 (exon 3), which shares high identity with the other members of the Kir2 family. Thus, it is likely that probes used in previous reports were nonspecific for Kir2.2. These blots using human atrium and multiple mouse tissues revealed bands of multiple sizes. As shown in Figure 5, our probes detected single transcripts of 6 and 2.2 Kb. This difference in transcript size between *KCNJ12* and *KCNJ18*, as well as non-specific detection of other Kir channels, may explain the previously observed pattern that has been interpreted as variable UTR extension. Sequences identified through RACE are shorter than bands of 6 and 2.2Kb detected on northern blot. Thus, there may be additional, unrecognized non-coding exons.

Kir2.6 shares 96-99% amino acid identity with Kir2.2 (depending on the SNPs present) and high homology of introns (>95%). Kir2.2 is a member of the strong inward rectifier subfamily (Takahashi et al., 1994; Preisig-Muller et al., 2002). It is thought that Kir2s maintain the resting membrane potential in excitable cells (Takahashi et al., 1994; Wible et al., 1995). Kir2.1 and Kir2.2 share over 70% identity at the amino acid level, overlap in expression, and may co-assemble, leading to the repolarizing I_{k1} current in mouse heart (Zaritsky et al., 2000; Zaritsky et al., 2001; Preisig-Muller et al., 2002; Zobel et al., 2003). While the role of Kir2 channels in skeletal muscle has received much less attention, it appears largely similar to that in cardiac myocytes. Increased or decreased ion channel transcription during thyrotoxicosis may cause drastic changes in resting membrane potential and potassium accumulation and can lead to weakness in otherwise normal patients. We propose that Kir2.6 levels are increased during thyrotoxicosis to aid in proper membrane potential maintenance, warding off more severe weakness.

Mutations in Kir2.6 cause susceptibility to TPP

We have found a total of 6 mutations in Kir2.6 associated with TPP. These mutations are largely localized in the channel's intracellular C-terminus with a single frame-shift truncation mutation in the pore-region. These mutations account for up to 33% of patients in the USA/Brazil/France group, indicating that other TPP genes exist. Kir2.6 mutations were identified in ~25% of Singaporean patients (7/27) but in only 1/83 patients from Hong Kong and 0/31 Thai patients. Thus, there are unique genetic contributions to TPP in different ethnic

populations. Genetic complexity is not surprising given the complex affect of thyroid hormones on both transcription and post-translational modification. These differences in mutation frequency between Asian populations are likely due to genetic heterogeneity between and (as for the Chinese population) within Asian populations.

Inward rectification is one of the most important properties of Kir channels, allowing for asymmetrically large current at hyperpolarized potentials. Rectification is caused by a voltage-dependent conduction-pore blockage by intracellular polyamines and Mg^{2+} (Lu, 2004). A potential gradient across the cell membrane removes this blockage during hyperpolarization but allow these polyvalent cations to occlude the ion-conducting pore during depolarizations. Rectification is important for setting the resting potential and aiding in repolarization of cells while not shunting current during depolarizations. We showed that none of the TPP mutations alter Kir2.6 rectification (Figure 9B).

The I144fs mutation results in a stop codon in the pore region and completely non-functional channels (Figure 9C-D). Truncated subunits lack the entire C-terminus and M2 membrane-spanning helix. The M2 helix lines a portion of the ion-conducting pore and is involved in inter-subunit coupling. The C-terminus is involved in both gating and inter-subunit assembly (Tinker et al., 1996; Soom et al., 2001). Co-expression studies showed that the I144fs mutation does not co-assemble with WT subunits (Figure 10), presumably leading to the TPP phenotype through haploinsufficiency (Figure 14).

Figure 14. Model of TPP pathophysiology.

Amorphic and antimorphic alleles would cause decreased K^+ currents leading to depolarization and gradual transitioning of voltage-gated channels to their inactivated states. Hypermorphic alleles, causing hyperpolarization, conversely, would cause difficulty reaching threshold. These opposite shifts in membrane excitability, when coupled with a stressor event, are both predicted to lead to the weakness and paralysis observed in TPP. How the genomic and non-genomic effects of thyrotoxicosis on other ion channels interact with these proposed Kir current alterations remains to be elucidated.
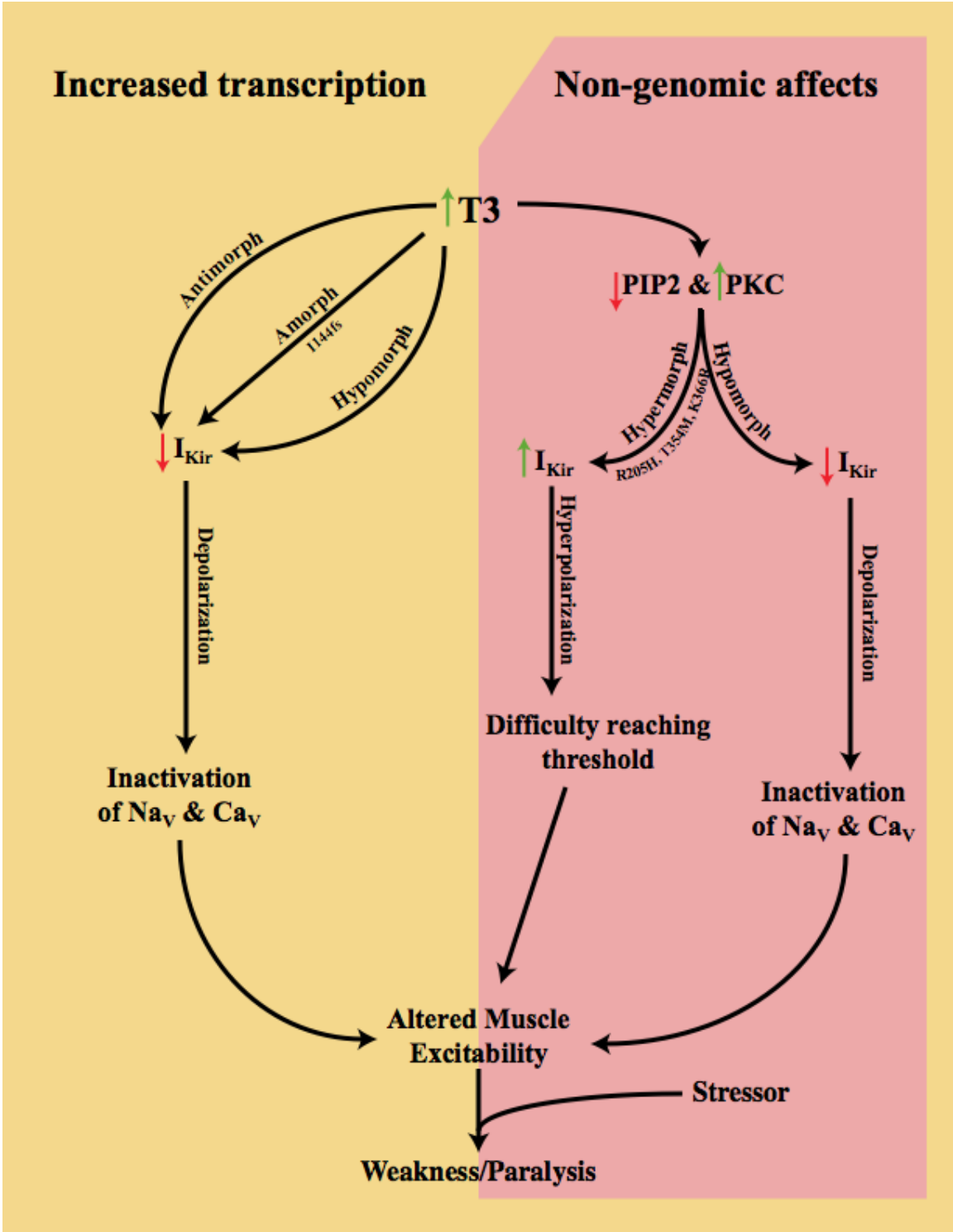
The T354M mutation also leads to a small decrease in overall whole-cell current (Figure 9C) that is attributable to alterations of neither conductance nor open channel probability (Figure 11C-D). Whether this small change is physiologically relevant is unclear. We found that Kir2.6 single channel conductance is unaltered by PKC activation while P_o is decreased dramatically in WT but not T354M channels (Figure 11B-C). The T354E mutation has properties identical to WT channels in the presence of activated PKC, indicating that phosphorylation of T354 causes current decrease by changing open probability. These data demonstrate that PKC activation leads to closure of WT channels but not T354M mutant channels. Such changes in PKC activity are expected during thyrotoxicosis and may result in weakness in the presence of the T354M hypermorphic mutation (Figure 14).

PKC is activated during thyrotoxicosis due to increased PIP_2 turnover (Lin et al., 1999; Kavok et al., 2001). Kir channels interact directly with PIP_2 in the membrane during normal gating, suggesting that currents are decreased during thyrotoxicosis by a decreased ability to open. This protein-lipid interaction occurs at a number of positively charged residues in the C-terminus. In ATS, a number of these residues are mutated and result in decreased PIP_2 affinity (Lopes et al., 2002). Two TPP mutations, R205H and K366R, occur in positively charged residues in the C-terminus and may alter PIP_2 affinity. Inside-out patches containing mutant or WT channels were perfused with polylysine to screen membrane charges and disrupt protein-lipid interactions (Lopes et al., 2002). We

found that the time required for half maximal current degradation for both of the mutants is significantly longer than that of WT channels (Figure 12D), suggesting that these are hypermorphic mutations (Figure 14).

The disease causing affects of two TPP associated mutations (R399X and Q407X) have not yet been fully elucidated. Both of these mutations are located at the very C-terminus of the channel and result in the absence of a putative PDZ interacting domain important for proper sub-cellular localization of Kir2.2 in skeletal muscle (Leonoudakis et al., 2004a; Leonoudakis et al., 2004b). We found that these mutant channels are functional in 293T cells and localize to the membrane in both these and C2C12 cells. However, mutant channels may either have improper trafficking or localization in native skeletal muscle. Such changes likely result in decreased or misplaced Kir2.6 currents, possibly in a dominant negative fashion. Ongoing experiments are aimed at addressing these questions.

We present a previously unreported paralog of Kir2.2 that encodes a strong inwardly rectifying potassium channel, Kir2.6, sharing up to 99% amino acid identity. As mutations in other ion channels are known to cause familial periodic paralysis, we screened this and other ion channels for mutations. We present genetic and electrophysiological evidence that mutations in Kir2.6 underlie TPP in a significant portion of patients. These mutations likely lead to paralysis only during thyrotoxicosis because Kir2.6 levels are increased by these conditions, non-genomic effects of T3 alter post-translational modifications, and muscle membrane potential is already metabolically stressed by changes in many other ionic currents. Further functional characterization will determine the

affects of the remainder of TPP associated mutations and whether mutant channels can co-assemble with other WT Kir subunits with physiologically relevant effects. Homologs of ion channel genes identified as the cause of familial periodic paralysis were later shown to cause cardiac arrhythmias including long-QT syndrome. It is therefore interesting to speculate that the atrial fibrillation frequently seen in thyrotoxic patients may be due, in part, to both genomic and non-genomic affects of thyroid hormones on inward rectifiers and other channels expressed in the heart.

Experimental Procedures

Identification of patients with TPP

We collected DNA and clinical data on unrelated index patients. TPP was diagnosed in patients with episodic flaccid paralysis, hypokalemia during at least one of the attacks, and altered thyroid function tests. Written consent was obtained from all subjects in compliance with the Institutional Review Boards and Ethics committees at the University of California at San Francisco, the Federal University of Sao Paulo, the University of Hong Kong, Groupe Hospitalier-Pitié-Salpêtrière, Ramathibodi Hospital, Singapore General Hospital, National University Hospital (Singapore), and the National Neuroscience Institute (Singapore). Ethnicity of both patients and controls was determined by self-report.

We confirmed the diagnosis of thyrotoxicosis through the findings of suppressed TSH and elevated free T4 and/or total T3, measured by an immunofluorimetric method (Delphia-Wallac, Finland); TSH-receptor antibodies

(TRAb) by a radioassay (BRAHMS, Germany); and anti-thyroid peroxidase and anti-thyroglobulin antibodies by radioimmunoassays (BRAHMS, Germany). Potassium was measured via ion-specific electrode (normal is between 3.5 and 5.0 mmol/L). Clinical results from select patients are summarized in Table 5.

Table 5. Clinical and lab findings of select TPP patients with Kir2.6 mutations

| Patient | Sex | Ethnicity | Age of Onset | Diagnosis of periodic paralysis | | | | Diagnosis of thyrotoxicosis | | | | Potassium Normal: 3.5-5 mmol/L | TSH Normal: 0.5-4.5 mIU/mL | T-T3 Normal: 70-200 ng/dL | T-T4 Normal: 4.5-12 ug/dL | F-T4 Normal: 0.8-1.5 ng/dL |
N (mutation)				Pattern	Tendon Reflexn	Duration	Period	Precipitating Factor	Goiter	Weight Loss	Tremor	Tachycardia					
2537 (Q407X)	M	Hispanic	28	Paraplegia	Hyperreflex	1h	Night	No	No	Yes	Yes	Yes	-	-	998	19	-
7348 (Q407X)	M	Caucasian	26	Quadriplegia	Areflex	12-24h	Day	No	Yes	Yes	Yes	Yes	3.2	-	445	26	>6
7162 (R399X)	M	Mixed	19	Paraplegia	Areflex	2h	Night	AE	Yes	Yes	Yes	Yes	2.7	<0.05	-	-	>6
7950 (Q407X)	M	Caucasian	22	Paraplegia	Areflex	4h	Night	AE	Yes	Yes	No	Yes	2	<0.05	-	-	6.7
7955 (Q407X)	M	Japanese	23	Paraplegia	Hyporeflex	6h	Night	No	Yes	Yes	No	Yes	1.5	<0.05	-	-	4.4
7656 (Q407X)	M	Mixed	44	Quadriplegia	N/A	2-4h	Night	No	Yes	Yes	Yes	Yes	2	<0.05	-	-	>6
9664 (R399R)	M	Caucasian	26	Paraplegia	Hyporeflex	4h	N/A	AM	No	Yes	No	No	1.7	<0.05	-	-	0.75
9665 (T354M)	M	Black	23	Quadriplegia	Hyporeflex	6h	Night	No	Yes	Yes	Yes	Yes	-	<0.05	-	-	9.4

The Brazilian population contains an extensive mixture of Europeans, Africans, and Native-Americans.

Low stringency PCR

Genomic DNA was extracted from leucocytes using PUREGENE DNA isolation blood kits (GENTRA Systems; Minneapolis, MN). PCR primers were designed against the GenBank Accession NM_021012 sequence with the forward primer containing two nucleotide mismatches to favor amplification of diverse products. Briefly, a standard outer PCR reaction (primers: TGGTGTCGTCTCTGTTCC/CTGGGCCCGTTCTGCTC) was performed employing 100-200ng of genomic DNA in 50μL containing 90% Platinum PCR SuperMix (Invitrogen; Carlsbad, CA). Cycling conditions were as follows: 5 min at 94°C followed by 38 cycles of 20 sec at 94°C, a low stringency annealing step of 30 sec at 56°C, and an extension step of 2 min at 72°C.

We performed nested PCR of Kir2.2 using 20 ng of outer PCR product in 50μL containing 10 mM Tris-HCl (pH 9 at 25°C), 50 mM KCl, 0.1% Triton X-100, 200 μM each dNTP, 1.5 mM MgCl2, 1 U Taq DNA polymerase and 25 pmol of forward and reverse primers (CGAGGAGGGCGAGTACATC/CAAGATGGTGATGGGCG) under the following conditions: 5 cycles at 66°C for 30 sec and 72°C for 1 minute, plus 30 cycles at 64°C for 30 sec and 72°C for 1 minute, each cycle preceded by a 94°C step. Resulting products were subcloned into pCR2.1 (Invitrogen; Carlsbad CA) and sequenced.

BAC Southern blot

Five µg of purified BAC DNA was digested with *EcoR*I and *BamH*I (New England Biolabs, Beverly, MA) for 16 hours and then fractionated on a 1% agarose gel before blotting to a Nylon membrane (Roche, Indianapolis, IN) by capillary transfer. *KCNJ12* PCR product was released from pCR2.1 by *EcoR*I digestion, gel-purified, and random prime-performed at 37°C using the Digoxigenin-labeled system (DIG Luminescent Detection Kit, Roche). Hybridization was performed at 68°C overnight in hybridization buffer (6X SSC, 5X Denhardt's reagent, 0.5% SDS, and 100 µg/mL salmon sperm DNA). The membrane was washed 2 X 20 minutes in 2X SSC/0.1% SDS at room temperature followed by 2 X 20 minute washes in SSC/0.1% SDS at 65°C. The membrane was then exposed for 40 minutes with Lumi-Film Chemiluminescent Detection film (Roche Applied Science) with an intensifying screen. The gel-band that matched with the blot-band was cut, purified, and subcloned into pBluescript SK(+). This clone contained a 2.6-Kb BAC DNA fragment containing *KCNJ18*.

For Figure 6, 20µg of BAC DNA was digested with either *BamHI* or *HindIII* and fractionated on a 0.8% agarose gel prior to transfer to an Amersham Hybond-N+ membrane (GE Healthcare) and probed as above. Overnight hybridization was performed at 40°C with biotinylated oligonucleotide per the manufacturer's instructions (North2South Chemiluminescent Hybridization and Detection Kit, Pierce). Exon 1 probes are CTGTTGGGAAGCCTGTTTC and GTCACGAGGGTAAGCCAAGC. Exon 3 probes are CAACCCCTACAGCATCGTGTC and TCCACACAGGTGGTGAACAT.

Characterizing the 5' and 3'UTRs of *KCNJ18*

Based on the differences between *KCNJ12* (NCBI database) and *KCNJ18* (2.6 Kb-clone), we performed 5' and 3' Rapid Amplification of cDNA Ends (RACE) to characterize both transcripts and their exon-intron genomic structure. The first round of RACE-PCR used 10µM of the provided adapter primer 1 and 10µM of the gene specific primer (5'-RACE: CTGCATCACACAGGGTGTGCGGCCGT, 3'-RACE CTGCTGCCCAGTGCCAACTCCTTCTGCTAT) in a 25-µL reaction containing 0.1 ng/µL of human testis or brain Marathon-Ready cDNA, followed by an inner PCR reaction using the nested adapter primer 2 and the nested gene specific primer (5'-RACE: CTGCATCACACAGGGTGTGCGGCCGT, 3'-RACE: GTCCTGGAGCAGCGGCCCTACAGACGGGG). RACE was performed per Advantage-GC 2 PCR kit manufacturer standard protocol (BD Biosciences). PCR products were then subcloned into pCR2.1-TOPO vector for sequencing.

According to the cloned consensus RACE products, we designed new primers flanking *KCNJ18* (see mutational analysis, below). The PCR was performed in a 25-µL reaction using 5 µL of substrate (0.1 ng/µL of human testis Marathon-Ready cDNA) (Clontech, Palo Alto, CA) under the following touchdown PCR conditions: 5 min at 94°C, followed by 38 cycles of 20 sec at 94°C, touchdown annealing temperature step of 30 sec at 68/ -0.5°C per cycle, and an extension step of 2 min at 72°C. This was repeated using skeletal muscle cDNA from FirstChoice RACE-Ready cDNA (Ambion, Austin, TX) to validate the full-

length *KCNJ18* cDNA. Products were subcloned into pCR2.1-TOPO and sequenced.

Kir2.6 Multiple Tissue Northern (MTN) blot expression

Exon 1 of *KCNJ12* (primers: GAGATCAGATAACAGCCGGCGGG/CTTCTCTGCAAAGCGGATCG) and *KCNJ18* (primers CTCTGTGGGACAGATACTGAAGCC/GACACGATGCTGTAGGGGTTG) were used as probes after random prime-labeling with ^{32}P dCTP at 37°C for 4 hours using Rediprime II Random Prime Labeling kit (Amersham Biosciences, City, UK). Ready-to-use Multiple Tissue Northern membrane (Clontech, Palo Alto, CA) was then hybridized at 68°C in ExpressHyb Hybridization Solution (BD Biosciences, Palo Alto, CA) at a concentration of 1-2 x 10^{6} cpm/mL (2-10ng/mL). After overnight hybridization, the membrane was washed 2 X 20 minutes in 2X SSC/0.05% SDS at room temperature, followed by another two washes for 20 minutes each in 0.1X SSC/0.1% SDS at 55°C for *KCNJ18* and at room temperature for *KCNJ12*. The timing of washes was optimized according to radioactivity counting and the blot was exposed for 60 hours with Kodak x-OMAT AR film (Eastman Kodak, Rochester, NY) film and an intensifying screen.

Promoter constructs

Inspection of the possible *KCNJ18* promoter sequence revealed a region containing a DR4 motif (5'-TGACCTggccTCACCTcaggg-3'), located 265bp upstream of exon 1. We used the above TRE sequence as an oligonucleotide with an inner EcoRI restriction site combined with NheI linker in the forward

strand (5'-CTAGCggaattccTGACCTGGCCTcACCTCAGGG-3') and BglII linker in the reverse (5'-TCTAGCCCTGAGGTgAGGCCAGGTCAggaattcc). The NheI/BglII-linked TRE sequence was ligated into pGL3-Basic (Promega, Madison, WI) to produce the WT construct. Negative controls were made either by disrupting the TRE sequence (5'-CTAGCggaattccTGgaCTGΔCTcgaCTCAGGG -3') (mutant construct), or by releasing the NheI/BglII fragment and recircularizing the vector ("Empty" pGL3). A positive control was constructed with two TRE binding motifs (2xDR-4pGL3).

T3 treatment and Luciferase assay

Wild-type, mutant, and empty vectors were used for transient transfection of C2C12 or 293T cells. Transfections were carried out in duplicate using Lipofectamine 2000 (Invitrogen) according to the manufacturer's instructions. C2C12 cells (1.25 X 10 cells/well for "proliferating" and 3 X 10 cells/well for "differentiated" stage, which is believed to be more similar to native muscle, in 24-well plates) were seeded each day prior to transfection. The cells were transfected with 0.5 µg of pGL3 construct, 0.1 µg of internal control plasmid pRL-TK (Promega) that constitutively expresses renilla luciferase, and 0.5 µg of expression plasmid for human thyroid receptor (TRβ). C2C12 cells were first cultured in Dulbecco's modified Eagle's minimal essential medium (DMEM) with 10% fetal bovine serum (FBS) and 10% horse serum (HS), followed by 10% (proliferating) or 2% (differentiated) horse serum solely, containing penicillin and streptomycin (100 µg/mL). T3-depleted serum was obtained by AG1-X8 resin (BioRad) treatment for 16h at room temperature. The cells were harvested 48

(proliferating) or 72 (differentiated) hours post-transfection. Serum-free medium (DMEM) supplemented with 2mg/mL of T3-free bovine serum albumin (Sigma) was used for transfection.

In both cell types, triiodothyronine (T3, Sigma) was added 6 hours after transfection to the labeled concentration. 293T cells were harvested 24h post-transfection. Cellular expression of the luciferases was assayed using a dual luciferase assay system (Promega). Light intensity was measured with a TD-20/20 DLR luminometer (Turner BioSystems). The assay was replicated five times. Relative light unit measures were obtained in duplicate in each assay.

Mutational analysis

The entire coding region (1.47 Kb) of *KCNJ18* was specifically amplified and sequenced in TPP patients and healthy controls. We performed PCR of *KCNJ18* (primers: ATGCTGTCCTCTCTGTTCC/GGGCCTCTCCCCGGCCA) using 20-100ng of genomic DNA in a 25μL reaction using the Advantage 2 polymerase mix (Clontech) with the addition of 5μL of GC-melt from the Advantage-GC 2 polymerase mix. Cycling conditions were: 95°C for 1 minute followed by 35 cycles of 94°C for 30 seconds and 67°C for 3 minutes, plus a final 3 minute extension at 67°C. All sequences were collected and analyzed with Sequencher (Gene Code Corporation, Ann Arbor, MI) software. Sequencing was performed twice in both directions for each sample. Uniqueness of *KCNJ18* sequencing was confirmed by the lack of polymorphisms at amino acids 15 and 430, at which *KCNJ18* and *KCNJ12* differ (Table 2).

Electrophysiology

293T cells were maintained as described above and transfected with 2µg DNA using Polyfect (Qiagen, Valencia CA). Currents were recorded 24-72 hours post transfection.

All recordings were conducted at room temperature using an Axopatch 200B Amplifier (Axon Instruments, Union City, CA) and pClamp6 for data acquisition. Data were analyzed using Igor Pro (Wavemetrics, Oswego, OR) and QUB (http://www.qub.buffalo.edu/). Pippettes (Kimax) of 1.5-3.5MΩ were coated with Sylgard 184 (Dow Corning Corporation, Midland, MI) and heat polished prior to use. Series resistance and capacitance compensation of 95% was used for all whole-cell recordings. For whole-cell recordings, each trial consisted of maintaining cells at resting membrane potential for 50ms, a 100ms test pulse between -60mV to +60mV in 10mV increments, and then returning cells to resting membrane potential. 5 trials were run per cell and used to create a per cell average. Data was sampled at 5kHz with a 2kHz low pass filter. Intracellular solution: 110mM K-Aspartate, 20mM KCl, 1mM $MgCl_2$, 10mM EGTA, 5mM Na_2-ATP, 5mM glucose, and 10mM HEPES (pH 7.4). Cells were bathed in a solution of 117mM NaCl, 30mM KCl, 2mM $CaCl_2$, 1mM $MgCl_2$, 10mM HEPES, 5mM glucose, and 2mM $NaHCO_3$ (pH 7.3) or the equivalent solution with TEA-Cl substituted for KCl to measure leak.

Single channel on-cell and multi-channel inside-out excised patch currents were recorded at 50kHz continuously for 1-7 minutes at the test voltage with a 1kHz low-pass filter. For single channel recordings, pipette and bath solution was

comprised of: 150mM KCl, 2mM $MgCl_2$, 1mM EGTA, and 10mM HEPES (pH 7.4). This solution was also used as the bath solution for excised patches while the pipette solution was identical to bath solution used for whole-cell recordings. Excised patches were held at -80mV during recordings. Where indicated, 100nM phorbol 12-myristate 13-acetate (PMA) or 300µg/ml polylysine (Sigma) was added. Cells were bathed in PMA at least 45 minutes prior to recording. After idealization, data for excised inside-out patches was summed and fit with an exponential function: base + $A*exp(-x/T_{50})$. Similar results can be obtained by instead fitting with a Hill or Boltzmann-style sigmoid function. Single channel current levels were calculated by curve fitting the sum of a number of Gaussian curves to the recorded data. Open probability was then calculated as the relative areas of these Gaussian curves. For the T354E and WT + PMA recordings, single-channel conductance was calculated at -60mV only, as other potentials lacked sufficient openings for reliable measurement. Data are reported as mean ± standard error (n = number of cells, patches, etc.) unless otherwise noted. For all figures, * denotes $p < 0.05$, ** $p < 0.01$, and *** $p < 0.001$.

CHAPTER 3

Heteromultimerization of Kir2.6

Summary

Inwardly rectifying potassium (Kir) channels have the potential to form heteromultimers both within and between their subfamilies. Kir2.1 can heteromultimerize with other Kir2 channels and with channels in other Kir subfamilies. Furthermore, Andersen-Tawil Syndrome (ATS) mutations in Kir2.1 are able to alter heteromeric channel function in a dominant negative manner. Given the recent discovery that mutations in Kir2.6 are associated with thyrotoxic hypokalemic periodic paralysis (TPP) we wondered if Kir2.6 might be able to heteromultimerize with other Kir channels found in skeletal muscle. Using electrophysiology, we show that Kir2.6 is able to coassemble with both Kir2.2 and Kir2.1 in an efficient manner, opening the possibility that TPP mutations might alter a larger swath of Kir channels than previously surmised.

Introduction

Inwardly rectifying potassium (Kir) channels play a vital role in both setting and maintaining the reversal potential and altering the excitability of cells in both neurons and muscle (Nichols and Lopatin, 1997; Lopatin and Nichols, 2001). A functional Kir channel is composed four subunits drawn from seven families, which are distinguished both by homology and physiology. Some Kir families are weakly rectifying (Kir1, Kir4, and Kir5), some modified by intracellular ATP levels (Kir1, Kir3, and Kir6) or G-proteins (Kir3), while still other have a small single

channel conductance (Kir7) or strongly rectify (Kir2) (Nichols and Lopatin, 1997; Krapivinsky et al., 1998).

While it has long been known that four subunits are required to form a functional Kir channel and different Kir subunit families are often coexpressed in the same cell, heteromeric Kir channels have received relatively little attention (Table 6) (Yang et al., 1995). The Kir2 subfamily is the largest Kir channel subfamily, with six members (Kir2.1-Kir2.6). Of these, Kir2.5, previously called Kir2.2v, represents a dominant negative subunit and has received little attention (Namba et al., 1996; Namba et al., 1997). It was originally reported that Kir2.1 does not coassemble with either members of its own subfamily (Kir2.2 or Kir2.3) or those from other subfamilies (Kir1.1 or Kir6.1) and that the M2 and proximal C-terminal regions confer the ability to heteromultimerize (Tinker et al., 1996). However, more recent studies have begun to contradict these findings. Firstly, knockout of Kir2.1 and Kir2.2 in mice results in non-linear changes in the I_{K1} current, which is composed of these two channels and maintains the resting membrane potential (Zaritsky et al., 2000; Zaritsky et al., 2001). More controlled studies of Kir2 subfamily coassembly have confirmed these results. Concatemers of Kir2.1-Kir2.2/Kir2.1-Kir2.3/Kir2.2-Kir2.3 are functional and coexpression of a wild-type form of one of these with a dominant-negative form of another results in near total current abrogation (Preisig-Muller et al., 2002). This also seems to be the case for coassembly of Kir2.1 with Kir2.4 (Schram et al., 2002). Heteromultimerization is not restricted to within subfamily combinations, however. Kir2.1 can heteromultimerize with both Kir3.1 and Kir3.4 as well as with

Kir4.1 (Fakler et al., 1996; Ishihara et al., 2009). Importantly, it is not the case that Kir2 subfamily members can heteromultimerize indiscriminately, as Kir2.1 does not heteromultimerize with Kir7.1 or the voltage-gate potassium channel subunits Kv1.1 or Kv1.3 (Tytgat et al., 1996; Preisig-Muller et al., 2002).

Table 6. Published results of heteromeric assembly.

	Kir1.1	Kir2.1	Kir2.2	Kir2.3	Kir2.4	Kir2.6	Kir3.1	Kir3.2	Kir3.3	Kir3.4	Kir4.1	Kir4.2	Kir5.1	Kir6.1	Kir6.2	Kir7.1
Kir1.1		?	?	?	?	?	?	?	?	?	?	?	?	?	?	?
Kir2.1			Yes	Yes	Yes	?	Yes	?	?	Yes	Yes	?	No	Yes	No	?
Kir2.2				Yes	Yes	?	?	?	?	Yes	Yes	?	No	Yes	Yes	?
Kir2.3					?	?	?	?	?	?	?	?	?	?	?	?
Kir2.4						?	?	?	?	?	?	?	No	?	?	?
Kir2.6							?	?	?	?	?	?	?	?	?	?
Kir3.1								Yes	?	Yes	?	?	No	Yes	?	?
Kir3.2									?	Yes	?	?	No	?	?	?
Kir3.3										?	?	?	?	?	?	?
Kir3.4											?	?	?	Yes	?	?
Kir4.1												Yes	No	Yes	?	?
Kir4.2													Yes	?	?	?
Kir5.1														No	?	?
Kir6.1															Yes	?
Kir6.2																?
Kir7.1																

"Yes" indicates the presence of heteromerization while "No" indicates evidence against heteromerization.

The Kir3 subfamily encodes a group of G-protein regulated Kir channels (GIRKs) with wide anatomical expression. These channels play an important role in the heart, where they alter the heart rate according to acetylcholine input. Kir3 subunits are capable of heteromultimerizing within the same subfamily. Specifically, Kir3.1 can coassemble with either Kir3.2 or Kir3.4, with the specificity of these interactions conferred by regions from the N- to C-terminus (Krapivinsky et al., 1995; Velimirovic et al., 1996; Woodward et al., 1997). As stated above, coassembly is not restricted to within subfamily combinations, though not all combinations prove functional (e.g. coassembly with Kir5.1) (Pessia et al., 1996). Somewhat similarly, both Kir3.1 and Kir3.4 are able to coassemble with Kir4.1, but the resulting channels are not functional (Tucker et al., 1996).

Coassembly of Kir4 and Kir5 subfamily members has received the greatest amount of investigation. Kir4.1 and Kir1.1 are both expressed in auditory outer hair cells, with Kir4.1 more strongly rectifying in the presence of intracellular polyamines than Kir1.1. This observation was exploited to demonstrate that the two channel subunits can functionally coassemble (Glowatzki et al., 1995). Kir4.1 and Kir2.1 have a wide anatomical overlap in expression. A mutation in Kir4.1 (E158N) that results in weaker rectification was used in a similar way to study Kir4.1/Kir2.1 coassembly to demonstrate that these two channels preferentially heteromultimerize rather than homomultimerize (Fakler et al., 1996). Kir5.1, when expressed by itself, is unable to produce functional channels (Bond et al.,

1994). Interestingly, this is no longer the case when coexpressed with Kir4.1, where the resulting currents are both potentiated and have a different shape, displaying a time-dependent increase rather than run-down (Pessia et al., 1996). Interestingly, the position of individual subunits within these heteromeric channels is important in determining the resulting current profile. Kir4.1/Kir5.1 heteromultimers preferentially coassemble in an alternating 4-5-4-5 pattern, rather than 4-4-5-5, with the later showing a time-dependent current run-down rather than a time-dependent current increase. While Kir4.1 coassembles readily with Kir1.1, Kir2.1 and Kir5.1, the same is not the case for Kir5.1. Kir5.1 does not heteromultimerize with Kir1.1, Kir2.1, Kir2.3, Kir3.1, Kir3.2 or Kir3.4 as indicated by no change in the resulting single channel properties (Pessia et al., 1996). Importantly, whole-cell studies have indicated that Kir5.1 acts as a negative regulator for Kir2.1, implying that there was a selection bias in previous single channel studies (Derst et al., 2001). Other whole-cell studies, however, have contradicted these findings and shown that Kir5.1 coassembles only with Kir4 subunits and not with Kir1.1, Kir2.1 or Kir6.2 (Konstas et al., 2003).

The Kir6 subfamily is regulated by ATP/ADP ratios and acts to link metabolism to cellular excitability, such as insulin release from pancreatic β cells. While homomers have properties identical to ATP-regulated Kir channels in many tissues, this is not always the case. Consequently, heteromultimerization of Kir6.1/Kir6.2 became of interest. Both biochemical and electrophysiological tests indicate that Kir6.1 and Kir6.2 can heteromultimerize to produce functional channels (Kono et al., 2000; Cui et al., 2001). Furthermore, these

heteromultimeric channels display an array of single channel properties that match many endogenous ATP-regulated Kir channels. This result is not non-specific, as similar experiments have shown no coassembly between either Kir6.1 or Kir6.2 and Kir2.1 (Cui et al., 2001).

With the recent cloning of Kir2.6 and its association with thyrotoxic hypokalemic periodic paralysis, TPP, we wondered whether Kir2.6 might coassemble with other Kir channel subunits. This is particularly important given the implication of heteromultimerization in Andersen-Tawil Syndrome pathophysiology (Preisig-Muller et al., 2002). There are a number of Kir channel subunits found in skeletal muscle. RT-PCR indicates that a rodent-specific isoform of Kir1.1 is expressed in skeletal muscle (Shuck et al., 1994; Kondo et al., 1996). Kir2.1 and Kir2.2 are expressed heavily in skeletal muscle. Also according to RT-PCR, the GIRKs Kir3.1 and Kir3.2 are found in skeletal muscle, with Kir3.1 expressed at a lower level (Isomoto et al., 1996). Finally, Northern blot analysis indicates that both ATP-regulated Kir channels, Kir6.1 and Kir6.2, are found in this tissue (Inagaki et al., 1995; Sakura et al., 1995). To test whether wild-type Kir2.6 might form functional heteromultimers, we coexpressed wild-type or dominant negative Kir2.6 with Kir2.1 or Kir2.2. Our results indicate that Kir2.6 is able to coassemble efficiently with at least some other Kir channels expressed in skeletal muscle.

Results

Construction and validation of IRES construct

We sought to exploit the ability of independent ribosomal entry site (IRES) based constructs to allow the expression of more than one gene of interest by the same promoter to explore heteromultimerization of Kir2.6. EGFP is commonly used to visualize transfected cells, but fusing it to either the N- or C-terminus of ion channels could alter their ability to coassemble. Consequently, we modified the base pIRES vector to add an additional IRES-EGFP 3' to the second multiple cloning site (Figure 15). This results in a tricistronic vector where either one or two Kir subunits can be coexpressed along with an EGFP marker without requiring protein fusion or cotransfection. To test the presence of heteromultimerization, we utilized the known dominant-negative effect of mutating the GYG selectivity filter of a subunit to AAA (Heginbotham et al., 1994; Slesinger et al., 1996). A similar dominant-negative strategy has been used by others previously (Tinker et al., 1996; Preisig-Muller et al., 2002; Schram et al., 2002; Ishihara et al., 2009).

To probe the efficacy of these constructs, we first subcloned wild-type Kir2.6 into MCS-A of the IRES construct and EGFP into MCS-B (Kir2.6-IRES-EGFP-IRES-EGFP). Cells expressing this construct have large currents (-60mV: -576±78pA/pF, -50mV: -443±61pA/pF, -40mV: -312±47pA/pF, -30mV: -180±37pA/pF, -20mV: -70±20pA/pF, -10mV: -15±6pA/pF, Figure 16). If, instead, the dominant-negative form of Kir2.6 (Kir2.6GYG->AAA) is expressed from MCS-B, significantly less current is found (approximately 73% less at -60mV,

124

p<0.05 for driving forces between -60mV and -20mV and >0.05 at more depolarized potential according to the Mann-Whitney U test). This is not due to the presence of a Kir2.6 subunit in MCS-B alone, as there is no decrease in current when instead wild-type Kir2.6 is coexpressed with itself (p>0.05 at all voltages). Kir2.6 expressed instead from MCS-B produces somewhat less current than when expressed from MCS-A (-404±54pA/pF vs. -576±78pA/pF at -60mV, p>0.05 at all voltages).

Figure 15. Creation strategy for IRES construct.

Starting with the base pIRES vector from clontech (A), EGFP was subcloned into the SalI and NotI sites of MCS-B (B). An EcoRV site was then added 3' to the NotI site (C). Site directed mutagenesis was then used to remove both the SalI and NotI sites of MCS-B and to convert the EcoRI site in MCS-A into an EcoRV site (D). This then allowed the subcloning of the entire IRES-EGFP cassette from D into C to create a tricistronic vector (E). A gene of interest can then be subcloned into either MCS for expression in mammalian cells.
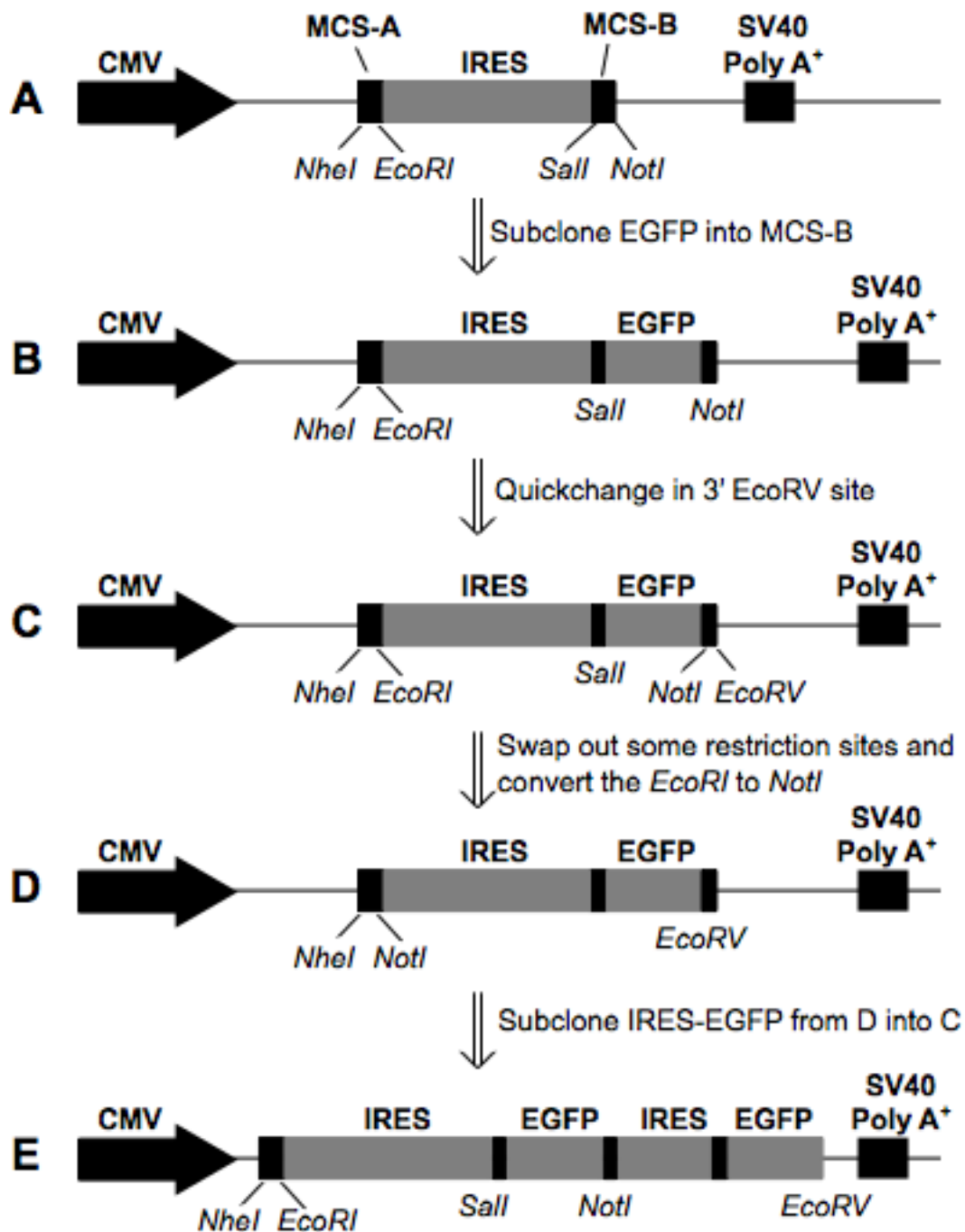
Figure 16. Wild-type and dominant-negative Kir2.6 efficiently coassemble.

Kir2.6 expressed from MCS-A (red circles, N=7) produces approximately -600pA/pF of inward current at -60mV driving force. When the dominant negative form is coexpressed from MCS-B (yellow square, N=6), the resulting current density is only approximately -150pA/pF. This seems to be due to expression of the dominant negative form, as expression of the wild-type form (purple inverted triangles, N=4) does not result in decreased current. For comparison, expression of wild-type Kir2.6 from MCS-B (blue triangles, N=5) results in approximately 33% less current density compared to wild-type Kir2.6 current density when expressed from MCS-A.
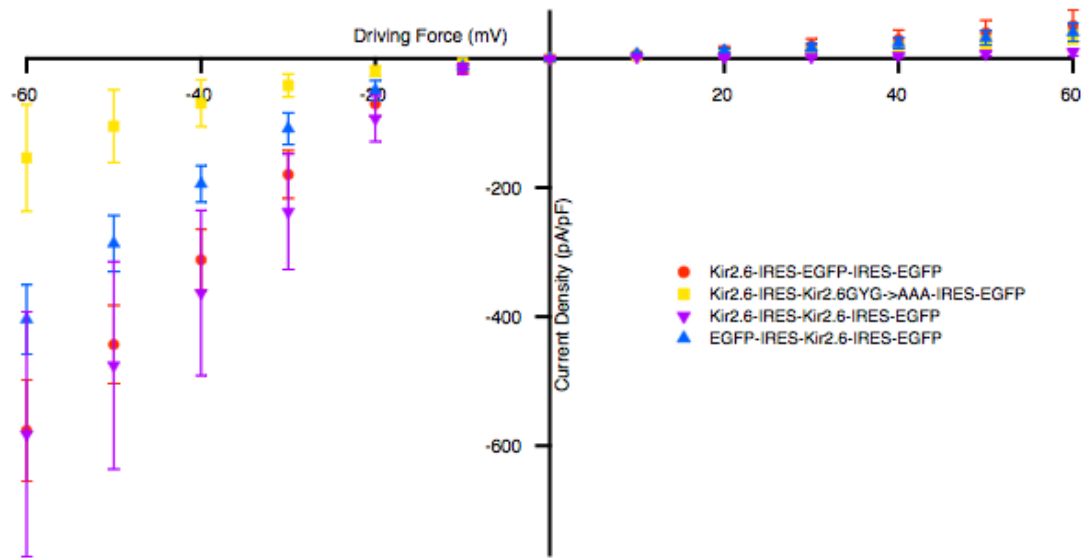
Kir2.2 and Kir2.6 functionally coassemble

Given the expression of Kir2.2 in skeletal muscle and the extremely high identity between Kir2.2 and Kir2.6, we wondered whether these two similar channels might be able to heteromultimerize as well (Takahashi et al., 1994; Ryan et al., 2010). When expressed by itself in the IRES construct, Kir2.2 produces large currents (-719±158pA/pF at -60mV, -511±119pA/pF at -50mV, -334±78pA/pF at -40mV, -188±41pA/pF at -30mV, -87±25pA/pF at -20mV, and -19±5pA/pF,

Figure 17). When, instead of EGFP, the dominant negative form of Kir2.6 is coexpressed with Kir2.2, significantly less current density is produced (approximately 78% less at -60mV driving force, $p<0.05$ for driving forces hyperpolarized to 0mV and >0.05 at all other voltages according to the Mann-Whitney U test).

Figure 17. Kir2.2 and Kir2.6 are able to efficiently coassemble.

Kir2.2, when expressed from MCS-A with EGFP in MCS-B, produces large inwardly rectifying currents, approximately -720pA/pF at -60mV driving force (red circles, N=6). When, instead of EGFP, a dominant negative form of Kir2.6 is expressed from MCS-B (blue squares, N=5), the resulting currents are much smaller, approximately -160pA/pF.

Driving Force (mV)

Current Density (pA/pF)

- ● Kir2.2-IRES-EGFP-IRES-EGFP
- ■ Kir2.2-IRES-Kir2.6GYG->AAA-IRES-EGFP
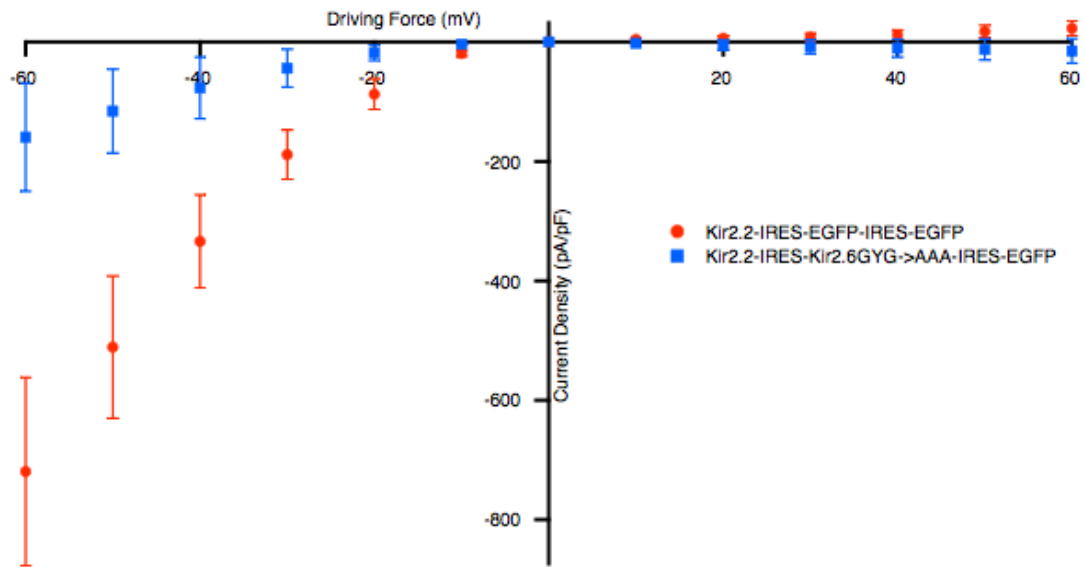
Kir2.6 and Kir2.1 can functionally coassemble

Kir2.1 is expressed heavily in skeletal muscle, where mutations in it result in the periodic paralytic phenotype seen in ATS patients (Raab-Graham et al., 1994; Plaster et al., 2001). It has also been suggested that Kir2.1 heteromerization contributes to ATS pathophysiology (Preisig-Muller et al., 2002). To determine if Kir2.1 is able to heteromultimerize with Kir2.6, we expressed these together in the IRES construct (Figure 18). Regardless of the relative positions of Kir2.1 and dominant-negative Kir2.6 within the constructs, a dominant negative effect was observed ($p < 0.05$ for all voltages between -60 and +50mV for Kir2.1 in MCS-A and -60 and -10mV for Kir2.1 in MCS-B according to the Mann-Whitney U test). This dominant-negative effect is highly efficient, with an approximate 99% reduction of current at -60mV driving force regardless of which MCS Kir2.1 was expressed from. It was also found that Kir2.1 produces approximately 50% less current density when expressed from MCS-B versus MCS-A (-1514±301pA/pF vs. -842±130pA/pF). This is not a non-specific effect of coexpressing the channels, as coexpression of Kir2.1 from MCS-A with wild-type Kir2.6 did not result in significantly decreased currents ($p > 0.05$ for all voltages).

Figure 18. Kir2.1 and Kir2.6 functionally coassemble.

Kir2.1 expressed from MCS-A (teal triangles, N=9) produces approximately -1500pA/pF of inward current at -60mV driving force. When the dominant negative form of Kir2.6 is coexpressed from MCS-B (blue inverted triangles, N=8), the resulting current density is approximately 0pA/pF. This seems to be due to expression of the dominant negative form of Kir2.6, as expression of the wild-type form (magenta rotated triangles, N=6) does not result in decreased current, having an approximate -1200pA/pF current density at -60mV. This effect was not due to the relative positions of the subunits within the IRES constructs as a dominant-negative effect was still observed when the subunits were swapped (EGFP in MCS-A, red circles, N=7; dominant-negative Kir2.6 in MCS-A, orange squares, N=7).

Driving Force (mV)

Current Density (pA/pF)

- ▲ Kir2.1-IRES-EGFP-IRES-EGFP
- ▼ Kir2.1-IRES-Kir2.6 GYG->AAA-IRES-EGFP
- ◄ Kir2.1-IRES-Kir2.6-IRES-EGFP
- ● EGFP-IRES-Kir2.1-IRES-EGFP
- ■ Kir2.6 GYG->AAA-IRES-Kir2.1-IRES-EGFP
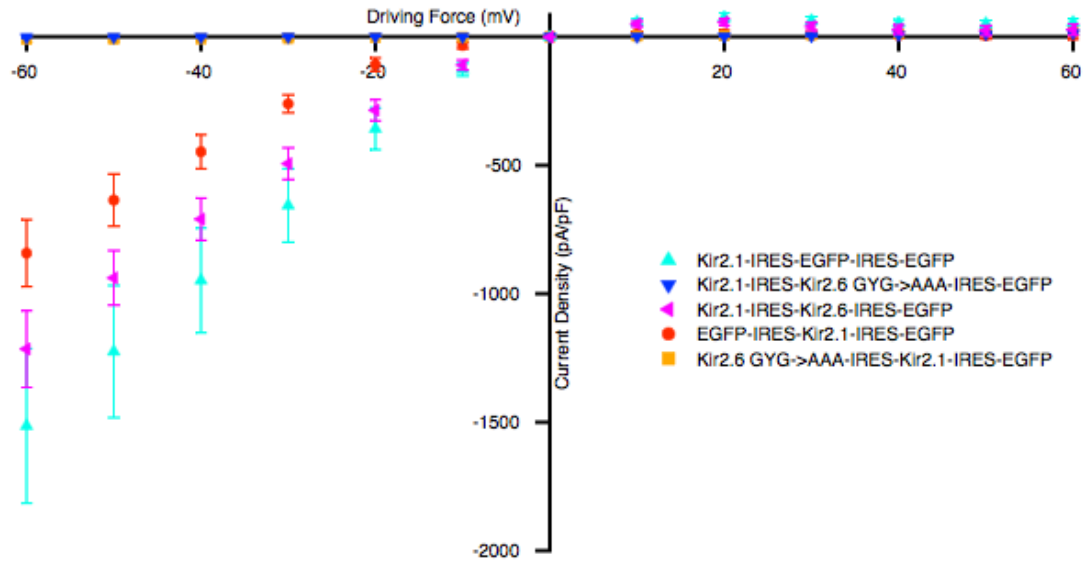
Discussion

Formation of heteromeric potassium channels were originally described for voltage-gated Shaker-related potassium channels (Isacoff et al., 1990; Liman et al., 1992). This was found to occur within, but usually not between, subfamilies, with specificity conferred by a range of areas in the N-terminus and M1 region.

More recently, Kir channel heteromerization has become of interest. Kir channels are able to efficiently coassemble with other subfamily members. Coexpression of wild-type and dominant-negative Kir2.1-4 channels results in near total current abrogation (Preisig-Muller et al., 2002; Schram et al., 2002). This is also the case for the Kir3 subfamily, where Kir3.1 can coassemble with Kir3.2 and Kir3.4, where heteromerization seems to be important for generating normal G-protein gated currents (Krapivinsky et al., 1995; Velimirovic et al., 1996).

For Kir channels, heteromultimerization can also occur between subfamilies. Kir2.1, for example, can heteromultimerize with Kir3.1, Kir3.4 and Kir4.1, but not Kir7.1 or the voltage-gated potassium channels Kv1.1 and Kv1.3, indicating that heteromerization is not completely indiscriminant (Fakler et al., 1996; Tytgat et al., 1996; Preisig-Muller et al., 2002; Ishihara et al., 2009). Coassembly of Kir4.1 and Kir5.1 rescues a lack of current from homomeric Kir5.1 channels and the resulting heteromeric channel has unqie current properties (Bond et al., 1994; Pessia et al., 1996). Not all heteromultimers are functional, as

exemplified by heteromultimers of Kir3.1 or Kir3.4 with Kir4.1 (Tucker et al., 1996).

Heteromerization may be important for both normal physiology and disease pathophysiology. Acetylcholine regulation of cardiac Kir currents seems to be conferred via heteromeric Kir3.1/3.4 channels (Krapivinsky et al., 1995). Kir2.1 mutations lead to ATS and these mutations are able to drastically alter the function of heteromeric channels formed with other subunits whose expression profile overlaps that of Kir2.1 (Preisig-Muller et al., 2002).

In the current study, we use electrophysiology to demonstrate that Kir2.6 can coassemble with both Kir2.1 and Kir2.2. Given that all of these are expressed heavily in skeletal muscle, it is likely that TPP mutations in Kir2.6 might spread their deleterious affects to a larger pool of channels, thereby increasing their efficacy and leading to disease. Future studies will need to determine the single channel properties of both wild-type and mutant heteromeric channels to further elucidate the degree to which heteromerization is important to TPP pathophysiology.

Experimental Procedures

Mutagenesis and subcloning

pIRES was obtained from Clontech (Mountainview, CA USA) and modified as described above (Figure 15). EGFP was originally subcloned from pEGFP-N1 (Clontech). The primers for these steps are listed in Table 7. For mutagenesis, Phusion high-fidelity DNA polymerase (Finnzymes, Espoo Finland) was used according to the manufacturer's instructions in a 25μL reaction. Cycling

conditions were: 98°C for 1 minute followed by 35 cycles of 98°C for 10 seconds and 68°C for 30 seconds per kilobase, plus a final 5 minute extension at 68°C. All sequences were subsequently sent for sequence confirmation. All restriction enzymes and T4 DNA ligase were purchased from New England Biolabs (Ipswich, MA USA) and used in accordance with the manufacturers instructions. Restriction enzyme products were gel purified prior to ligation with a QIAquick Gel Extraction Kit (Qiagen, Valencia, CA USA).

Table 7. Primers used for heteromerization studies.

Primer	Sequence	Use
66F	CGCTAGCCTGTCGTCTCTGTT	NheI primer for Kir2.6
52R	AAGAATTCTAGATCTCTGACCC	EcoRI primer for Kir2.6
65F	CGTCGACCTGTCGTCTCTGTT	SalI primer for Kir2.6
51R	CGATGCGGCCGCTAGATCTCTGACCCCCGTC	NotI primer for Kir2.6
70F/R	CGCAGACCACCATCGCCGCCGCGCTGCGCTGTGTGACG CGTCACACAGCGCAGCGCGGCGGCGATGGTGGTCTGCG	Convert GYG in Kir2.6 to AAA
53F	AAGCTAGCCGCCACCATGGTGAGCAAG	NheI primer for EGFP
60R	AAGAATTCCTACTTGTACAGCTCGTCCATG	EcoRI primer for EGFP
54F	AAGTCGACCGCCACCATGGTGAGCAAG	SalI primer for EGFP
59R	GCGGCCGCCTACTTGTACAGCTCGTCCATG	NotI primer for EGFP
68F	AAGCGGCCGCTGCATCTAGGGCGGCCAATTC	NotI primer for IRES
68R	AAGATATCCTACTTGTACAGCTCGTCCATG	EcoRV primer for EGFP
69F/R	GGATCCTCTAGAGTAGACCGCCACCATGG CCATGGTGGCGGTCTACTCTAGAGGATCC	Remove SalI site from IRES-EGFP
83F	AAGCTAGCGTAGAACCACAAGGCTCCCA	NheI primer for Kir2.1
83R	AAGAATTCCCCATCTTGACCAGTACCGT	EcoRI primer for Kir2.1
84F	AAGTCGACGTAGAACCACAAGGCTCCCA	SalI primer for Kir2.1
84R	AAGCGGCCGCCCCATCTTGACCAGTACCGT	NotI primer for Kir2.1
85F	CGCTAGCCTGTCGTCTCTGTT	NheI primer for Kir2.2
85R	AAGAATTCTAGATCTCTGACTCCCGTC	EcoRI primer for Kir2.2
86F	CGTCGACCTGTCGTCTCTGTT	SalI primer for Kir2.2
86R	CGATGCGGCCGCTAGATCTCTGACTCCCGTC	NotI primer for Kir2.2
97F	CGCTAGCGTACCCAGCTTGCTTGTTCT	NheI primer for Kir3.2
97R	AAGAATTCGATACGAATGGCTACATTTTGG	EcoRI primer for Kir3.2
98F	CGTCGACGTACCCAGCTTGCTTGTTCT	SalI primer for Kir3.2
98R	CGATGCGGCCGCGATACGAATGGCTACATTTTGG	NotI primer for Kir3.2
99F/R	CCTTAGTGCCAAAGAGCTAGCGGAGCTGG CCAGCTCCGCTAGCTCTTTGGCACTAAGG	Remove internal NheI site from Kir3.2
100F/R	GGGGACTTGAGGTATTCTCACATTGTGG CCACAATGTGAGAATACCTCAAGTCCCC	Remove internal EcoRI site from Kir3.2
101F/R	CCGGGGATCCGTATTCTCTAGAGCAAGC GCTTGCTCTAGAGAATACGGATCCCCGG	Remove 5' EcoRI
102F	GGGTGACTCGAGACGACGGATCCGCGG CCGCGGATCCGTCGTCTCGAGTCACCC	Remove 3' SalI
118F	CGCTAGCGGATCCGCCATGCTGTCCC	NheI primer for Kir6.2
118R	AAGAATTCCTCAACTGCGGTCCTCATC	EcoRI primer for Kir6.2
119F	CGTCGACGGATCCGCCATGCTGTCCC	SalI primer for Kir6.2
119R	CGTCGACCTCAACTGCGGTCCTCATC	NotI primer for Kir6.2

Electrophysiology

293T cells were maintained at 37°C with 5% CO_2 in DMEM supplemented with 10% FBS and 1% penicillin/streptomycin. Cells were transfected with 2μg DNA using Polyfect (Qiagen, Valencia, CA USA) with currents recorded 24-72 hours after transfection. Kir3.2 constructs where cotransfected with Gβ and Gγ to increase current density.

Recordings were conducted at room temperature using an Axopatch 200B Amplifier (Axon Instruments, Union City, CA USA) and pClamp6 for data acquisition. Data were analyzed with Igor Pro (Wavemetrics, Oswego, OR USA). Pippettes (Kimax Brand from Fisher Scientific, Waltham, MA USA) of 1.5-3.5MΩ were coated with Sylgard 184 (Dow Corning Corporation, Midland, MI USA) and heat polished prior to use. Series resistance and capacitance compensation of 95% was used for all whole-cell recordings. For whole-cell recordings, each trial consisted of maintaining cells at resting membrane potential for 50ms, a 100ms test pulse between -60mV to +60mV in 10mV increments, and then returning cells to resting membrane potential. 5 trials were run per cell and used to create a per cell average. Data was sampled at 5kHz with a 2kHz low pass filter. Intracellular solution: 110mM K-Aspartate, 20mM KCl, 1mM $MgCl_2$, 10mM EGTA, 5mM Na_2-ATP, 5mM glucose, and 10mM HEPES (pH 7.4). Cells were bathed in a solution of 117mM NaCl, 30mM KCl, 2mM $CaCl_2$, 1mM $MgCl_2$, 10mM HEPES, 5mM glucose, and 2mM $NaHCO_3$ (pH 7.3) or the equivalent solution with TEA-Cl substituted for KCl to measure leak.

Data are reported as mean ± standard error (n = number of cells). P-values are calculated with a Mann-Whitney U test.

CHAPTER 4

Theoretical Reconstruction of Thyrotoxic Periodic Paralysis

Caused by Alteration of Kir Currents

Summary

Mutations in Kir2.6 have previously been shown to contribute to thyrotoxic periodic paralysis. As this channel is absent in mice and hyperthyroidism in mice does not lead to paralysis, it seems that creation of an animal model of this disorder will not be a simple task. We present a computational model of skeletal muscle altered to mimic hyperthyroidism where Kir conductances can be altered both in amplitude and subcellular localization. We show that Kir channel levels must be tightly regulated during hyperthyroidism, with too little leading to spontaneous activity and too much leading to inactivity. Furthermore, alteration of the subcellular localization of Kir conductances can also lead to altered membrane activity during hyperthyroidism. These results support previous theories of thyrotoxic periodic paralysis pathophysiology and further point to the importance of regulated potassium accumulation in the T-tubular system to normal skeletal muscle excitability.

Introduction

We have recently reported the discovery of mutations in an inwardly rectifying potassium channel (Kir2.6) associated with thyrotoxic hypokalemic periodic paralysis (TPP) (Ryan et al., 2010). TPP is characterized by periodic bouts of skeletal muscle weakness or paralysis on the background of an underlying thyroid disorder, treatment of which prevents attacks. TPP mutations

in Kir2.6 result in a variety of physiological defects, from complete loss of function and, presumably, haploinsufficiency (I144fs) to excess current during hyperthyroid conditions, such as increased phosphatidylinositol 4,5-bisphosphate turnover (R205H and K366R) or protein kinase C activity (T354M). Other mutations (R399X and Q407X) do not seem to alter Kir2.6 currents directly, but may alter either membrane-trafficking or subcellular localization. Kir channels in skeletal muscle are localized to the T-tubular system, where they seem to contribute to clearance of excess potassium accumulated during action potentials (Adrian and Bryant, 1974; Clark et al., 2001; Leonoudakis et al., 2001). This has led to the theory that Kir current levels must be kept within a controlled range, outside of which during hyperthyroidism, a clinically meaningful phenotype is precipitated.

The normal step of creating a mouse model of TPP is untenable as mice lack Kir2.6 (similar to a double I144fs TPP patient) but, when made hyperthyroid, do not present TPP symptomology. This suggests that mouse skeletal muscle endocrine response is fundamentally different from that of humans. Instead, *in silico* modeling may be informative in testing TPP pathophysiology.

Mathematical descriptions of neuronal electrical properties long predate the invention of modern electrophysiology or computers (Rushton, 1934; Curtis and Cole, 1938; Hodgkin and Rushton, 1946; Lapicque, 2007). The mathematical description of ion channels in the squid giant axon by Hodgkin and Huxley created an experimental basis for the incorporation of physiologically meaningful

active elements into then largely passive models of electrical activity (Hodgkin and Huxley, 1952).

Hodgkin-Huxley style numerical models of skeletal muscle have gone through a large number of alterations and refinements since the first model created in 1970 (Adrian et al., 1970). Firstly, while both sarcoplasmic and T-tubular membrane were first modeled as separate compartments, appropriate placement of ion channels required refinement (Adrian and Peachey, 1973). This alone was sufficient to allow functional predictions from earlier findings of chloride channel conductance differences between normal and myotonic muscle (Lipicky et al., 1971; Adrian and Marshall, 1976). Similarly simple models have been used to predict how alterations in sodium channel inactivation can lead to myotonia and paralysis (Cannon et al., 1993). More complex models have focused on accurately representing the T-tubular system and making further refinements to ion channel conductances and placements (van Veen et al., 1992; Henneberg and Roberge, 1997). Recently, these models have been further extended such that all model conductances are physiologically relevant, model compartmental sizes are anatomically accurate, and T-tubular accumulation of potassium, which had been previously surmised to affect skeletal muscle action potential properties (Adrian and Bryant, 1974), is modeled in accordance with experimental observations (Wallinga et al., 1999).

The aim of the present study was to extend these previous models to test how alteration of Kir conductance magnitude and location might affect skeletal muscle activity and lead to TPP. Previous work by others has suggested that

voltage-gated sodium and potassium conductances can change in cardiac tissue due to hyperthyroidism (Harrison and Clausen, 1998; Le Bouter et al., 2003). We have increased these conductances to an extent necessary to produce disease relevant alterations in excitability. Our findings indicate that inwardly rectifying potassium currents must be kept within a regulated window during hyperthyroidism. If levels are kept too low, potassium accumulates in the T-tubular system and results in drastic depolarization and inactivation of voltage-gated channels. If levels are kept too high, normal levels of stimulation are unable to elicit reliable activation. Furthermore, if the subcellular localization of otherwise normal Kir conductances is altered, even by a few percent, normal levels of current input are unable to initiate action potential production.

Results

Model construction

The basic model used has been described previously (Wallinga et al., 1999). We altered the ζ parameter (T-tubule volume to surface ratio) in accordance with the original source (Peachey, 1965). The extracellular potassium concentration was changed to 2mM to reproduce hypokalemia. To test the effects of varying multiple parameters in an efficient manner, two models were created. The first model, labeled the "high-throughput" model, consists of 5 sarcolemmal segments each with 5 T-tubular compartments. The second model, labeled "full-scale" model, consists of 10 sarcolemmal segments each with 20 T-tubular compartments. The allowed error in the membrane current density, 1e-6 $\mu A/cm^2$, was chosen as a tradeoff between computational time and accuracy, for

which sarcolemmal action potential conduction velocity serves as a surrogate (Figure 19). The resulting model produces action potentials and potassium accumulation similar to that previously described (Figure 20) (Wallinga et al., 1999).

The sodium, voltage-gated potassium, inwardly rectifying potassium, and η_{Kir} parameters were altered with each run of the model. To test how alterations of current densities associated with hyperthyroidism might affect excitability, sodium and voltage-gated potassium conductance levels were increased 1, 3, 5 or 10-fold in each combination (Table 8). For further study, the proportion of Kir conductances normally restricted to T-tubular compartments was decreased from 1 to 0.5, 0.1, 0.05, or 0.01. There were a total of 320 unique parameter combinations. For the benefit of time, the small-scale model was used to sample this parameter space. Further probing was done with the full-scale model.

Figure 19. Computation time and accuracy versus model error tolerance.

The time for computation of the full-scale model (red circles) increases as the allowable membrane current density, or tolerance, decreases. There is a converse relationship with the sarcolemmal conduction velocity (blue triangles) and tolerance. When tolerance is set too high (1e-3 or higher), action potentials propagate at an infinite speed (1e-2) or even backward in time (1e-1). With decreasing tolerance, this value, which acts as a surrogate for accuracy, approaches a steady state value.
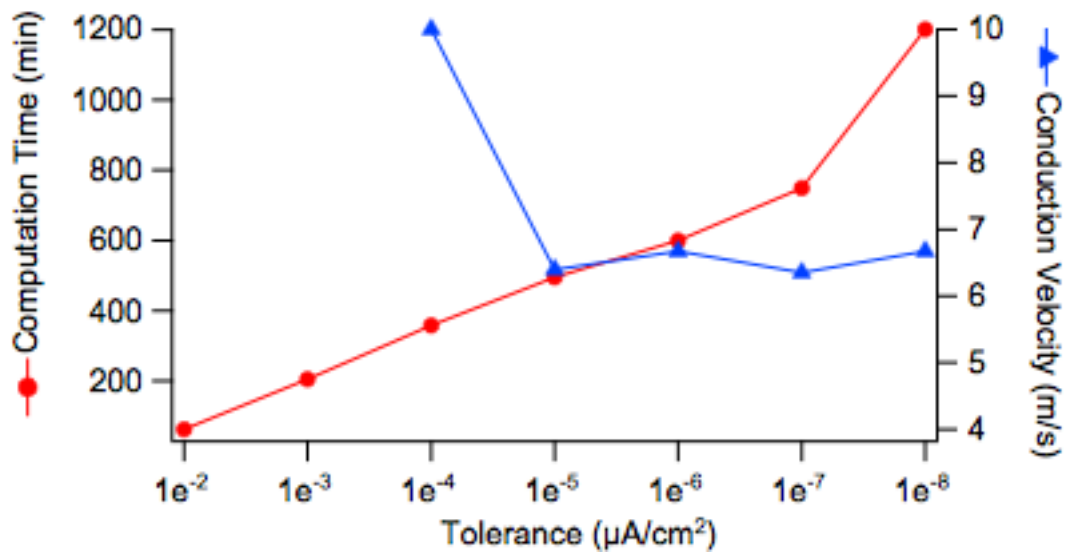
Figure 20. Example results from full-scale model with default parameters.

After allowing the model 1000ms to reach steady-state, a brief stimulation produces stereotypical action potentials, A. The sarcolemmal action potential (solid red line, here from the third sarcolemmal segment) has a normal shape and time-course with an appreciable after-hyperpolarization. The outer T-tubular action potential (dotted blue line) has a lower amplitude and delayed onset compared to that seen in the sarcoplasmic membrane. The inner-tubule membrane is further delayed but has an action potential of intermediate amplitude. The currents underlying this action potential, B, are similar to those previously described for this model. Potassium accumulates with each action potential, C, and continues to do so until reaching a plateau after continuous stimulation, D. These results are from the full-scale model.
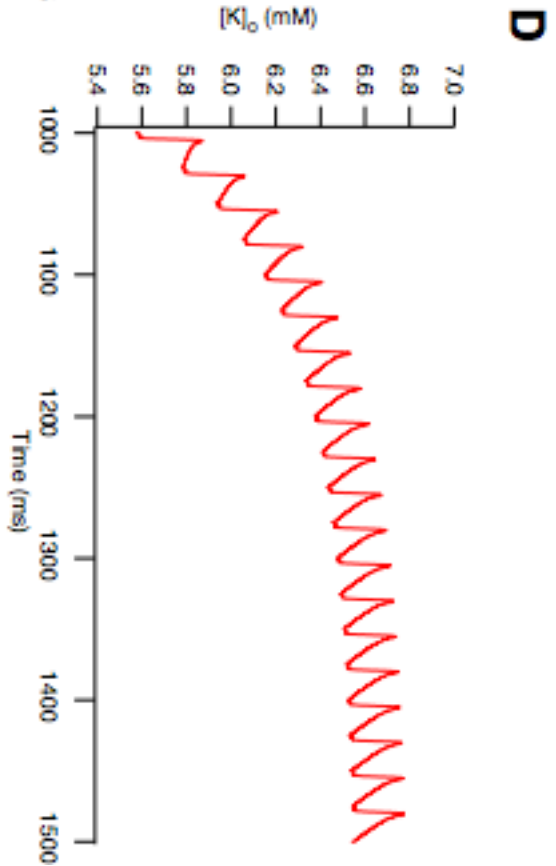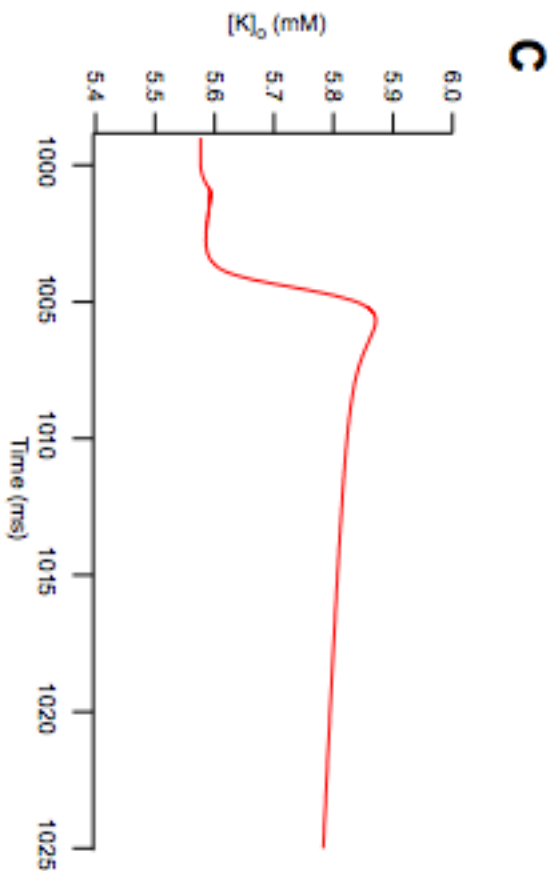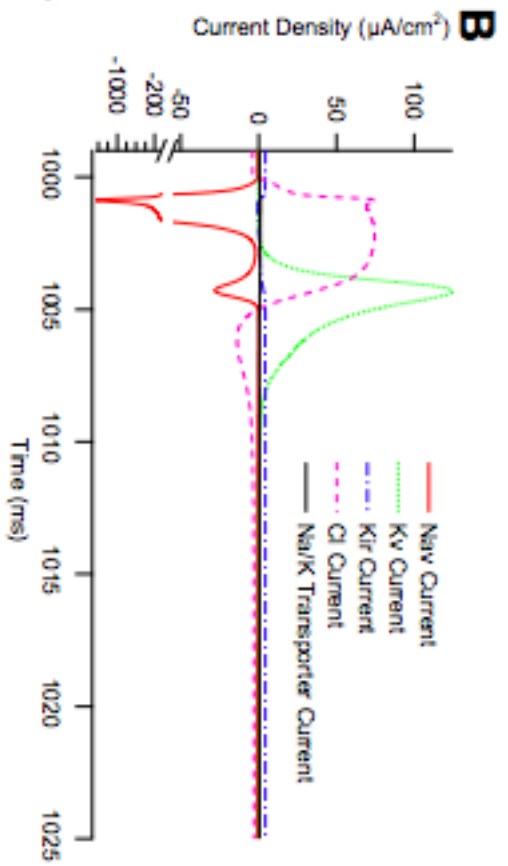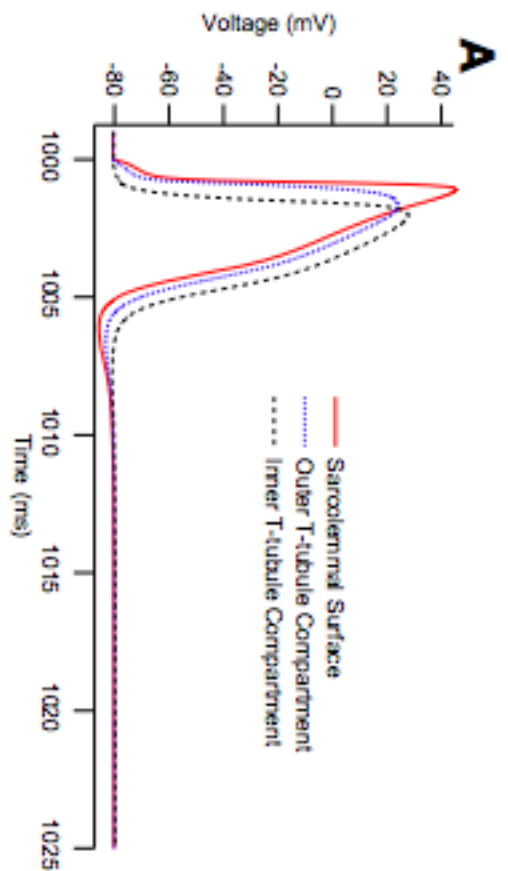
Table 8. Parameter variation for high throughput model.

Bold values indicate default values for current density. The current density for each conductance type was increased 1, 3, 5, or 10-fold. For alterations of channel distribution, η_{Kir}, the default value is 1. A value of 0.5 indicates that 50% of Kir channels are maintained in the T-tubules with the other 50% free to traffic to the sarcolemmal surface.

	Current Density (μA/cm^2)			
i_{Na}	**268**	804	1340	2680
i_{Kv}	**21.6**	64.8	108	2160
i_{Kir}	**0.44**	1.31	2.18	4.37
	Channel Distribution			
η_{Kir}	0.01	0.05	0.1	0.5

Results of high-throughput model

The high-throughput model was first allowed to reach a steady-state value by running without stimulation for 1000ms. Thereafter, the model was stimulated at 40Hz for 250ms. The combination of parameters can produce five possible outcomes, of which three are seen in the high-throughput results (Figure 21). Firstly, there may be no evoked action potentials, denoted by black. Secondly, there may initially be no evoked action potentials, with normal action potentials appearing after repetitive stimulation, denoted by gray. Thirdly, the model may produce normal reliably provoked action potentials, denoted by green. Alternatively, while normal action potentials are initially evoked, the model quickly enters a state of spontaneous high-frequency activity, denoted by yellow. Finally, the model may enter a state of high-frequency activity without the need for outside stimulation, denoted by red.

The default state for the model produces normal evoked action potentials (Figure 22, top left panel, bottom left circle). Increasing the voltage-gated potassium channel conductance (gK_v) either 3, 5, or 10-fold while holding the sodium (gNa_v) and Kir (gK_{ir}) conductances stable also results in normal evoked action potentials. Increasing gNa_v while holding gK_{ir} constant produces spontaneous high-frequency activity, regardless of alterations in gK_v. For states presumably mimicking hyperthyroidism (gNa_v=1340 or 2680 and gK_v=108 or 268), spontaneous activity is produced when gK_{ir} remains unaltered. As gK_{ir} is increased, the model's ability to produce normal evoked action potentials at heightened levels of gNa_v and gK_v also increases (3-fold and 5-fold increases in

gK$_{ir}$, Figure 22 top-right and bottom-left, respectively). This alteration rescues the spontaneous activity phenotype otherwise produced by the hyperthyroid state. There are bounds, however, by which gK$_{ir}$ can be increased and still have the model produce normal activity. Increasing gK$_{ir}$ 10-fold results in no evoked activity, regardless of the level of sodium or voltage-gated potassium conductance (Figure 22, bottom right). This suggests that gK$_{ir}$ must be increased during hyperthyroidism to maintain normal electrical activity, but that increasing this too much also results in altered activity.

Figure 21. Possible model outcomes.

Running either the high-throughput or full-scale model with a variety of parameters produces five possible results. After allowing the model to reach steady state, 40Hz stimulation for 250ms (high-throughput model) or 500ms (full-scale model) results in either no evoked action potentials (left top, black), initial failures followed by evoked action potentials (right top, gray, only found in full-scale model), normal evoked action potentials (left middle, green), initially normal evoked action potentials followed by spontaneous activity (right bottom, yellow, only found in full-scale model), and spontaneous high-frequency activity not requiring stimulation (left bottom, red).
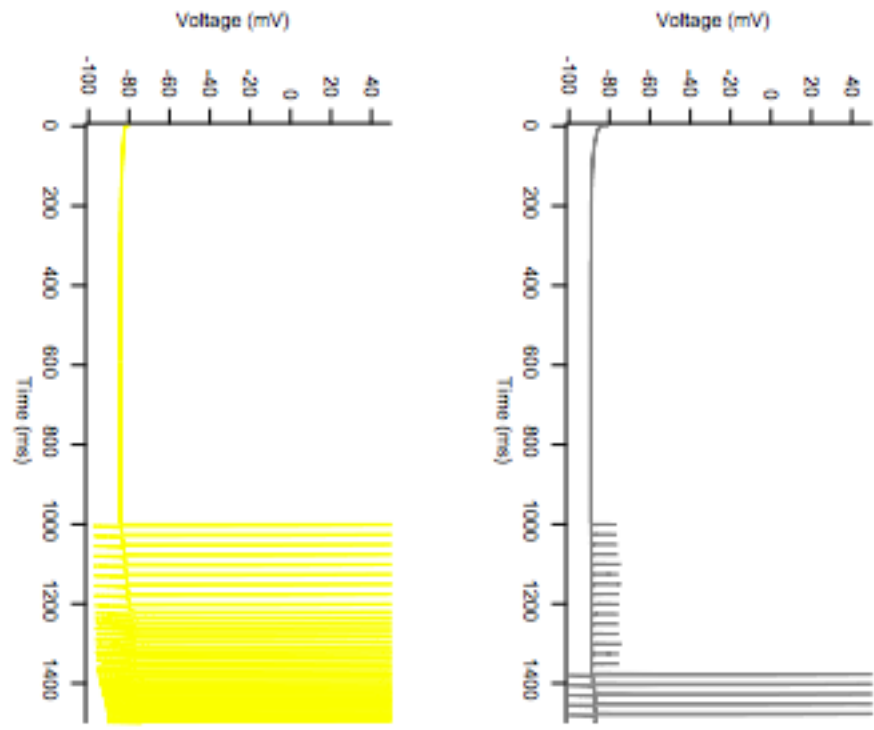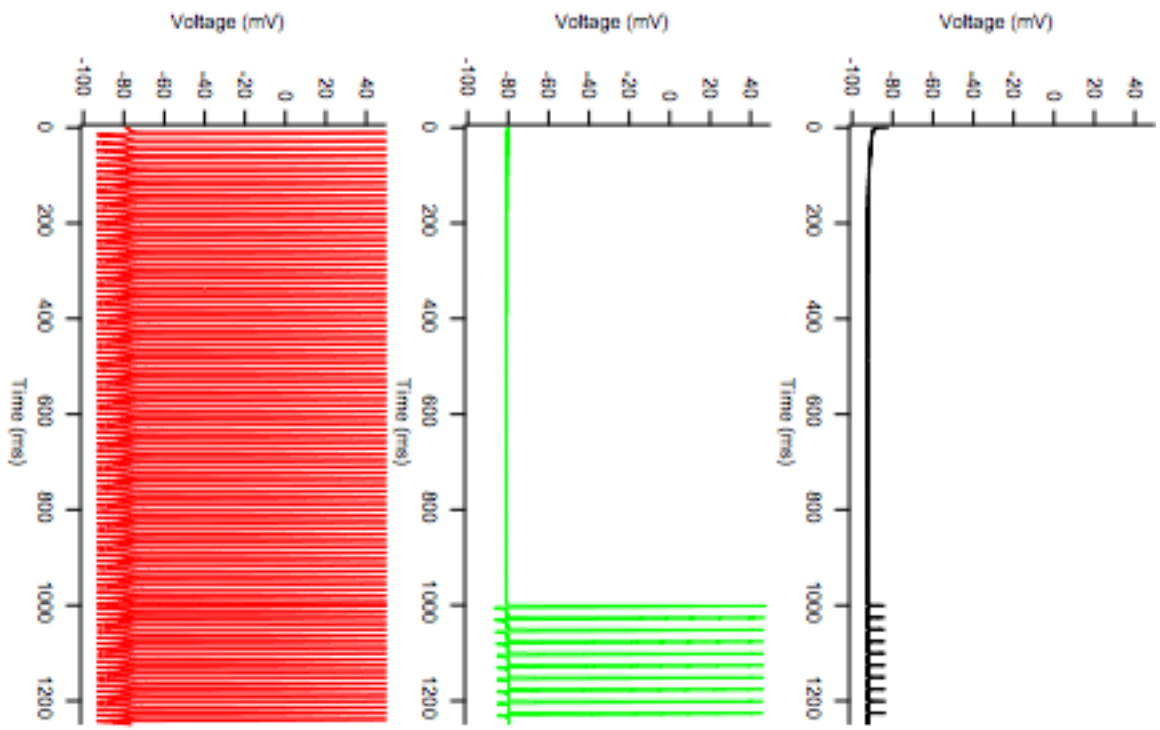
Figure 22. Summary of high-throughput model results.

Circles indicate activity as specified above (Figure 21). gK_{ir} indicates the fold change from default of the inward rectifier potassium channel conductance and applies to each graph independently (default value, top left; 3-fold increase, top right; 5-fold increase, bottom left; 10-fold increase, bottom right) whereas gNa_v and gK_v indicate the current density of voltage-gated sodium and potassium channels in $\mu A/cm^2$, respectively, as specified in Table 8.
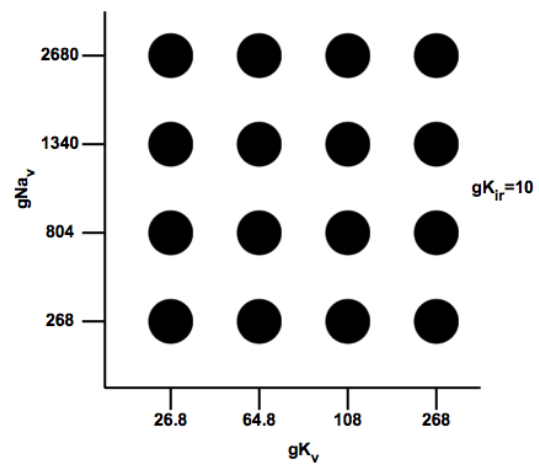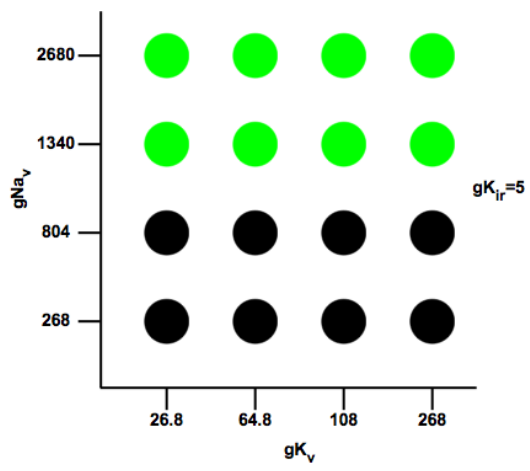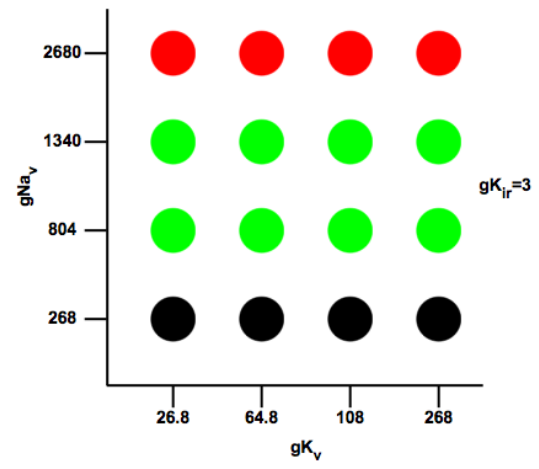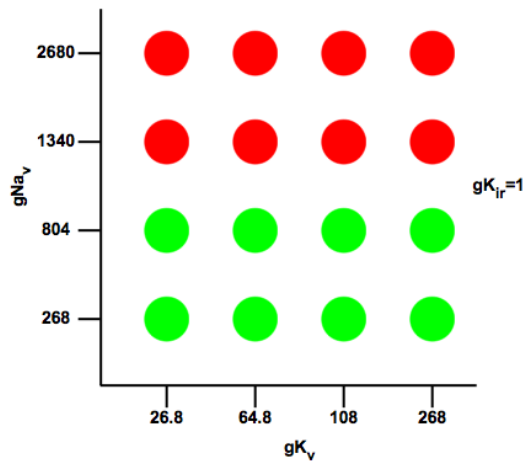
Full-scale model results

We sought to confirm the results from the high-throughput model with the larger full-scale model. Specifically, the exact window within which gK_{ir} must be held during hyperthyroidism was probed. These results recapitulate the results of the high-throughput model (Figure 23). In short, in a hyperthyroid state, a baseline level of gK_{ir} results in spontaneous high-frequency activity. As gK_{ir} is increased, the model transitions into a narrow border region where normal evoked action potentials are initially observed with spontaneous activity developing with further stimulation. Further increases in gK_{ir} results in a window of normal evoked action potentials, as seen in the high-throughput model. Increasing gK_{ir} even further produces another narrow transition region in which action potentials are only evoked after a number of failed stimulations. Finally, further increases in gK_{ir} results in a total absence of evoked action potentials.

We were curious if excess potassium accumulation underlies the models in which normal action potentials are initially produced with spontaneous activity evolving with continued stimulation. As shown below, potassium levels increase dramatically in these models, eventually reaching a plateau above 30mM external potassium within the T-tubular compartments (Figure 24). The amount of accumulation decreases toward the sarcolemmal surface, as would be expected given the clamping of the external milieu at 2mM potassium. The threshold for inducing this spontaneous activity is accumulation of approximately 8.5mM potassium.

Figure 23. Kir conductances must be maintained within a precise window for normal activity during hyperthyroidism.

Sodium and voltage-gated potassium channel conductances were increased to levels presumed to mimic hyperthyroidism (5 or 10-fold increase) in the full-scale model. gK_{ir} conductance was increased up to 10-fold to elucidate the resulting activity type. Notation of activity is in accordance with the graph above (Figure 21).

gNa = 2680 (μA/cm^2), ηK$_{ir}$=1

gK$_v$ (μA/cm^2)

gK$_{ir}$ (fold)

gNa = 1340 (μA/cm^2), ηK$_{ir}$ = 1

gK$_v$ (μA/cm^2)

gK$_{ir}$ (fold)
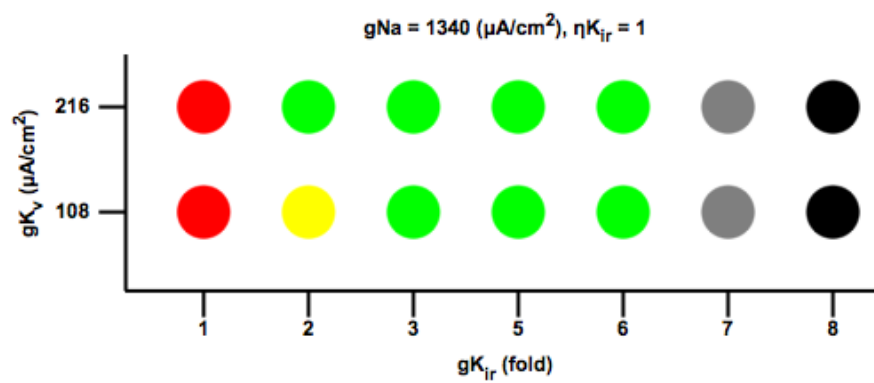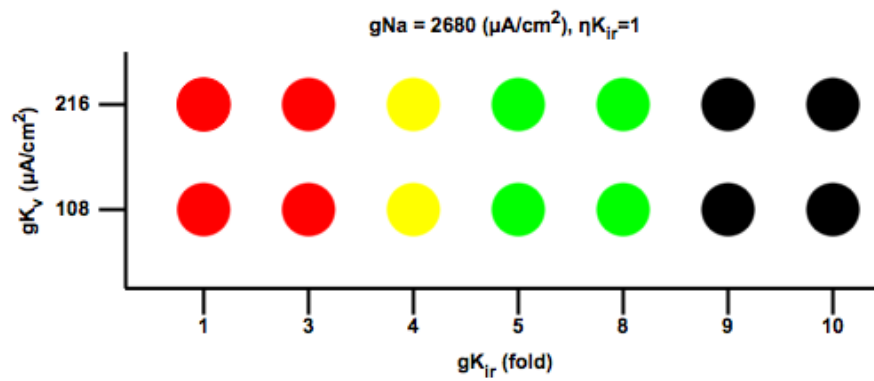
Figure 24. Excess potassium accumulation accompanies spontaneous activity.

T-tubular potassium levels increase with each action potential. During a spontaneous high-frequency train of action potentials potassium levels can increase dramatically. Here, position refers to the distance of the T-tubular compartment from the sarcolemmal surface with $0\mu m$ the outermost compartment. Potassium levels, indicated by the color scale, increase toward the innermost T-tubular compartment. This accumulation corresponds to the activity graphed above (Figure 21, yellow).
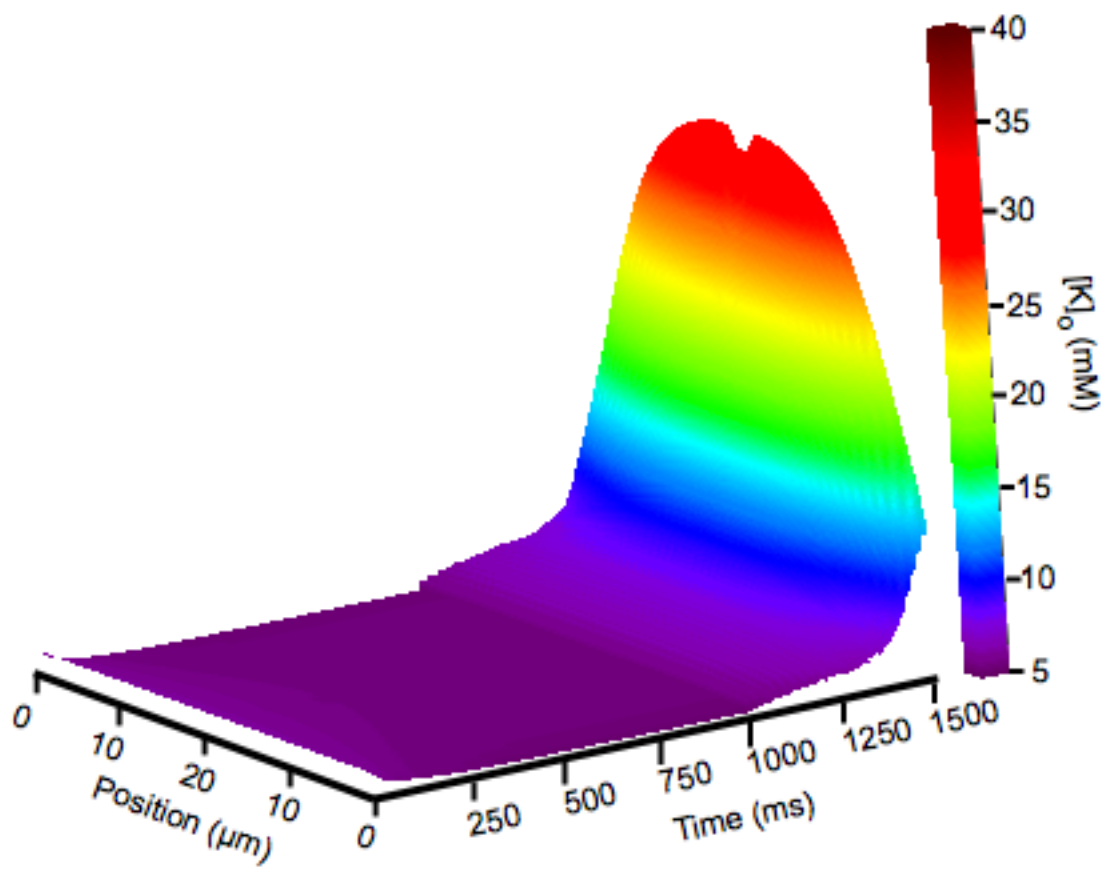
Effect of altering Kir conductance location

We were then curious what would happen if the subcellular localization restriction of Kir2 channels, which are normally concentrated in the T-tubules, is loosened, as predicted from the R399X and Q407X Kir2.6 mutations in TPP patients. We focused on the edges of normal function determined above with our full-scale model. At the highest levels of gK_{ir}, a shift of as little as 5% of Kir conductance from the T-tubules to the sarcolemmal surface can result in altered activation (Figure 25). A larger shift of conductance is required for larger values of gNa. At lower levels of gK_{ir}, a much greater amount of the T-tubular Kir conductance must traffic to the sarcolemmal surface to elicit altered function. In general, it seems that increases in gNa result in needing more gK_v for repolarization and, therefore, more gK_{ir} to clear potassium accumulated in the T-tubules due to current through voltage-gated potassium channels. As there is a 3:1 ratio between the T-tubule and sarcolemmal membrane, the minimum effective ηK_{ir} is 0.75, as this would represent random distribution throughout all compartments.

Figure 25. Small alterations in Kir conductance localization can lead to altered membrane excitability.

The distribution of T-tubular Kir conductances (ηK_{ir}) was varied as indicated with the specified sodium, voltage-gated potassium and inwardly rectifying potassium levels. Activation is indicated as above (Figure 21). A greater shift of ηK_{ir} is required to alter excitability for smaller changes to gK_{ir}. In general, more gK_{ir} is required to compensate for increasing levels of gK_v.

A   gNa = 2680 (µA/cm^2), gK$_V$ = 216 (µA/cm^2)

B   gNa = 2680 (µA/cm^2), gK$_V$ = 108 (µA/cm^2)

C   gNa = 1340 (µA/cm^2), gK$_V$ = 216 (µA/cm^2)

D   gNa = 1340 (µA/cm^2), gK$_V$ = 108 (µA/cm^2)

165
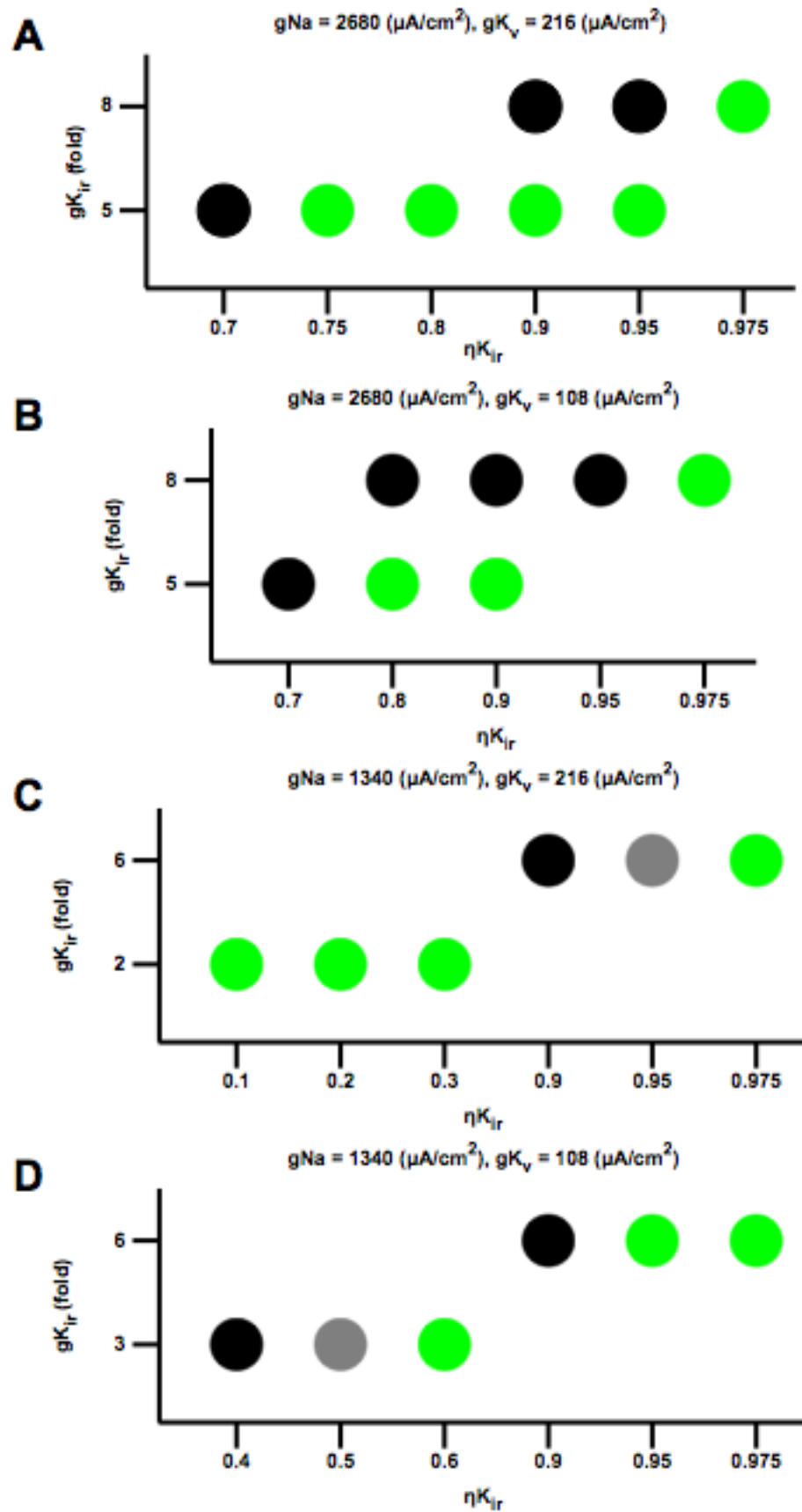
Discussion

Computational methods have previously been used to probe the pathophysiology of skeletal muscle ion channel disorders (Adrian and Peachey, 1973; Cannon et al., 1993). Here, we have modified a previously developed model to test how Kir2.6 mutations might result in the TPP phenotype in skeletal muscle. During hyperthyroidism, voltage-gated sodium, voltage-gated potassium and Kir2.6 levels increase (Harrison and Clausen, 1998; Le Bouter et al., 2003; Ryan et al., 2010). Our most striking finding is that Kir levels must increase to maintain normal excitability in this state. This seems to be due to increased sodium current driving more potassium ions into the T-tubular milieu during repolarization. Kir channels then serve to clear this accumulated potassium and diminishing this ability leads to malfunction.

Malfunction in the T-tubule system is believed to be involved in other skeletal muscle channelopathies. In myotonia congenita, decreased chloride conductance, due to mutated chloride channels, leads to prolonged stimulation initiated but self-sustained trains of action potentials (Adrian and Bryant, 1974; Koch et al., 1992; George et al., 1993). It was observed that decreasing the chloride conductance resulted in a depolarized resting potential after a train of action potentials. This depolarization is not present if the T-tubule system is decoupled from the sarcoplasmic surface, suggesting that ionic accumulation in the T-tubule system exacerbated by altered chloride conductance underlies the disorder. Later computational simulations have confirmed these suspicions (Adrian and Marshall, 1976). A similar situation has been observed in

166

hyperkalemic periodic paralysis caused by sodium channel mutations affecting inactivation (Ptacek et al., 1991; Rojas et al., 1991; Cannon et al., 1993). Here, increased sodium currents increase T-tubular potassium accumulation and result in a greatly depolarized stable state. Without a T-tubular system, these results are not observed.

Our results apply not only to TPP, but also to Andersen-Tawil syndrome, where typically dominant-negative mutations in Kir2.1 can cause a similar periodic paralytic phenotype (Plaster et al., 2001). From our results, it seems that decreased Kir2.1 conductance should not normally lead to significantly altered skeletal muscle physiology, as a small Kir conductance is sufficient to clear accumulated potassium. However, even small increases in sodium or voltage-gated potassium currents due to stressors may lead to enough voltage-gated potassium current that the now depleted pool of Kir channels are unable to clear, resulting in depolarization and disease.

This model demonstrates the importance of potassium accumulation and clearance in the T-tubules to skeletal muscle physiology. Any alteration to skeletal muscle function that alters the balance of voltage-gated potassium channel current and Kir current is likely to lead to altered excitability. Interestingly, alteration of the subcellular localization of Kir conductances also leads to altered excitability, though not through altered potassium accumulation. This model also demonstrates the power of *in silico* methods to complement standard electrophysiology in probing disease pathophysiology. This is true not only because some disorders are difficult, if not impossible, to meaningfully

167

model in mice, but because the speed of these computational methods allows the completion of a larger variety of experiments, the more interesting of which might then be confirmed via standard techniques.

Experimental Procedures

All computations were performed on a 3GHz 686-based personal computer (Intel, Santa Clara, CA). The model has been described previously (Wallinga et al., 1999), and was implemented in Fortran 95/2003 as the original code is no longer available. Parameters were stored in an SQL database (MySQL, www.mysql.com) for which C was used to interconnect. The Gnu Fortran and Gnu C Compilers (GNU, www.gnu.org) were used for compilation. Runge-Kutta with the Cash-Karp adaptive step size was used for numeric integration (Press, 1996). Source code is provided in Appendix II. The maximum time-step for the model was 0.5ms and the maximum current-clamp error was set to 1e-6 μA/cm^2. A maximum of 50,000 iterations were performed per step prior to resorting to classic 4th/5th order Runge-Kutta for numeric integration. For the high-throughput model, the simulation was allowed to rest for 1000ms prior to 40Hz stimulation for 250ms. For the full-scale model the stimulation lasted for a total of 500ms. 64-bit IEEE floating point arithmetic was used for all calculations. Classic 4th order Runge-Kutta was performed after each step to compute the change in accumulated potassium.

Acknowledgements

CHAPTER 5

Dead ends, loose ends, and future questions

Dead ends

Copy number variations (CNVs) are segments of DNA, from 1 kilobase (Kb) to several megabases (Mb) in length, which show variability in number across multiple genomes. CNVs can cause either an increase (duplication) or decrease (deletion) in the relative copy number of a gene or genes in a region. CNVs have been of recent interest in disease research, as some are associated with neurologic and psychiatric disorders, such as early onset Alzheimer's disease, schizophrenia, bipolar disorder, autosomal dominant leukodystrophy, and Parkinson's disease (Lee and Lupski, 2006; Padiath et al., 2006; Cook and Scherer, 2008). In humans, CNVs are particularly enriched around segmental duplications in the pericentromeric region (Goidts et al., 2006). These regions also constitute a large percentage of the difference between the human and great ape genomes (Marques-Bonet et al., 2009).

KCNJ18 seems to have arisen recently in evolutionary time, with presence in humans and some other great apes, but not non-primates. Interestingly, *KCNJ18* seems to have arisen due to a pericentromeric segmental duplication (Figure 26). We wondered if copy number variations in it might be associated with TPP and might account for cases where *KCNJ18* mutations are not present. To that end, we formed a collaboration with Evan Eichler's lab at the University of Washington and helped in the design of probes against the bacterial artificial chromosome (BAC) containing *KCNJ18*. We sent 15 DNA samples from TPP

patients who lack KCNJ18 mutations, 11 samples from patients with paroxysmal kinesigenic dyskinesia (PKD), 3 samples from patients with spinocerebellar ataxia type-4 (SCA4), and 3 samples from patients with familial adult myoclonic epilepsy (FAME) for array comparative genomics hybridization (aCGH) analysis with a particular focus on the area around *KCNJ18*. Analysis of the results was performed in a blinded manner. The aCGH analysis suggested a number of deletion events around *KCNJ18*, however upon unblinding none of these were correlated specifically with TPP and, in fact, tended to cluster around a group of DNAs, suggesting the results are spurious (Table 9). A similar result was found for other locations and the other disorders probed (not shown). This indicates that copy number variations of *KCNJ18* are unlikely to be causative for TPP.

Figure 26. Comparison of BACs for KCNJ12 and KCNJ18.

The BACs containing *KCNJ12* (RP-11728E14) and *KCNJ18* (RP11-437N10) were compared with miropeats (http://www.genome.ou.edu/miropeats.html). The width of each rectangle on the BACs indicates the width of the duplication between the BACs, with a 1Kb minimum. Lines connect the relative placement of these duplication within each BAC. For reference, *KCNJ12*/*KCNJ18* lie at the edge of the black duplication with exon 1 being unique.

RP11-728E14

RP11-437N10

0.0   100.0   200.0 KBases

172
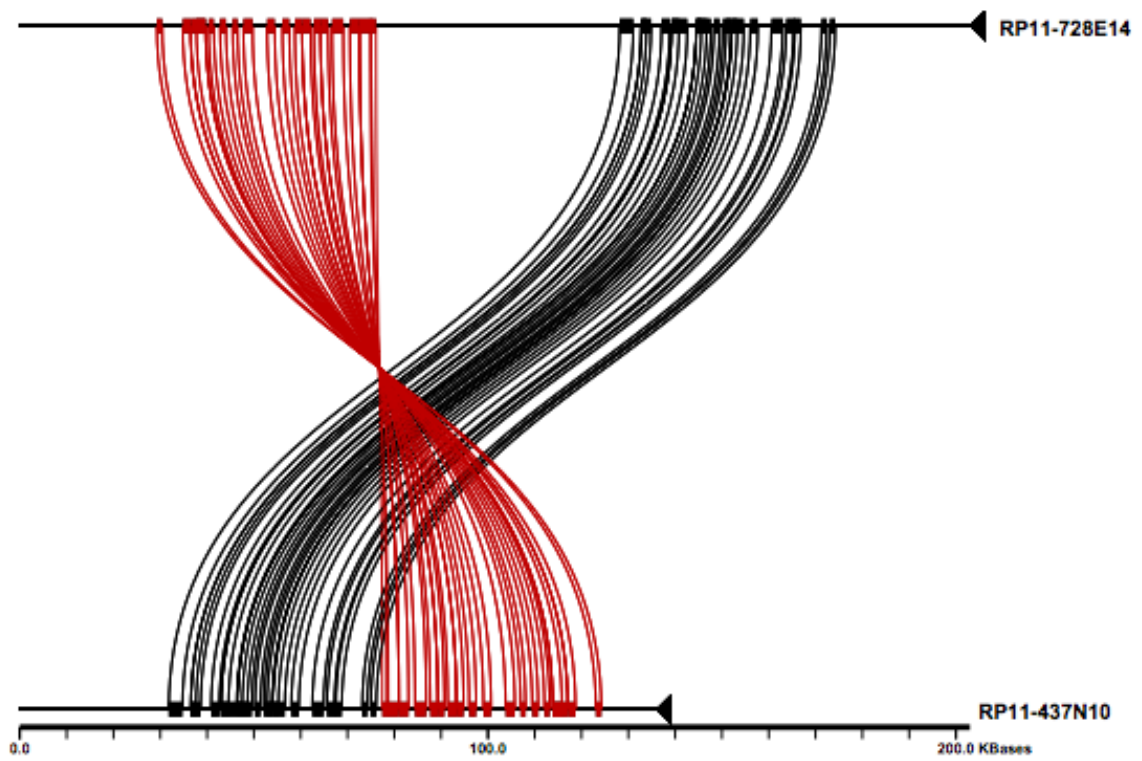
Table 9. Significant aCGH results for all samples around KCNJ18.

Kindred #DNA	Disease	Position #1 z-score	Position #2 z-score
2694 #20711	TPP	-2.00	-2.12
3735 #25251	TPP		
4512 #29128	TPP	-0.99	-0.91
4611 #29744	TPP	-1.13	-0.94
50044 #100363	TPP	-1.35	-1.21
50045 #100368	TPP	-1.23	-1.22
50096 #100798	TPP	-2.23	-2.00
7450 #45426	TPP	-2.10	-2.28
7958 #48528	TPP	-2.29	-2.61
7958 #48527	TPP	-0.98	-1.02
7958 #48526	TPP	-1.94	-2.08
7962 #50281	TPP	-0.80	-0.40
7963 #48537	TPP		
9149 #52641	TPP	-1.65	-2.14
9661 #57425	TPP	0.19	0.35
5471 #34767	PKD	-1.26	-1.40
4874 #35104	PKD	0.01	-0.18
4962 #31786	PKD	-0.89	-0.83
3391 #23880	PKD	-2.3	-1.75
3323 #35090	PKD	-1.21	-0.96
3534 #24322	PKD	-1.59	-2.25
3538 #24624	PKD	-1.88	-1.82
3446 #24129	PKD	0.32	0.86
5212 #33237	PKD	-1.18	-0.74
2916 #22890	PKD	-0.92	-1.90
3994 #27376	PKD	-1.97	-1.61
1875 #13297	SCA4	-1.94	
1875 #18957	SCA4	-1.40	-1.99
1875 #17275	SCA4	-0.54	-0.84
3782 #25441	FAME	-2.18	-1.99
3783 #25445	FAME	-0.84	-0.95
3780 #25425	FAME	0.73	

Position #1 is bases 4202-6201 and position #2 is bases 35231-37815 of the NCBI sequence of BAC RP11-437N10. TPP: thyrotoxic hypokalemic periodic paralysis, PKD: paroxysmal kinesigenic dyskinesia, SCA4: spinocerebellar ataxia type-4, FAME: familial adult myoclonic epilepsy. Highlighted cells indicate a statistically significant change.

Loose Ends

I was curious if the R399X and Q407X mutations result in altered subcellular localization. Firstly, I transfected EGFP fused wild-type and mutant channels into C2C12 cell, which are derived from mouse myotubes. Interestingly, both mutant and wild-type channels traffic efficiently to the membrane with no obvious subcellular distribution. The likely reason for this is the lack of a coherent t-tubular system in C2C12 cells when compared to native skeletal muscle. I then became interested in using native mouse skeletal muscle infected with a virus delivering wild-type or mutant Kir2.6, but unmodified human Kir2.6 does not traffic appropriately in native rodent skeletal muscle (C. Vandenberg, personal communication). Consequently, I sought out primate skeletal muscle with which to probe subcellular localization.

Skeletal muscle was harvested from the extensor digitorum longus of two Macaques by Jonathon Horton's lab. This tissue was digested and cultured as described previously (Partridge, 1997). Kir2.6 was modified to contain a hemagglutinin (HA) epitope tag on its extracellular surface (primers: 5'-'ccatatgacgtgcctgactatgctggaggCCACGGCCGCACACC-3', 5'-agtcaggcacgtcatatgggtagccaccGCCCTCAGCCGGCTCC-3') and subcloned into pSicoR from Tyler Jacks (Ventura et al., 2004). Immunofluorescence demonstrated that this tissue has an extremely high background fluorescence intensity, which is also seen in other native skeletal muscle samples (H. Bernstein, personal communication). I was unable to find a fluorophore outside the range of macaque skeletal muscle autofluorescence. This made it impossible

to discern signal from background. Hopefully future studies will be able to surmount this hurdle, either with different fluorophores or using a different source of skeletal muscle.

I have previously shown that activation of PKC results in a decreased open probability of wild-type but not mutant T354M Kir2.6 (Ryan et al., 2010). I sought to demonstrate that PKC directly phosphorylates T354 by constructing a fusion protein of the C-terminus of Kir2.6 to Glutathione S-transferase (GST) in the pGex-6P1 vector (GE Healthcare). Both the wild-type and mutant constructs were then transfected into Rosetta cells (EMD Biosciences), grown until reaching an OD_{600} of 0.6-2.0, and expression induced with IPTG for three hours at 37°C. The fusion protein was then extracted, bound to GST-beads, and washed according to the manufacturers protocol. Some batches were then digested with PreScission protease (GE Healthcare) according to the manufacturers directions. The purified protein was then incubated in kinase buffer and PKC-θ (Calbiochem) with radioactive ATP according to the manufacturers instructions. Both the GST fused wild-type and mutant proteins showed significant radioactive signal. Cutting the protein with PreScission protease produced a much fainter band that was also present in both the wild-type and mutant proteins, suggesting that there are likely multiple phosphorylation sites on the C-terminus, with T354 being just one, or that the PKC used phosphorylates Serines or Threonines in a non-specific manner. Future studies with either other PKC isotypes or further mutated C-terminal segments may be able to surmount this issue.

Future Questions

In this thesis I describe the discovery of a novel inwardly rectifying ion channel, Kir2.6, and mutations in it associated with TPP. I have described how many of these mutations alter Kir2.6 function and created a theory as to how alteration of Kir2.6 function might lead to TPP. I have also shown that Kir2.6 can heteromultimerize with at least some other Kir channels found in skeletal muscle, providing a mechanism for TPP mutations to affect a larger population of channels. I have, furthermore, used a computational model to demonstrate that mutations in Kir2.6 lead to TPP through either the alteration of T-tubular potassium clearance or due to an inability of normal stimulation to lead to action potential initiation due to altered Kir channel subcellular localization. However, many questions remain.

Firstly, as discussed above, it has not been demonstrated that either the R399X or Q407X mutations result in altered subcellular localization. Kir2.6 is presumed to localize in the T-tubular membrane (Leonoudakis et al., 2004a; Leonoudakis et al., 2004b). Firstly, this will need to be demonstrated, which will be complicated as the creation of an antibody that distinguishes Kir2.2 and Kir2.6 is not trivial. Secondly, while some primates seem to have a *KCNJ18* in their genome, it has not been shown that this is expressed. An epitope tagged channel could be infected into native tissue, as attempted above, but care will have to be taken to ensure that an observed affect is not spurious and due to overexpression.

Increased PIP_2 turnover and PKC activation have previously been described as non-genomic effects of hyperthyroidism (Lin et al., 1999; Kavok et al., 2001). While I have demonstrated that some TPP mutations result in altered sensitivity to these effects, it is unclear what the exact change in PIP_2 turnover or PKC activation is as a function of time. Specifically, while some mutations in Kir2.6 (R205H and K366R) result in altered PIP_2 interaction, is the change in PIP_2 turnover during hyperthyroidism sufficient for this to result in TPP? Similarly, is the change in PKC activation over time sufficient for Kir2.6 channels with the T354M to produce enough extra current to result in TPP? The most direct method for testing these questions would be to obtain skeletal muscle biopsies from patients. This would also allow the direct comparison of *in silico* results (CHAPTER 4) to *in vivo* results and the direct determination, in humans, of the affect of hyperthyroidism on sodium and potassium channel levels.

I have shown using electrophysiology that Kir2.6 can coassemble with at least some other Kir channels expressed in skeletal muscle (CHAPTER 3). The first obvious follow-up would be to see if immunoprecipitation of one subunit type in an electrophysiologically indicated heteromultimer also results in precipitation of other subunit types. This seems quite likely from previous results, but have not been shown.

Kir2.2 from chicken, which shares a high degree of identity to human Kir2.6, has recently been crystallized (Tao et al., 2009). This opens the possibility both for modeling mutations onto the current structure and the creation of new structures from the same protocol. Modeling of the R205H onto the available

structure has already resulted in one interesting prediction (Figure 27). It seems that the Arginine in position 205 does not interact directly with PIP_2 in the membrane. Rather, it seems to form an inter-subunit hydrogen bond with E242 that is absent in the case of the R205H mutation. One prediction would be that this inter-subunit bond is helpful in aiding gating movements and that the R205H mutation alters the energetics of these conformational changes. Direct crystallization of TPP mutation containing constructs may yield other interesting results.

Figure 27. R205 in the chicken Kir2.2 crystal structure forms an inter-subunit hydrogen bond.

The crystal structure of chicken Kir2.2 (PDB 3JYC) with each subunit colored uniquely, top, shows that there is a hydrogen bond between R205 (red) and E242 (green) indicated by a light blue line. Modeling a Histidine into this position, bottom, removes the inter-subunit bond.
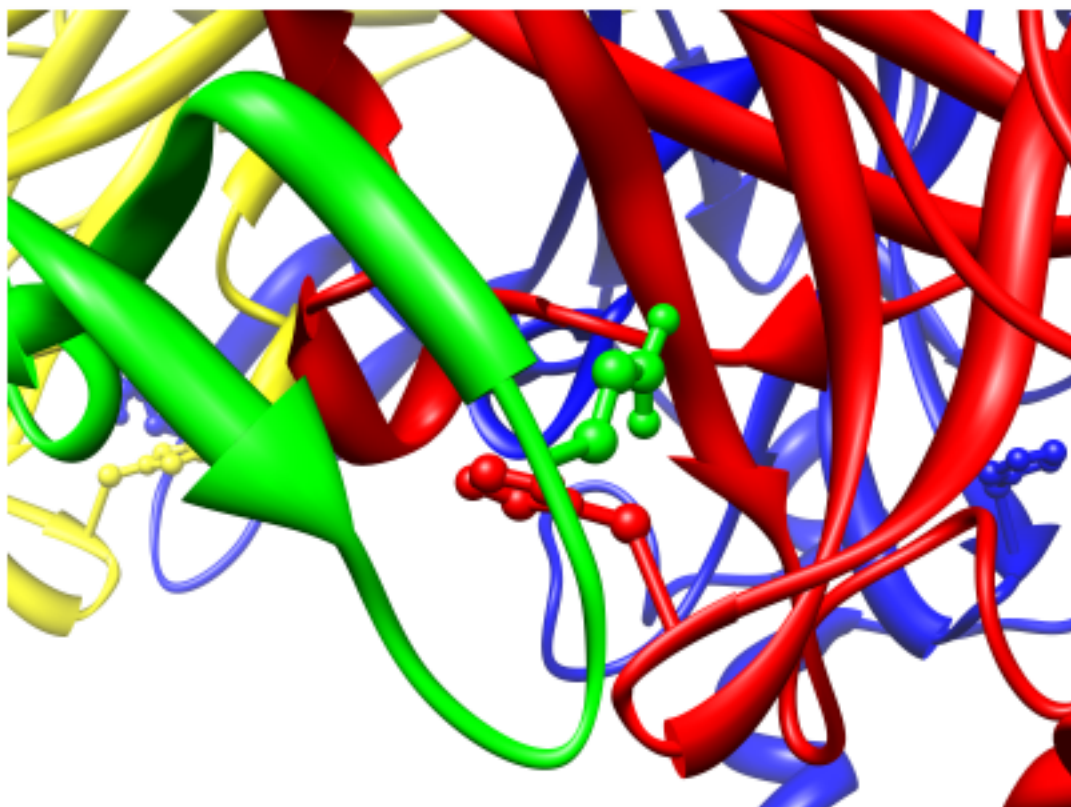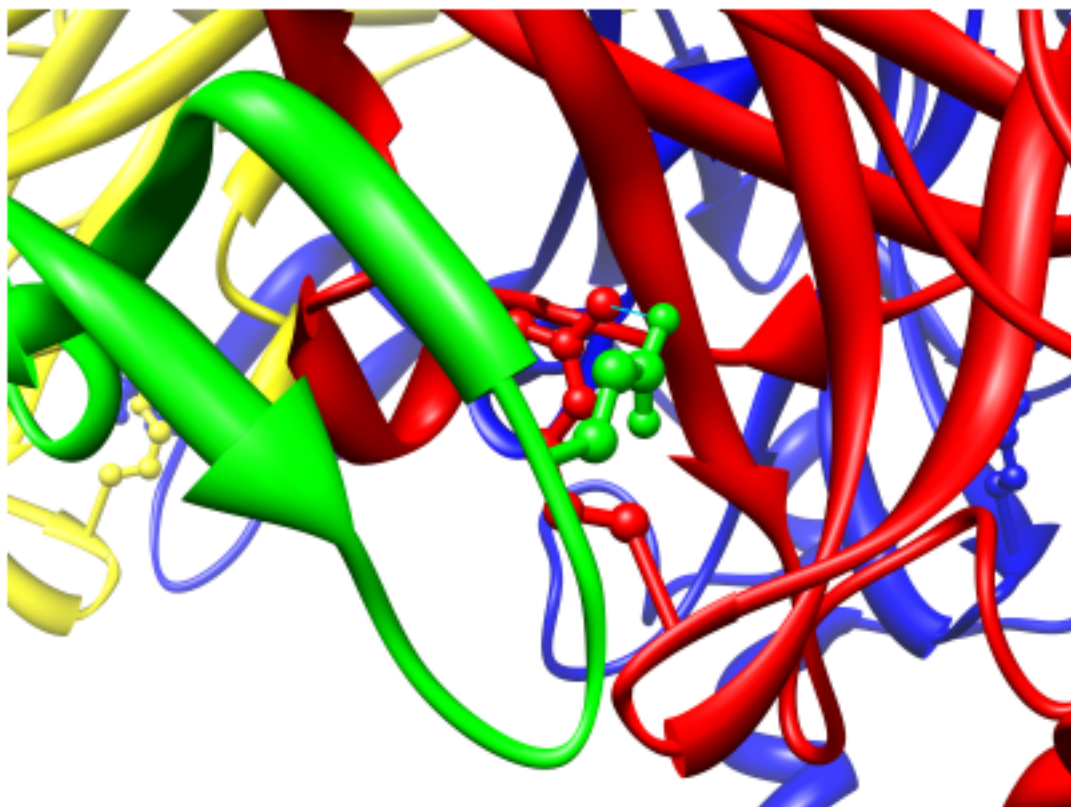
REFERENCES

Abraham, M. R., Jahangir, A., Alekseev, A. E. and Terzic, A. (1999). Channelopathies of inwardly rectifying potassium channels. Faseb J 13, 1901-1910.

Adrian, R. H. and Bryant, S. H. (1974). On the repetitive discharge in myotonic muscle fibres. J Physiol 240, 505-515.

Adrian, R. H., Chandler, W. K. and Hodgkin, A. L. (1970). Voltage clamp experiments in striated muscle fibres. J Physiol 208, 607-644.

Adrian, R. H. and Marshall, M. W. (1976). Action potentials reconstructed in normal and myotonic muscle fibres. J Physiol 258, 125-143.

Adrian, R. H. and Peachey, L. D. (1973). Reconstruction of the action potential of frog sartorius muscle. J Physiol 235, 103-131.

Bailey, J. A., Yavor, A. M., Massa, H. F., Trask, B. J. and Eichler, E. E. (2001). Segmental duplications: organization and impact within the current human genome project assembly. Genome Res 11, 1005-1017.

Bassett, J. H., Harvey, C. B. and Williams, G. R. (2003). Mechanisms of thyroid hormone receptor-specific nuclear and extra nuclear actions. Mol Cell Endocrinol 213, 1-11.

Bond, C. T., Pessia, M., Xia, X. M., Lagrutta, A., Kavanaugh, M. P. and Adelman, J. P. (1994). Cloning and expression of a family of inward rectifier potassium channels. Receptors Channels 2, 183-191.

Bulman, D. E., Scoggan, K. A., van Oene, M. D., Nicolle, M. W., Hahn, A. F., Tollar, L. L. and Ebers, G. C. (1999). A novel sodium channel mutation in a family with hypokalemic periodic paralysis. Neurology 53, 1932-1936.

Cannon, S. C., Brown, R. H., Jr. and Corey, D. P. (1993). Theoretical reconstruction of myotonia and paralysis caused by incomplete inactivation of sodium channels. Biophys J 65, 270-288.

Catterall, W. A. (2000). From ionic currents to molecular mechanisms: the structure and function of voltage-gated sodium channels. Neuron 26, 13-25.

Clark, R. B., Tremblay, A., Melnyk, P., Allen, B. G., Giles, W. R. and Fiset, C. (2001). T-tubule localization of the inward-rectifier K(+) channel in mouse ventricular myocytes: a role in K(+) accumulation. J Physiol 537, 979-992.

Cook, E. H., Jr. and Scherer, S. W. (2008). Copy-number variations associated with neuropsychiatric conditions. Nature 455, 919-923.

Cui, Y., Giblin, J. P., Clapp, L. H. and Tinker, A. (2001). A mechanism for ATP-sensitive potassium channel diversity: Functional coassembly of two pore-forming subunits. Proc Natl Acad Sci U S A 98, 729-734.

Curtis, H. J. and Cole, K. S. (1938). Transverse Electric Impedance of the Squid Giant Axon. J Gen Physiol 21, 757-765.

Derst, C., Karschin, C., Wischmeyer, E., Hirsch, J. R., Preisig-Muller, R., Rajan, S., Engel, H., Grzeschik, K., Daut, J. and Karschin, A. (2001). Genetic and

functional linkage of Kir5.1 and Kir2.1 channel subunits. FEBS Lett 491, 305-311.

Donaldson, M. R., Jensen, J. L., Tristani-Firouzi, M., Tawil, R., Bendahhou, S., Suarez, W. A., Cobo, A. M., Poza, J. J., Behr, E., Wagstaff, J*., et al.* (2003). PIP2 binding residues of Kir2.1 are common targets of mutations causing Andersen syndrome. Neurology 60, 1811-1816.

Dutzler, R. (2006). The ClC family of chloride channels and transporters. Curr Opin Struct Biol 16, 439-446.

Eichler, E. E., Clark, R. A. and She, X. (2004). An assessment of the sequence gaps: unfinished business in a finished human genome. Nat Rev Genet 5, 345-354.

Fakler, B., Bond, C. T., Adelman, J. P. and Ruppersberg, J. P. (1996). Heterooligomeric assembly of inward-rectifier K+ channels from subunits of different subfamilies: Kir2.1 (IRK1) and Kir4.1 (BIR10). Pflugers Arch 433, 77-83.

George, A. L., Jr., Crackower, M. A., Abdalla, J. A., Hudson, A. J. and Ebers, G. C. (1993). Molecular basis of Thomsen's disease (autosomal dominant myotonia congenita). Nat Genet 3, 305-310.

Glowatzki, E., Fakler, G., Brandle, U., Rexhausen, U., Zenner, H. P., Ruppersberg, J. P. and Fakler, B. (1995). Subunit-dependent assembly of inward-rectifier K+ channels. Proc Biol Sci 261, 251-261.

Goidts, V., Cooper, D. N., Armengol, L., Schempp, W., Conroy, J., Estivill, X., Nowak, N., Hameister, H. and Kehrer-Sawatzki, H. (2006). Complex patterns of copy number variation at sites of segmental duplications: an important category of structural variation in the human genome. Hum Genet 120, 270-284.

Grottesi, A., Sands, Z. A. and Sansom, M. S. (2005). Potassium channels: complete and undistorted. Curr Biol 15, R771-774.

Harrison, A. P. and Clausen, T. (1998). Thyroid hormone-induced upregulation of Na+ channels and Na(+)-K+ pumps: implications for contractility. Am J Physiol 274, R864-867.

Heginbotham, L., Lu, Z., Abramson, T. and MacKinnon, R. (1994). Mutations in the K+ channel signature sequence. Biophys J 66, 1061-1067.

Henneberg, K. A. and Roberge, F. A. (1997). Simulation of propagation along an isolated skeletal muscle fiber in an isotropic volume conductor. Ann Biomed Eng 25, 5-28.

Hodgkin, A. L. and Huxley, A. F. (1952). A quantitative description of membrane current and its application to conduction and excitation in nerve. J Physiol 117, 500-544.

Hodgkin, A. L. and Rushton, W. A. H. (1946). The Electrical Constants of a Crustacean Nerve Fibre. Proc Roy Soc Lond B 133, 444-479.

Hugnot, J. P., Pedeutour, F., Le Calvez, C., Grosgeorge, J., Passage, E., Fontes, M. and Lazdunski, M. (1997). The human inward rectifying K+ channel Kir 2.2 (KCNJ12) gene: gene structure, assignment to chromosome 17p11.1, and identification of a simple tandem repeat polymorphism. Genomics 39, 113-116.

Inagaki, N., Tsuura, Y., Namba, N., Masuda, K., Gonoi, T., Horie, M., Seino, Y., Mizuta, M. and Seino, S. (1995). Cloning and functional characterization of a novel ATP-sensitive potassium channel ubiquitously expressed in rat tissues, including pancreatic islets, pituitary, skeletal muscle, and heart. J Biol Chem 270, 5691-5694.

Isacoff, E. Y., Jan, Y. N. and Jan, L. Y. (1990). Evidence for the formation of heteromultimeric potassium channels in Xenopus oocytes. Nature 345, 530-534.

Ishihara, K., Yamamoto, T. and Kubo, Y. (2009). Heteromeric assembly of inward rectifier channel subunit Kir2.1 with Kir3.1 and with Kir3.4. Biochem Biophys Res Commun 380, 832-837.

Isomoto, S., Kondo, C., Takahashi, N., Matsumoto, S., Yamada, M., Takumi, T., Horio, Y. and Kurachi, Y. (1996). A novel ubiquitously distributed isoform of GIRK2 (GIRK2B) enhances GIRK1 expression of the G-protein-gated K+ current in Xenopus oocytes. Biochem Biophys Res Commun 218, 286-291.

Jan, L. Y. and Jan, Y. N. (1997). Cloned potassium channels from eukaryotes and prokaryotes. Annu Rev Neurosci 20, 91-123.

Karle, C. A., Zitron, E., Zhang, W., Wendt-Nordahl, G., Kathofer, S., Thomas, D., Gut, B., Scholz, E., Vahl, C. F., Katus, H. A. and Kiehn, J. (2002). Human cardiac inwardly-rectifying K+ channel Kir(2.1b) is inhibited by direct protein kinase C-dependent regulation in human isolated cardiomyocytes and in an expression system. Circulation 106, 1493-1499.

Kavok, N. S., Krasilnikova, O. A. and Babenko, N. A. (2001). Thyroxine signal transduction in liver cells involves phospholipase C and phospholipase D activation. Genomic independent action of thyroid hormone. BMC Cell Biol 2, 5.

Kelley, D. E., Gharib, H., Kennedy, F. P., Duda, R. J., Jr. and McManis, P. G. (1989). Thyrotoxic periodic paralysis. Report of 10 cases and review of electromyographic findings. Arch Intern Med 149, 2597-2600.

Koch, M. C., Steinmeyer, K., Lorenz, C., Ricker, K., Wolf, F., Otto, M., Zoll, B., Lehmann-Horn, F., Grzeschik, K. H. and Jentsch, T. J. (1992). The skeletal muscle chloride channel in dominant and recessive human myotonia. Science 257, 797-800.

Kondo, C., Isomoto, S., Matsumoto, S., Yamada, M., Horio, Y., Yamashita, S., Takemura-Kameda, K., Matsuzawa, Y. and Kurachi, Y. (1996). Cloning and functional expression of a novel isoform of ROMK inwardly rectifying ATP-dependent K+ channel, ROMK6 (Kir1.1f). FEBS Lett 399, 122-126.

Kono, Y., Horie, M., Takano, M., Otani, H., Xie, L. H., Akao, M., Tsuji, K. and Sasayama, S. (2000). The properties of the Kir6.1-6.2 tandem channel co-expressed with SUR2A. Pflugers Arch 440, 692-698.

Konstas, A. A., Korbmacher, C. and Tucker, S. J. (2003). Identification of domains that control the heteromeric assembly of Kir5.1/Kir4.0 potassium channels. Am J Physiol Cell Physiol 284, C910-917.

Krapivinsky, G., Krapivinsky, L., Wickman, K. and Clapham, D. E. (1995). G beta gamma binds directly to the G protein-gated K+ channel, IKACh. J Biol Chem 270, 29059-29062.

Krapivinsky, G., Medina, I., Eng, L., Krapivinsky, L., Yang, Y. and Clapham, D. E. (1998). A novel inward rectifier K+ channel with unique pore properties. Neuron 20, 995-1005.

Kung, A. W. (2002). Thyrotoxic Periodic Paralysis., In Oxford textbook of endocrinology and diabetes, J. A. H. Wass, S. M. Shalet, and E. A. M. Gale, eds. (Oxford ; New York: Oxford University Press), pp. 427-429.

Kung, A. W. (2006). Clinical review: Thyrotoxic periodic paralysis: a diagnostic challenge. J Clin Endocrinol Metab 91, 2490-2495.

Lapicque, L. (2007). Quantitative investigations of electrical nerve excitation treated as polarization. 1907. Biol Cybern 97, 341-349.

Le Bouter, S., Demolombe, S., Chambellan, A., Bellocq, C., Aimond, F., Toumaniantz, G., Lande, G., Siavoshian, S., Baro, I., Pond, A. L.*, et al.* (2003). Microarray analysis reveals complex remodeling of cardiac ion channel expression with altered thyroid status: relation to cellular and integrated electrophysiology. Circ Res 92, 234-242.

Lee, J. A. and Lupski, J. R. (2006). Genomic rearrangements and gene copy-number alterations as a cause of nervous system disorders. Neuron 52, 103-121.

Leonoudakis, D., Conti, L. R., Anderson, S., Radeke, C. M., McGuire, L. M., Adams, M. E., Froehner, S. C., Yates, J. R., 3rd and Vandenberg, C. A. (2004a). Protein trafficking and anchoring complexes revealed by proteomic analysis of inward rectifier potassium channel (Kir2.x)-associated proteins. J Biol Chem 279, 22331-22346.

Leonoudakis, D., Conti, L. R., Radeke, C. M., McGuire, L. M. and Vandenberg, C. A. (2004b). A multiprotein trafficking complex composed of SAP97, CASK, Veli, and Mint1 is associated with inward rectifier Kir2 potassium channels. J Biol Chem 279, 19051-19063.

Leonoudakis, D., Mailliard, W., Wingerd, K., Clegg, D. and Vandenberg, C. (2001). Inward rectifier potassium channel Kir2.2 is associated with synapse-associated protein SAP97. J Cell Sci 114, 987-998.

Liman, E. R., Tytgat, J. and Hess, P. (1992). Subunit stoichiometry of a mammalian K+ channel determined by construction of multimeric cDNAs. Neuron 9, 861-871.

Lin, H. Y., Davis, F. B., Gordinier, J. K., Martino, L. J. and Davis, P. J. (1999). Thyroid hormone induces activation of mitogen-activated protein kinase in cultured cells. Am J Physiol 276, C1014-1024.

Lipicky, R. J., Bryant, S. H. and Salmon, J. H. (1971). Cable parameters, sodium, potassium, chloride, and water content, and potassium efflux in isolated external intercostal muscle of normal volunteers and patients with myotonia congenita. J Clin Invest 50, 2091-2103.

Long, S. B., Campbell, E. B. and Mackinnon, R. (2005). Crystal structure of a mammalian voltage-dependent Shaker family K+ channel. Science 309, 897-903.

Lopes, C. M., Zhang, H., Rohacs, T., Jin, T., Yang, J. and Logothetis, D. E. (2002). Alterations in conserved Kir channel-PIP2 interactions underlie channelopathies. Neuron 34, 933-944.

Lu, Z. (2004). Mechanism of rectification in inward-rectifier K+ channels. Annu Rev Physiol 66, 103-129.

Marques-Bonet, T., Kidd, J. M., Ventura, M., Graves, T. A., Cheng, Z., Hillier, L. W., Jiang, Z., Baker, C., Malfavon-Borja, R., Fulton, L. A*., et al.* (2009). A burst of segmental duplications in the genome of the African great ape ancestor. Nature 457, 877-881.

Miller, C. (2006). ClC chloride channels viewed through a transporter lens. Nature 440, 484-489.

Namba, N., Inagaki, N., Gonoi, T., Seino, Y. and Seino, S. (1996). Kir2.2v: a possible negative regulator of the inwardly rectifying K+ channel Kir2.2. FEBS Lett 386, 211-214.

Namba, N., Mori, R., Tanaka, H., Kondo, I., Narahara, K. and Seino, Y. (1997). The inwardly rectifying potassium channel subunit Kir2.2v (KCNJN1) maps to 17p11.2-->p11.1. Cytogenet Cell Genet 79, 85-87.

Nemzek, J. A., Kruger, J. M., Walshaw, R. and Hauptman, J. G. (1994). Acute onset of hypokalemia and muscular weakness in four hyperthyroid cats. J Am Vet Med Assoc 205, 65-68.

Nichols, C. G. and Lopatin, A. N. (1997). Inward rectifier potassium channels. Annu Rev Physiol 59, 171-191.

Padiath, Q. S., Saigoh, K., Schiffmann, R., Asahara, H., Yamada, T., Koeppen, A., Hogan, K., Ptacek, L. J. and Fu, Y. H. (2006). Lamin B1 duplications cause autosomal dominant leukodystrophy. Nat Genet 38, 1114-1123.

Partridge, T. A. (1997). Tissue Culture of Skeletal Muscle, In Basic Cell Culture Protocols, J. W. Pollard, and J. M. Walker, eds. (Totowa, NJ: Humana Press Inc.), pp. 131-144.

Peachey, L. D. (1965). The sarcoplasmic reticulum and transverse tubules of the frog's sartorius. J Cell Biol 25, Suppl:209-231.

Pessia, M., Tucker, S. J., Lee, K., Bond, C. T. and Adelman, J. P. (1996). Subunit positional effects revealed by novel heteromeric inwardly rectifying K+ channels. Embo J 15, 2980-2987.

Plaster, N. M., Tawil, R., Tristani-Firouzi, M., Canun, S., Bendahhou, S., Tsunoda, A., Donaldson, M. R., Iannaccone, S. T., Brunt, E., Barohn, R*., et al.* (2001). Mutations in Kir2.1 cause the developmental and episodic electrical phenotypes of Andersen's syndrome. Cell 105, 511-519.

Preisig-Muller, R., Schlichthorl, G., Goerge, T., Heinen, S., Bruggemann, A., Rajan, S., Derst, C., Veh, R. W. and Daut, J. (2002). Heteromerization of Kir2.x potassium channels contributes to the phenotype of Andersen's syndrome. Proc Natl Acad Sci U S A 99, 7774-7779.

Press, W. (1996). Numerical Recipes in Fortran 90, Vol 2, 2 edn (Cambridge: Cambridge University Press).

Ptacek, L. J., George, A. L., Jr., Griggs, R. C., Tawil, R., Kallen, R. G., Barchi, R. L., Robertson, M. and Leppert, M. F. (1991). Identification of a mutation in the gene causing hyperkalemic periodic paralysis. Cell 67, 1021-1027.

185

Ptacek, L. J., Tawil, R., Griggs, R. C., Engel, A. G., Layzer, R. B., Kwiecinski, H., McManis, P. G., Santiago, L., Moore, M., Fouad, G. and et al. (1994). Dihydropyridine receptor mutations cause hypokalemic periodic paralysis. Cell 77, 863-868.

Raab-Graham, K. F., Radeke, C. M. and Vandenberg, C. A. (1994). Molecular cloning and expression of a human heart inward rectifier potassium channel. Neuroreport 5, 2501-2505.

Rojas, C. V., Wang, J. Z., Schwartz, L. S., Hoffman, E. P., Powell, B. R. and Brown, R. H., Jr. (1991). A Met-to-Val mutation in the skeletal muscle Na+ channel alpha-subunit in hyperkalaemic periodic paralysis. Nature 354, 387-389.

Rushton, W. A. (1934). A physical analysis of the relation between threshold and interpolar length in the electric excitation of medullated nerve. J Physiol 82, 332-352.

Ryan, D. P., Dias da Silva, M. R., Soong, T. W., Fontaine, B., Donaldson, M. R., Kung, A. W., Jongjaroenprasert, W., Liang, M. C., Khoo, D. H., Cheah, J. S., *et al.* (2010). Mutations in Potassium Channel Kir2.6 Cause Susceptibility to Thyrotoxic Hypokalemic Periodic Paralysis. Cell 140, 88-98.

Ryan, D. P. and Ptácek, L. J. (2008). Ion Channel Disorders, In The molecular and genetic basis of neurologic and psychiatric disease, R. N. Rosenberg, S. DiMauro, H. L. Paulson, L. J. Ptácek, and E. J. Nestler, eds. (Philadelphia: Lippincott Williams & Wilkins), pp. 550-568.

Sakura, H., Ammala, C., Smith, P. A., Gribble, F. M. and Ashcroft, F. M. (1995). Cloning and functional expression of the cDNA encoding a novel ATP-sensitive potassium channel subunit expressed in pancreatic beta-cells, brain, heart and skeletal muscle. FEBS Lett 377, 338-344.

Schram, G., Melnyk, P., Pourrier, M., Wang, Z. and Nattel, S. (2002). Kir2.4 and Kir2.1 K(+) channel subunits co-assemble: a potential new contributor to inward rectifier current heterogeneity. J Physiol 544, 337-349.

Shuck, M. E., Bock, J. H., Benjamin, C. W., Tsai, T. D., Lee, K. S., Slightom, J. L. and Bienkowski, M. J. (1994). Cloning and characterization of multiple forms of the human kidney ROM-K potassium channel. J Biol Chem 269, 24261-24270.

Silva, M. R., Chiamolera, M. I., Kasamatsu, T. S., Cerutti, J. M. and Maciel, R. M. (2004). Thyrotoxic hypokalemic periodic paralysis, an endocrine emergency: clinical and genetic features in 25 patients. Arq Bras Endocrinol Metabol 48, 196-215.

Slesinger, P. A., Patil, N., Liao, Y. J., Jan, Y. N., Jan, L. Y. and Cox, D. R. (1996). Functional effects of the mouse weaver mutation on G protein-gated inwardly rectifying K+ channels. Neuron 16, 321-331.

Soom, M., Schonherr, R., Kubo, Y., Kirsch, C., Klinger, R. and Heinemann, S. H. (2001). Multiple PIP2 binding sites in Kir2.1 inwardly rectifying potassium channels. FEBS Lett 490, 49-53.

Takahashi, N., Morishige, K., Jahangir, A., Yamada, M., Findlay, I., Koyama, H. and Kurachi, Y. (1994). Molecular cloning and functional expression of

cDNA encoding a second class of inward rectifier potassium channels in the mouse brain. J Biol Chem 269, 23274-23279.

Tao, X., Avalos, J. L., Chen, J. and MacKinnon, R. (2009). Crystal structure of the eukaryotic strong inward-rectifier K+ channel Kir2.2 at 3.1 A resolution. Science 326, 1668-1674.

Tinker, A., Jan, Y. N. and Jan, L. Y. (1996). Regions responsible for the assembly of inwardly rectifying potassium channels. Cell 87, 857-868.

Tucker, S. J., Bond, C. T., Herson, P., Pessia, M. and Adelman, J. P. (1996). Inhibitory interactions between two inward rectifier K+ channel subunits mediated by the transmembrane domains. J Biol Chem 271, 5866-5870.

Tytgat, J., Buyse, G., Eggermont, J., Droogmans, G., Nilius, B. and Daenens, P. (1996). Do voltage-gated Kv1.1 and inward rectifier Kir2.1 potassium channels form heteromultimers? FEBS Lett 390, 280-284.

van Veen, B. K., Rijkhoff, N. J., Rutten, W. L., Wallinga, W. and Boom, H. B. (1992). Potential distribution and single-fibre action potentials in a radially bounded muscle model. Med Biol Eng Comput 30, 303-310.

Velimirovic, B. M., Gordon, E. A., Lim, N. F., Navarro, B. and Clapham, D. E. (1996). The K+ channel inward rectifier subunits form a channel similar to neuronal G protein-gated K+ channel. FEBS Lett 379, 31-37.

Ventura, A., Meissner, A., Dillon, C. P., McManus, M., Sharp, P. A., Van Parijs, L., Jaenisch, R. and Jacks, T. (2004). Cre-lox-regulated conditional RNA interference from transgenes. Proc Natl Acad Sci U S A 101, 10380-10385.

Wallinga, W., Meijer, S. L., Alberink, M. J., Vliek, M., Wienk, E. D. and Ypey, D. L. (1999). Modelling action potentials and membrane currents of mammalian skeletal muscle fibres in coherence with potassium concentration changes in the T-tubular system. Eur Biophys J 28, 317-329.

Wible, B. A., De Biasi, M., Majumder, K., Taglialatela, M. and Brown, A. M. (1995). Cloning and functional expression of an inwardly rectifying K+ channel from human atrium. Circ Res 76, 343-350.

Woodward, R., Stevens, E. B. and Murrell-Lagnado, R. D. (1997). Molecular determinants for assembly of G-protein-activated inwardly rectifying K+ channels. J Biol Chem 272, 10823-10830.

Yang, J., Jan, Y. N. and Jan, L. Y. (1995). Determination of the subunit stoichiometry of an inwardly rectifying potassium channel. Neuron 15, 1441-1447.

Yu, F. H. and Catterall, W. A. (2003). Overview of the voltage-gated sodium channel family. Genome Biol 4, 207.

Zaritsky, J. J., Eckman, D. M., Wellman, G. C., Nelson, M. T. and Schwarz, T. L. (2000). Targeted disruption of Kir2.1 and Kir2.2 genes reveals the essential role of the inwardly rectifying K(+) current in K(+)-mediated vasodilation. Circ Res 87, 160-166.

Zaritsky, J. J., Redell, J. B., Tempel, B. L. and Schwarz, T. L. (2001). The consequences of disrupting cardiac inwardly rectifying K(+) current (I(K1))

as revealed by the targeted deletion of the murine Kir2.1 and Kir2.2 genes. J Physiol 533, 697-710.

Zobel, C., Cho, H. C., Nguyen, T. T., Pekhletski, R., Diaz, R. J., Wilson, G. J. and Backx, P. H. (2003). Molecular dissection of the inward rectifier potassium current (IK1) in rabbit cardiomyocytes: evidence for heteromeric co-assembly of Kir2.1 and Kir2.2. J Physiol 550, 365-372.

APPENDIX 1.

Common Reference Sequence of KCNJ18

The reference sequenced used above in chapter 2 represents a genotype close to KCNJ12. For the sake of posterity, I have included, below, a reference sequence that should represent the most commonly observed genotype. This sequence is also quite close to that used for recordings.

Figure 28. Common genotype reference sequence of KCNJ18

This sequence represents the most common genotype found in either patients or controls and is also similar to the sequence used in all constructs.

```
agcaggccacagggcggcttgggcacagtcagctttccgtcctgttgggaagcctgtttctgctttcagtgc        72

ctacgtggtgtcaggaacgccggtcacagtgaacgcctgcaggaccacactgctgcatcgtctctgtgtggga       144

cagatactgaagccagggcttggcttaccctcgtgacagtctccggag^gatgttctagtgactggatccttt       216

ccagctggtgcctgggaaatggcagccactactaattcagccttgaagacagtaccgtgcctactccagcccc       288

attacgtagaagacagaactcaagagg^agccgcctgcctggagctagctggggggtgagccagggtccccc       360

        M  T  A  A  S  R  A  N  P  Y  S  I  V  S  L            15
aaccccgggg ATG ACC GCG GCC AGC CGG GCC AAC CCC TAC AGC ATC GTG TCA TTG         415

  E  E  D  G  L  H  L  V  T  M  S  G  A  N  G  F  G  N          33
GAG GAG GAC GGG CTG CAC CTG GTC ACC ATG TCG GGC GCC AAC GGC TTC GGC AAC        469

  G  K  V  H  T  Q  H  R  C  R  N  R  F  V  K  K  N  G          51
GGC AAG GTG CAC ACG CAG CAC AGG TGC CGC AAC CGC TTC GTC AAG AAG AAT GGC        523

  Q  C  N  I  A  F  A  N  M  D  E  K  S  Q  R  Y  L  A          69
CAG TGC AAC ATT GCG TTC GCC AAC ATG GAC GAG AAG TCA CAG CGC TAC CTG GCT        577

  D  M  F  T  T  C  V  D  I  R  N  R  Y  M  L  L  I  F          87
GAC ATG TTC ACC ACC TGT GTG GAC ATC CGC TGG CGC TAC ATG CTG CTC ATC TTC        631

  S  L  A  F  L  A  S  W  L  L  F  G  V  I  F  N  V  I          105
TCG CTG GCC TTC CTT GCC TCC TGG CTG CTG TTC GGC GTC ATC TTC TGG GTC ATC        685

  A  V  A  H  G  D  L  E  P  A  E  G  H  G  R  T  P  C          123
GCG GTG GCA CAC GGT GAC CTG GAG CCG GCT GAG GGC CAC GGC CGC ACA CCC TGT        739

  V  M  Q  V  H  G  F  M  A  A  F  L  F  S  I  E  T  Q          141
GTG ATG CAG GTG CAC GGC TTC ATG GCG GCC TTC CTC TTC TCC ATC GAG ACG CAG        793

  T  T  I  G  Y  G  L  R  C  V  T  E  E  C  K  V  A  V          159
ACC ACC ATC GGC TAC GGG CTG CGC TGT GTG ACG GAG GAG TGC TTG GTG GCC GTC        847

  F  M  V  V  A  Q  S  I  V  G  C  I  I  D  S  F  M  I          177
TTC ATG GTG GTG GCC CAG TCC ATC GTG GGC TGC ATC ATC GAC TCC TTC ATG ATT        901

  G  A  I  M  A  K  M  A  R  P  K  K  R  A  H  T  L  L          195
GGT GCC ATC ATG GCC AAG ATG GCA AGG CCC AAG AAG CGG GCA CAC ACG CTG CTG        955

  F  S  H  N  A  V  V  A  L  R  D  G  K  L  C  L  M  W          213
TTC AGC CAC AAC GCC GTG GTG GCC CTG CGT GAC GGC AAG CTC TGC CTC ATG TGG        1009

  R  V  G  N  L  R  K  S  H  I  V  E  A  H  V  R  A  Q          231
CGT GTG GGC AAC CTG CGC AAG AGC CAC ATT GTG GAG GCC CAT GTG CGC GCG CAG        1063

  L  I  K  P  R  V  T  E  E  G  E  Y  I  P  L  D  Q  V          249
CTC ATC AAG CCG CGG GTC ACC GAG GAG GGC GAG TAC ATC CCG CTG GAC CAG GTC        1117

  D  I  D  V  G  F  D  K  G  L  D  R  I  F  L  V  S  P          267
GAC ATC GAT GTG GGC TTC GAC AAG GGC CTG GAC CGC ATC TTT CTG GTG TCG CCC        1171

  I  T  I  L  H  E  I  D  E  A  S  P  L  F  G  I  S  N          285
ATC ACC ATC TTG CAT GAA ATT GAC GAG GCC AGC CCG CTC TTC GGC ATC AGC CGG        1225

  Q  D  L  E  T  D  D  F  E  I  V  V  I  L  E  G  M  V          303
CAG GAC CTG GAG ACG GAC GAC TTT GAG ATC GTG GTC ATC CTG GAA GGC ATG GTG        1279

  E  A  T  A  M  T  T  Q  A  R  S  S  Y  L  A  N  E  I          321
GAG GCC ACA GCC ATG ACC ACC CAG GCC CGC AGC TCC TAC CTG GCC AAT GAG ATC        1333

  L  W  G  H  R  F  E  P  V  L  F  E  E  K  N  Q  Y  K          339
CTG TGG GGT CAC CGC TTT GAG CCC GTG CTC TTC GAG GAG AAG AAC CAG TAC AAG        1387

  I  D  Y  S  H  F  H  K  T  Y  E  V  P  S  T  P  R  C          357
ATT GAC TAC TCG CAC TTC CAC AAG ACC TAT GAG GTG CCC TCT ACG CCC CGC TGC        1441

  S  A  K  D  L  V  E  N  K  F  L  L  P  S  A  N  S  F          375
AGT GCG AAG GAT CTG GTA GAG AAC AAG TTC CTG CTG CCC AGC GCC AAC TCC TTC        1495

  C  Y  E  N  E  L  A  F  L  S  R  D  E  D  E  A  D          393
TGC TAT GAG AAC GAG CTG GCC TTC CTG AGC CGT GAC GAG GAG GAT GAG GCG GAC        1549

  G  D  Q  D  G  R  S  R  D  G  L  S  P  Q  A  R  H  D          411
GGA GAC CAG GAC GGC CGA AGC CGG GAT GGC CTC AGC CCC CAG GCC AGG CAT GAC        1603

  F  D  R  L  Q  A  G  G  G  V  L  E  Q  R  P  Y  R  R          429
TTT GAC AGA CTC CAG GCT GGC GGC GGG GTC CTG GAG CAG CTG CCC TAC AGA CGG        1657

  G  S  E  I  STOP                                                433
GGG TCA GAG ATC tgagccaaccttggccgacatgcagcatccaccctggccggggagaggcccgc         1724

ggtcgctcaggggccctgggtttgagcagaacggggccagtgccctgggttgcagactcagtagcgttttag      1796

tcgttttatgtttcttgcaaaggcctcagaaggttggccggagagggggcagccagagcggcagcccccgg      1868

cctcagaggctatcacaggctcagggcaaagaagtggcctcctgggggggccaggccacgggggccagggctt     1940

ctgcctgaagatggcgctgcagcctgcgtggaagcagcccagctcgatggtggtcccagcctctgctgtcca      2012

aggctggctagctgcgctgctcctgctcggtgtttaacttgggcagaaacacgggttcagcttttctcgac      2084

cttagcttgggtgagactgtttacaaaaaaaaaaaaataccatgcaattggagaaaaaaattttcattcata      2156

gggggcaaaaagaacaattagaattccatgggtctgccagg                                     2197
```

APPENDIX 2.

Source Code for Monte-Carlo Model

The following Igor Pro code can be run to reproduce the monte-carlo model related to the PIP$_2$ experiments. To use it, first run *setup(x)*, where *x* is a value between 1 and 3 and indicates the channel to simulate. Then, run *get_idealized()* an appropriate amount of times for the number of channels in each simulation. The resulting wave, `idealized`, should have its last 2 points removed and the remainder curvefit via, *fit()*. The results can then be stored and the process repeated an appropriate number of times. To alter the sampling frequency, edit the `IDEALSIZE` variable in the *setup()* function.

```
Function Exp_Xoffset(w,x) : FitFunc
        Wave w
        Variable x

        //CurveFitDialog/ These comments were created by the Curve Fitting dialog.
Altering them will
        //CurveFitDialog/ make the function less convenient to work with in the Curve
Fitting dialog.
        //CurveFitDialog/ Equation:
        //CurveFitDialog/ f(x) = base + A*exp(-x/T50)
        //CurveFitDialog/ End of Equation
        //CurveFitDialog/ Independent Variables 1
        //CurveFitDialog/ x
        //CurveFitDialog/ Coefficients 3
        //CurveFitDialog/ w[0] = base
        //CurveFitDialog/ w[1] = A
        //CurveFitDialog/ w[2] = T50

        return w[0] + w[1]*exp(-x/w[2])
End



//Set the initial states for the various channel types
function setup(channel)
        Variable channel

        Variable/G IDEALSIZE = 13000000   //50kHz
        Variable/G INVFREQ = 260000/IDEALSIZE
        Variable/G STACKSIZE = 3000

        if(channel == 1)
                //WT
                Variable/G initial_Po = 0.658395
                Variable/G init_base = 0.84659
                Variable/G init_A = 7.8166
                Variable/G init_x50 = 38.982
                Variable/G channels = 11
        elseif(channel == 2)
                //R205H
```

```
                    Variable/G initial_Po = 0.546529
                    Variable/G init_base = 0
                    Variable/G init_A = 6.0012
                    Variable/G init_x50 = 55.341
                    Variable/G channels = 9
            else
                    //K366R
                    Variable/G initial_Po = 0.491019
                    Variable/G init_base = 1.0222
                    Variable/G init_A = 8.9244
                    Variable/G init_x50 = 58.469
                    Variable/G channels = 19
            endif

            Variable/G open_mu = 220.0
            Variable/G initial_closed_mu = 40.0
            Make/O/D/n=(IDEALSIZE) idealized = 0
            SetScale/P x 0,INVFREQ/1000,"seconds", idealized
end

//Compute the initial state, 0 is closed 1 is open
function initial_state()
            Variable ran
            NVAR initial_Po

            ran = 5+enoise(5)
            if(ran>=10*initial_Po)
                    return 0
            else
                    return 1
            endif
end

//      Given a given mean open interval and an open probability, calculate the mean
//      of the Gaussian distribution of the closed state duration
function compute_closed_mu(Po, mu_o)
            Variable Po, mu_o

            NVAR initial_Po
            Variable output
            return (mu_o/(Po*initial_Po)) - mu_o
end

// Get a random interval from a Gaussian distribution
function get_interval(mu)
            Variable mu

            Variable output;

            // get random number from the appropriate distribution
            do
                    //output = mu + gnoise(mu)
                    //output = gammaNoise(2,mu/2)
                    output = expNoise(mu)
            while(output < 0.0)

            return output
end

// Alter the closed state mu according to where we are in time
function change_mu(position)
            Variable position

            Variable Po
            NVAR init_base, init_A, init_x50
            NVAR open_mu,INVFREQ

            Po = exp(-(position/1000)/init_x50) + init_base/(init_A + init_base)
            return compute_closed_mu(Po, open_mu)
end

function convert_to_idealized(initial_state, open_stack, closed_stack, open_i, closed_i)
            Variable initial_state, open_i, closed_i
```

```
        Wave open_stack, closed_stack

        Wave idealized
        NVAR IDEALSIZE, INVFREQ
        NVAR init_max, init_base, init_x50,init_n
        Variable i, j, k, m
        Variable state, position, interval

        position = 0
        state = initial_state
        j = 0
        m = 0

        for(i=0; i<(open_i + closed_i +2); i+=1)
                if(state == 0)
                        interval = closed_stack[j]
                        j+=1
                else
                        interval = open_stack[m]
                        m+=1
                endif

                for(k=0; k<interval/INVFREQ; k+=1)
                        idealized[position] += state
                        position+=1
                        if(position >= IDEALSIZE)
                                break
                        endif
                endfor

                if(state == 0)
                        state = 1
                else
                        state = 0
                endif
        endfor
end

function get_idealized()
        Variable Po
        Variable position
        Variable closed_mu
        Variable open_i, closed_i
        Variable state, init_state
        NVAR STACKSIZE, initial_Po, initial_closed_mu, open_mu

        Make/O/N=(3000) open_stack, closed_stack

        Po = initial_Po
        position = 0.0
        closed_mu = initial_closed_mu
        open_i = 0
        closed_i = 0

        // Get the initial state
        init_state = initial_state()
        state = init_state

        // Fill the open and closed stacks
        do
                if(state == 1)
                        open_stack[open_i] = get_interval(open_mu)
                        position += open_stack[open_i]
                        open_i+=1
                        if(open_i >= 3000)
                                printf "exceeded the open stack size at %f\n",position
                        endif
                        state = 0
                else
                        closed_mu = change_mu(position)
                        closed_stack[closed_i] = get_interval(closed_mu)
                        position += closed_stack[closed_i]
                        closed_i+=1
```

194

```
                              if(closed_i >= 3000)
                                      printf "exceeded the closed stack size at %f\n",position
                              endif
                              state = 1
                      endif
              while(position <= 260000.0)

              // Convert the stacks to an idealized trace
              convert_to_idealized(init_state, open_stack, closed_stack, open_i, closed_i)
end

function fit()
      NVAR init_base, init_A, init_x50
      Variable V_FitOptions = 4

      Make/D/N=3/O W_coef

      w_coef[0] = {init_base, init_A, init_x50}
      FuncFit/NTHR=0/TBOX=768 Exp_Xoffset W_coef  idealized /D
end
```

Appendix 3.

Source Code for Skeletal Muscle Model

The following code is configured to draw the values for sodium channel conductance, voltage-gated potassium channel conductance, inward-rectifier potassium channel conductance, and inward-rectifier potassium channel from a table in a MySQL database. Results for each run are stored in two files, V_xxxx.dat and Ko_xxxx.dat, where xxxx is the id number of the parameter set from the MySQL database. Database connection should be configured in the file mysql_functions.c, which is written in C. The remainder of the code is written Fortran 95/2003. All configurable options are held within the file named constants.f90. Importantly, the precision of all floating point variables is set by TYP, which is currently set to 64-bit IEEE floating point (or similar). Variables of interest are under "Variable parameters". Namely, num_segments sets the number of sarcolemmal segments in the model and num_compartments sets the number of t-tubular compartments into which the associated t-tubular region is divided. The model uses a fifth-order Cash-Karp Runge-Kutta method for numeric integration, which is driven by the ***odeint()*** function. This function was taken from Numerical Recipes in Fortran 90, and not included. The contents and usage of the various files should be apparent from their names.

```
----mysql_functions.c----
#include <stdio.h>
#include <stdlib.h>
#include <string.h>
#include "mysql/mysql.h"

struct params {
        int id;
        double gNa;
        double gKv;
        double gKir;
        double eta_Kir;
```

```c
};

void get_values_(struct params *param) {
        MYSQL conn;
        MYSQL_RES *result;
        MYSQL_ROW row;
        char *host = "localhost";
        char *user = "root";
        char *password = NULL;
        char *database = "model";
        unsigned int port = 0;
        char *socket = NULL;
        unsigned long flag = CLIENT_MULTI_STATEMENTS;
        int i, num_fields;
        char query[] = "SELECT id,gNa,gKv,gKir,eta_Kir from parameters where started IS
NULL limit 1";
        size_t bytes;

        //Initiate the connection
        if(mysql_init(&conn)==NULL) {
                printf("Failed to initiate connection\n");
                exit(1);
        }
        if(!mysql_real_connect(&conn,host,user,password,database,port,socket,flag)) {
                printf("Failed to connect to the database\n");
                exit(1);
        }

        //Query the database
        bytes = strlen(query);
        mysql_real_query(&conn, query, bytes);
        result = mysql_store_result(&conn);

        //Extract the values
        while(row = mysql_fetch_row(result)) {
                param->id = atoi(row[0]);
                param->gNa = strtod(row[1],NULL);
                param->gKv = strtod(row[2],NULL);
                param->gKir = strtod(row[3],NULL);
                param->eta_Kir = strtod(row[4],NULL);
        }

        //Free the results
        mysql_free_result(result);

        //Create the update query
        sprintf(query,"UPDATE parameters set started=now() where id=%d",param->id);
        bytes = strlen(query);

        //Update the table
        mysql_real_query(&conn, query, bytes);
        result = mysql_store_result(&conn);
        mysql_free_result(result);

        //Cleanup
        mysql_close(&conn);
}

void set_done_(int *id) {
        MYSQL conn;
        MYSQL_RES *result;
        MYSQL_ROW row;
        char *host = "localhost";
        char *user = "root";
        char *password = NULL;
        char *database = "model";
        unsigned int port = 0;
        char *socket = NULL;
        unsigned long flag = CLIENT_MULTI_STATEMENTS;
        int i, num_fields;
        char query[50];
        size_t bytes;
```

```c
        //Initiate the connection
        if(mysql_init(&conn)==NULL) {
                printf("Failed to initiate connection\n");
                exit(1);
        }
        if(!mysql_real_connect(&conn,host,user,password,database,port,socket,flag)) {
                printf("Failed to connect to the database\n");
                exit(1);
        }

        //construct the query
        sprintf(query,"UPDATE parameters set completed=now() where id=%d",*id);
        bytes = strlen(query);

        //Update the table
        mysql_real_query(&conn, query, bytes);

        //Cleanup
        mysql_close(&conn);
}

void get_total_(int *total, float *diff) {
        MYSQL conn;
        MYSQL_RES *result;
        MYSQL_ROW row;
        char *host = "localhost";
        char *user = "root";
        char *password = NULL;
        char *database = "model";
        unsigned int port = 0;
        char *socket = NULL;
        unsigned long flag = 0;
        int i, num_fields;
        char query[100] = "SELECT count(1) from parameters where started is NULL";
        size_t bytes = strlen(query);

        //Initiate the connection
        if(mysql_init(&conn)==NULL) {
                printf("Failed to initiate connection\n");
                exit(1);
        }
        if(!mysql_real_connect(&conn,host,user,password,database,port,socket,flag)) {
                printf("Failed to connect to the database\n");
                exit(1);
        }

        //Perform the query
        mysql_real_query(&conn, query, bytes);
        result = mysql_store_result(&conn);

        //Extract the values
        while(row = mysql_fetch_row(result)) {
                *total = atoi(row[0]);
        }

        //Free the results
        mysql_free_result(result);

        //Cleanup
        mysql_close(&conn);
}
```
----constants.f90----
```fortran
module constants
        ! We'll set some constants that are used throughout the simulation
        implicit none
        save

        !Figure out double precision
        integer, parameter :: SGL = selected_real_kind(6,37)         !2 byte float
        integer, parameter :: DBL = selected_real_kind(15,307)       !4 byte float
        integer, parameter :: QAD = selected_real_kind(33,4931)      !4 byte float
        integer, parameter :: I1B = selected_int_kind(2)     !1 byte integer
        integer, parameter :: I2B = selected_int_kind(4)     !2 byte integer
```

```fortran
      integer, parameter :: I4B = selected_int_kind(9)       !4 byte integer
      integer, parameter :: I8B = selected_int_kind(18)      !8 byte integer
      integer, parameter :: TYP = DBL                        !Use double precision
      integer, parameter :: ITYP = I4B                       !single precision integers


      !Gating parameters
      real(kind=TYP), parameter :: A_a = 150._TYP            !mV
      real(kind=TYP), parameter :: A_h_K = 7.5_TYP           !mV
      real(kind=TYP), parameter :: A_S = 5.8_TYP             !mV
      real(kind=TYP), parameter :: K_a_h = 14.7_TYP          !mV
      real(kind=TYP), parameter :: K_a_m = 10._TYP           !mV
      real(kind=TYP), parameter :: K_a_n = 7._TYP            !mV
      real(kind=TYP), parameter :: K_b_h = 9._TYP            !mV
      real(kind=TYP), parameter :: K_b_m = 18._TYP           !mV
      real(kind=TYP), parameter :: K_b_n = 40._TYP           !mV
      real(kind=TYP), parameter :: V_a = 70._TYP             !mV
      real(kind=TYP), parameter :: V_h = -45._TYP            !mV
      real(kind=TYP), parameter :: V_h_K = -40._TYP          !mV
      real(kind=TYP), parameter :: V_m = -46._TYP            !mV
      real(kind=TYP), parameter :: V_n = -40._TYP            !mV
      real(kind=TYP), parameter :: V_S = -78._TYP            !mV
      real(kind=TYP), parameter :: a_hat_m = 0.288_TYP       !ms**-1 mV**-1
      real(kind=TYP), parameter :: a_hat_n = 0.0131_TYP      !ms**-1 mV**-1
      real(kind=TYP), parameter :: a_hat_h = 0.0081_TYP      !ms**-1
      real(kind=TYP), parameter :: B_hat_h = 4.38_TYP        !ms**-1
      real(kind=TYP), parameter :: B_hat_m = 1.38_TYP        !ms**-1
      real(kind=TYP), parameter :: B_hat_n = 0.067_TYP       !ms**-1


      !Physical Constants
      integer, parameter :: Cm = 1                           !uF/Cm^2
      real(kind=TYP), parameter :: F = 96485._TYP            !C/mol
      real(kind=TYP), parameter :: GL = 3.7_TYP              !mS/cm
      real(kind=TYP), parameter :: lower_r = 20.E-4_TYP      !cm
      real(kind=TYP), parameter :: R = 8.31441_TYP           !J/(Kelvin*moles)
      real(kind=TYP), parameter :: Ra = 150._TYP             !Ohm-cm^2
      real(kind=TYP), parameter :: Ri = 125._TYP             !Ohm-cm
      real(kind=TYP), parameter :: T = 293._TYP              !Kelvin
      real(kind=TYP), parameter :: delta_x = 100.E-4_TYP     !cm
      real(kind=TYP), parameter :: rho = 0.003_TYP           !dimensionless
      real(kind=TYP),      parameter      ::     zeta     =     rho*(lower_r**2)*delta_x/
(0.6_TYP*(lower_r**2)*3800*delta_x)
      real(kind=TYP), parameter :: sigma_t = 0.34_TYP        !dimensionless
      real(kind=TYP), parameter :: pi = 3.14159265358979323846264338327950288419 7_TYP


      !Conductances and affiliated parameters
      real(kind=TYP) :: g_hat_Na = 268._TYP                  !mS/cm**2
      real(kind=TYP) :: g_hat_K_DR = 21.6_TYP                !mS/cm**2
      real(kind=TYP), parameter :: g_hat_Cl = 6.55_TYP       !mS/cm**2
      real(kind=TYP), parameter :: G_K_original = 3.7_TYP    !mS/cm**2
      real(kind=TYP) :: G_K = G_K_original
      real(kind=TYP) :: g_hat_K_IR
      real(kind=TYP), parameter :: Na_o = 133._TYP           !mM
      real(kind=TYP), parameter :: Na_i = 12.7_TYP           !mM
      real(kind=TYP), parameter :: K_o = 2.0_TYP             !mM
      real(kind=TYP), parameter :: K_i = 150.9_TYP           !mM
      real(kind=TYP), parameter :: Cl_o = 128._TYP           !mM
      real(kind=TYP), parameter :: Cl_i = 5.7_TYP            !mM
      real(kind=TYP), parameter :: J_hat_NaK= 207.0E-6_TYP   !umol/cm**2
      real(kind=TYP), parameter :: K_K = 950._TYP            !mM**2
      real(kind=TYP), parameter :: K_mK = 1._TYP             !mM
      real(kind=TYP), parameter :: K_mNa = 13._TYP           !mM
      real(kind=TYP), parameter :: K_S = 1._TYP              !mM**2
      real(kind=TYP), parameter :: S_i = 10._TYP             !mM
      real(kind=TYP), parameter :: delta = 0.4_TYP           !dimensionless
      real(kind=TYP), parameter :: eta_Na = 0.1_TYP          !
      real(kind=TYP), parameter :: eta_K_DR = 0.45_TYP       !
      real(kind=TYP) :: eta_K_IR = 1.0_TYP            !
      real(kind=TYP), parameter :: eta_Cl = 0.1_TYP          !
      real(kind=TYP), parameter :: eta_NaK = 0.1_TYP         !
      real(kind=TYP), parameter :: tau_K = 350._TYP          !ms


      !Stimulation setup
```

```fortran
        real(kind=TYP), parameter :: stim_offset = 1000.0            !offset  from  0ms  for
the first stimulation
        real(kind=TYP), parameter :: stim_duration = 0.85_TYP        !duration  (in  ms)  of
the stimulation
        real(kind=TYP), parameter :: inter_stimulation_interval = 25.0     !interval
between stimuli (ms)
        integer(kind=ITYP), parameter :: MAXITER = 50000            !Maximum    number   of
iterations per step

        !Precompute some stuff
        real(kind=TYP), parameter :: area = 2 * pi * lower_r * delta_x
        real(kind=TYP), parameter :: total_t_area = rho * pi * delta_x * (lower_r**2) /
zeta
        real(kind=TYP), parameter :: area_ratio = total_t_area/area
        real(kind=TYP),           parameter        ::          ISS_constant         =
(1000*pi*(lower_r**2))/(delta_x*Ri*area)
        real(kind=TYP), parameter :: E_Na = 1000 * (R*T/F) * log(Na_o/Na_i)
        real(kind=TYP), parameter :: E_K = 1000 * (R*T/F) * log(K_o/K_i)
        real(kind=TYP), parameter :: E_Cl = 1000 * (R*T/F) * log(Cl_i/Cl_o)
        real(kind=TYP), parameter :: K_R = K_o * exp(-1 * delta * E_K * F/(1000*R*T))
        real(kind=TYP), parameter :: sigma = (exp(Na_o/67.3_TYP) - 1)/7._TYP

        !Variable parameters
        real(kind=TYP), parameter :: Duration = 1500._TYP
        real(kind=TYP), parameter :: stimulation_orig = -350._TYP
        real(kind=TYP), parameter :: i_error = 1.0e-6_TYP
        real(kind=TYP), parameter :: step_size = 0.5_TYP
        integer(kind=ITYP), parameter :: num_segments = 10
        integer(kind=ITYP), parameter :: num_compartments = 20

        !Size constants based on parameters above
        integer(kind=ITYP), parameter :: num_comps = num_segments * num_compartments
        integer(kind=ITYP), parameter :: num_segs = num_segments * (num_compartments + 1)
        integer(kind=ITYP), parameter :: mem_v_end = num_segments
        integer(kind=ITYP), parameter :: mem_y_end = 5 * (num_segments)
        integer(kind=ITYP), parameter :: num_y = 5 * num_segs
        integer(kind=ITYP), parameter :: num_mem_y = 5 * num_segments
        integer(kind=ITYP), parameter :: num_comp_y = num_y - num_mem_y

        !Global variables that will be filled initially
        real(kind=TYP), dimension(num_compartments) :: G_L
        real(kind=TYP), dimension(num_compartments) :: t_area
end module constants




----capacitance.f90----
!----------------------------------------------------------------------
!
! Capacitive current (uA/cm^2)
!
!----------------------------------------------------------------------
subroutine cap(voltage, previous, step, output)
        use constants
        implicit none
        real(kind=TYP), dimension(num_segs), intent(in) :: voltage
        real(kind=TYP), dimension(num_segs), intent(in) :: previous
        real(kind=TYP), intent(in) :: step
        real(kind=TYP), dimension(num_segs), intent(out) :: output

        output = Cm * (voltage - previous)/step

        return
end subroutine cap




----RK4.f90----
module rkfuncs
contains
!----------------------------------------------------------------------
!
! Sodium channel fast-inactivation alpha rate constant (1/ms)
```

200

```fortran
!
!-----------------------------------------------------------------------
function alpha_h(voltage) result(output)
        use constants
        implicit none
        real(kind=TYP), dimension(:) :: voltage
        real(kind=TYP), dimension(size(voltage)) :: output

        output = a_hat_h * exp(-(voltage - V_h)/K_a_h)

        return
end function alpha_h

!-----------------------------------------------------------------------
!
! Sodium channel fast-inactivation beta rate constant (1/ms)
!
!-----------------------------------------------------------------------
function beta_h(voltage) result(output)
        use constants
        implicit none
        real(kind=TYP), dimension(:) :: voltage
        real(kind=TYP), dimension(size(voltage)) :: output

        output = b_hat_h/(1 + exp(-(voltage - V_h)/K_b_h))

        return
end function beta_h

!-----------------------------------------------------------------------
!
! Sodium channel activation alpha rate constant (1/ms)
!
!-----------------------------------------------------------------------
function alpha_m(voltage) result(output)
        use constants
        implicit none
        real(kind=TYP), dimension(:) :: voltage
        real(kind=TYP), dimension(size(voltage)) :: output

        !Local variables
        integer :: i
        i = 1

        output = a_hat_m * (voltage - V_m)/(1 - exp(-(voltage - V_m)/K_a_m))

        !Check for NaN
        do i=1, size(output), 1
                if(isnan(output(i)) .EQV. .TRUE.) then
                        output(i) = 2.88_TYP  !Approximately
                end if
        end do

        return
end function alpha_m

!-----------------------------------------------------------------------
!
! Sodium channel activation beta rate constant (1/ms)
!
!-----------------------------------------------------------------------
function beta_m(voltage) result(output)
        use constants
        implicit none
        real(kind=TYP), dimension(:) :: voltage
        real(kind=TYP), dimension(size(voltage)) :: output

        output = b_hat_m * exp(-(voltage - V_m)/K_b_m)

        return
end function beta_m

!-----------------------------------------------------------------------
```

```fortran
!
! Kv-channel activation alpha constant (1/ms)
!
!----------------------------------------------------------------------
function alpha_n(voltage) result(output)
        use constants
        implicit none
        real(kind=TYP), dimension(:) :: voltage
        real(kind=TYP), dimension(size(voltage)) :: output
        integer :: i

        output = a_hat_n * (voltage - V_n)/(1 - exp(-(voltage - V_n)/K_a_n))

        !Check for NaN
        do i=1, size(output), 1
                if(isnan(output(i)) .EQV. .TRUE.) then
                        output(i) = 0.0917_TYP !Approximately
                end if
        end do

        return
end function alpha_n

!----------------------------------------------------------------------
!
! Kv-channel activation beta constant (1/ms)
!
!----------------------------------------------------------------------
function beta_n(voltage) result(output)
        use constants
        implicit none

        real(kind=TYP), dimension(:) :: voltage
        real(kind=TYP), dimension(size(voltage)) :: output

        output = b_hat_n * exp(-(voltage - V_n)/K_b_n)

        return
end function beta_n

!----------------------------------------------------------------------
!
! Sodium channel slow-inactivation steady-state value (dimensionless)
!
!----------------------------------------------------------------------
function S_inf(voltage) result(output)
        use constants
        implicit none

        real(kind=TYP), dimension(:) :: voltage
        real(kind=TYP), dimension(size(voltage)) :: output

        output = 1/(1 + exp((voltage - V_S)/A_S))

        return
end function S_inf

!----------------------------------------------------------------------
!
! Sodium channel slow-inactivation time constant (dimensionless)
!
!----------------------------------------------------------------------
function Tau_S(voltage) result(output)
        use constants
        implicit none

        real(kind=TYP), dimension(:) :: voltage
        real(kind=TYP), dimension(size(voltage)) :: output

        output = 1000*60._TYP/(0.2_TYP + 5.65_TYP * ((voltage + 90._TYP)/100._TYP)**2)

        return
end function Tau_S
```

202

```fortran
!-----------------------------------------------------------------------
!
! Sodium channel slow-inactivation alpha rate constant (1/ms)
!
!-----------------------------------------------------------------------
function alpha_S(voltage) result(output)
        use constants
        implicit none
        real(kind=TYP), dimension(:) :: voltage
        real(kind=TYP), dimension(size(voltage)) :: output

        !Local variables
        integer :: i

        do i=1, size(voltage), 1
                if(voltage(i) >= -40._TYP) then
                        output(i) = 0._TYP
                else
                        output(i) = (-127140*exp(0.224_TYP*voltage(i)) - &
                                3.474e-5_TYP*exp(-0.04391*voltage(i))) * &
                                (voltage(i)           +          37.78_TYP)/(1           +
exp(0.311_TYP*(voltage(i)+79.23_TYP)))
                end if
        end do

        return
end function alpha_S

!-----------------------------------------------------------------------
!
! Sodium channel slow-inactivation beta rate constant (1/ms)
!
!-----------------------------------------------------------------------
function beta_S(voltage) result(output)
        use constants
        implicit none
        real(kind=TYP), dimension(:) :: voltage
        real(kind=TYP), dimension(size(voltage)) :: output

        !local variables
        integer :: i

        do i=1, size(voltage), 1
                if(voltage(i) >= -40._TYP) then
                        output(i)   =   0.3_TYP   *   exp(-2.535e-7_TYP*voltage(i))/(1+exp(-
0.1_TYP*(voltage(i)+32._TYP)))
                else
                        output(i)       =       0.1212_TYP*exp(-0.01052*voltage(i))/(1+exp(-
0.1378*(voltage(i)+40.14_TYP)))
                end if
        end do

        return
end function beta_S

!-----------------------------------------------------------------------
!
! Kv-channel inactivation component at steady-state (dimensionless)
!
!-----------------------------------------------------------------------
function h_K_inf(voltage) result(output)
        use constants
        implicit none

        real(kind=TYP), dimension(:) :: voltage
        real(kind=TYP), dimension(size(voltage)) :: output

        output = 1/(1 + exp((voltage - V_h_K)/A_h_K))

        return
end function h_K_inf
```

203

```fortran
!------------------------------------------------------------------------
!
! Kv-channel time-component of steady-state inactivation (ms)
!
!------------------------------------------------------------------------
function Tau_h_K(voltage) result(output)
        use constants
        implicit none

        real(kind=TYP), dimension(:) :: voltage
        real(kind=TYP), dimension(size(voltage)) :: output

        output = exp(-(voltage + 40._TYP)/25.75_TYP)

        return
end function Tau_h_K
end module rkfuncs


!------------------------------------------------------------------------
!
! Differential equations for ion channel gating parameters
! (dimensionless)
!
!------------------------------------------------------------------------
subroutine derivs(y, output, voltage)
        use constants
        use rkfuncs

        implicit none
        real(kind=TYP), dimension(num_y), intent(in) :: y
        real(kind=TYP), dimension(num_y), intent(out) :: output
        real(kind=TYP), dimension(num_segs), intent(in) :: voltage

        real(kind=TYP), dimension(num_segs) :: d_inf_local

        !local variables
        output(1::5) = alpha_m(voltage) * (1 - y(1::5)) - beta_m(voltage) * y(1::5)
        !m
        output(2::5) = alpha_n(voltage) * (1 - y(2::5)) - beta_n(voltage) * y(2::5)
        !n
        output(3::5) = alpha_h(voltage) * (1 - y(3::5)) - beta_h(voltage) * y(3::5)
        !h
        output(4::5) = (h_K_inf(voltage) - y(4::5))/Tau_h_K(voltage)
        !hK
        output(5::5) = (S_inf(voltage) - y(5::5))/Tau_S(voltage)                  !s
!       output(5::5) = alpha_S(voltage) * (1 - y(5::5)) - beta_S(voltage) * y(5::5)
        !s

        return
end subroutine derivs


!------------------------------------------------------------------------
!
! If we're iterating around the stimulation, we need to just use classic
! RK4 at the lower point
!
!------------------------------------------------------------------------
subroutine RK4int(y, step, voltage)
        use constants
        implicit none

        real(kind=TYP), dimension(num_y), intent(inout) :: y
        real(kind=TYP), intent(in) :: step
        real(kind=TYP), dimension(num_segs), intent(in) :: voltage

        !Local Variables
        real(kind=TYP), dimension(num_y) :: k1, k2, k3, k4

        call derivs(y, k1, voltage)
        call derivs(y + 0.5_TYP * step * k1, k2, voltage)
        call derivs(y + 0.5_TYP * step * k2, k3, voltage)
        call derivs(y + k3, k4, voltage)
        y = y + step * (k1 + 2*k2 + 2*k3 + k4)/6
```

```fortran
        return
end subroutine RK4int

----stimulation.f90----
!----------------------------------------------------------------------
!
! stimulation(stim,position,duration) calculates and returns the
! appropriate stimulation that occurs at a given point in time. The
! function takes the arguements: stim, the user-input stimulation;
! position, where we are (in ms) in the simulation; and duration, the
! user input duration of the experiment.
!
! There is undoubtedly a more efficient way of doing this.
!
!----------------------------------------------------------------------
real(kind=TYP) function stimulation(position)
        use constants
        implicit none

        real(kind=TYP), intent(in) :: position

        !local variables
        real(kind=TYP) :: pos          !temporary position

        pos = stim_offset
        stimulation = 0.
        if(position <= pos) then
                stimulation = 0.
        else
                do while(pos < Duration)
                        pos = pos + stim_duration
                        if(position <= pos) then
                                stimulation = stimulation_orig
                                exit
                        end if
                        pos = pos + inter_stimulation_interval - stim_duration
                        if(position <= pos) then
                                stimulation = 0.
                                exit
                        end if
                end do
        end if

        return
end function stimulation

----chloride.f90----
!----------------------------------------------------------------------
!
! Chloride-channel surface-membrane current density (uA/cm^2)
!
!----------------------------------------------------------------------
subroutine i_Cl_func(voltage,output)
        use constants
        implicit none

        real(kind=TYP), dimension(num_segments), intent(in) :: voltage
        real(kind=TYP), dimension(num_segments), intent(out) :: output

        !Local Variables
        real(kind=TYP), dimension(num_segments) :: a
        call a_func(voltage, a)

        output =  g_hat_Cl * (voltage - E_Cl) * a**4

        return
end subroutine i_Cl_func

!----------------------------------------------------------------------
!
! Chloride-channel T-tubule membrane current density (uA/cm^2)
!
```

```fortran
!----------------------------------------------------------------------
subroutine i_Cl_t_func(voltage,output)
        use constants
        implicit none

        real(kind=TYP), dimension(num_comps),intent(in) :: voltage
        real(kind=TYP), dimension(num_comps),intent(out) :: output

        !Local Variables
        real(kind=TYP), dimension(num_comps) :: a
        call a_t_func(voltage, a)

        output = g_hat_Cl * eta_Cl * (voltage - E_Cl) * a**4

        return
end subroutine i_Cl_t_func

!----------------------------------------------------------------------
!
! Boltzmann distribution for gCl (dimensionless)
!
!----------------------------------------------------------------------
subroutine a_func(voltage, output)
        use constants
        implicit none
        real(kind=TYP), dimension(num_segments), intent(in) :: voltage
        real(kind=TYP), dimension(num_segments), intent(out) :: output

        output = 1/(1 + exp((voltage - V_a)/A_a))
        return
end subroutine a_func

subroutine a_t_func(voltage, output)
        use constants
        implicit none
        real(kind=TYP), dimension(num_comps), intent(in) :: voltage
        real(kind=TYP), dimension(num_comps), intent(out) :: output

        output = 1/(1 + exp((voltage - V_a)/A_a))
return
end subroutine a_t_func

----potassium.f90----
!----------------------------------------------------------------------
!
! Potassium reversal potential (mV)
!
!----------------------------------------------------------------------
subroutine E_K_t_func(k_o_local, output)
        use constants
        real(kind=TYP), dimension(num_comps), intent(in) :: k_o_local
        real(kind=TYP), dimension(num_comps), intent(out) :: output

        output = 1000 * (R*T/F) * log(k_o_local/k_i)

        return
end subroutine E_K_t_func

!----------------------------------------------------------------------
!
! Surface-membrane Kv-channel current density (uA/cm^2)
!
!----------------------------------------------------------------------
subroutine i_K_DR_func(voltage, y, output)
        use constants
        real(kind=TYP), dimension(num_segments), intent(in) :: voltage
        real(kind=TYP), dimension(num_mem_y), intent(in) :: y
        real(kind=TYP), dimension(num_segments), intent(out) :: output

        !Local variables
        real(kind=TYP), dimension(num_segments) :: g_K_DR
        call g_K_DR_func(y,g_K_DR)
```

```fortran
        output = g_K_DR * (voltage - E_K)
        return
end subroutine i_K_DR_func

!-----------------------------------------------------------------------
!
! T-tubule membrane Kv-channel current density (uA/cm^2)
!
!-----------------------------------------------------------------------
subroutine i_K_DR_t_func(voltage, y, k_o_local, output)
        use constants
        real(kind=TYP), dimension(num_comps), intent(in) :: voltage
        real(kind=TYP), dimension(num_comp_y), intent(in) :: y
        real(kind=TYP), dimension(num_comps), intent(in) :: k_o_local
        real(kind=TYP), dimension(num_comps), intent(out) :: output

        !Local variables
        real(kind=TYP), dimension(num_comps) :: E_K_t
        real(kind=TYP), dimension(num_comps) :: g_K_DR_t

        call g_K_DR_t_func(y, g_K_DR_t)
        call E_K_t_func(K_o_local, E_K_t)
        output = eta_K_DR * g_K_DR_t * (voltage - E_K_t)

        return
end subroutine i_K_DR_t_func

!-----------------------------------------------------------------------
!
! Kv-channel surface conductance (mS/cm^2)
!
!-----------------------------------------------------------------------
subroutine g_K_DR_func(y, output)
        use constants
        real(kind=TYP), dimension(num_mem_y), intent(in) :: y
        real(kind=TYP), dimension(num_segments), intent(out) :: output

        output = g_hat_K_DR * y(4::5) * y(2::5) ** 4

        return
end subroutine g_K_DR_func

subroutine g_K_DR_t_func(y, output)
        use constants
        real(kind=TYP), dimension(num_comp_y), intent(in) :: y
        real(kind=TYP), dimension(num_comps), intent(out) :: output

        output = g_hat_K_DR * y(4::5) * y(2::5) ** 4

        return
end subroutine g_K_DR_t_func

!-----------------------------------------------------------------------
!
! Surface membrane Kir channel current density (uA/cm^2)
!
!-----------------------------------------------------------------------
subroutine i_K_IR_func(voltage, output)
        use constants
        implicit none

        real(kind=TYP), dimension(num_segments), intent(in) :: voltage
        real(kind=TYP), dimension(num_segments), intent(out) :: output

        !Local variables
        real(kind=TYP), dimension(num_segments) :: g_K_IR
        call g_K_IR_func(voltage,g_K_IR)

        output = g_K_IR * (voltage - E_K)

        return
end subroutine i_K_IR_func
```

```fortran
!-----------------------------------------------------------------------
!
! T-tubule membrane Kir channel current density (uA/cm^2)
!
!-----------------------------------------------------------------------
subroutine i_K_IR_t_func(voltage, k_o_local, output)
        use constants
        implicit none

        real(kind=TYP), dimension(num_comps), intent(in) :: voltage
        real(kind=TYP), dimension(num_comps), intent(in) :: k_o_local
        real(kind=TYP), dimension(num_comps), intent(out) :: output

        !Local variables
        real(kind=TYP), dimension(num_comps) :: g_K_IR
        real(kind=TYP), dimension(num_comps) :: E_K_local
        call g_K_IR_t_func(voltage,k_o_local,g_K_IR)
        call E_K_t_func(k_o_local,E_K_local)

        output = eta_k_IR * g_K_IR * (voltage - E_K_local)

        return
end subroutine i_K_IR_t_func

!-----------------------------------------------------------------------
!
! Surface conductance of Kir channels (uA/cm^2)
!
!-----------------------------------------------------------------------
subroutine g_K_IR_func(voltage,output)
        use constants
        implicit none

        real(kind=TYP), dimension(num_segments), intent(in) :: voltage
        real(kind=TYP), dimension(num_segments), intent(out) :: output

        !Local variables
        real(kind=TYP), dimension(num_segments) :: y
        call y_func(voltage,y)

        output = g_hat_K_IR * y

        return
end subroutine g_K_IR_func

subroutine g_K_IR_t_func(voltage,k_o_local,output)
        use constants
        implicit none

        real(kind=TYP), dimension(num_comps), intent(in) :: voltage
        real(kind=TYP), dimension(num_comps), intent(in) :: k_o_local
        real(kind=TYP), dimension(num_comps), intent(out) :: output

        !Local variables
        real(kind=TYP), dimension(num_comps) :: y
        real(kind=TYP), dimension(num_comps) :: g_hat_K_IR_t
        call y_t_func(voltage,k_o_local,y)
        call g_hat_K_IR_t_func(voltage,k_o_local,g_hat_K_IR_t)

        output = g_hat_K_IR_t * y

        return
end subroutine g_K_IR_t_func

!-----------------------------------------------------------------------
!
! Tubular conductance of Kir channels (uA/cm^2)
!
!-----------------------------------------------------------------------
subroutine g_hat_K_IR_t_func(voltage,k_o_local,output)
        use constants
        implicit none
```

```fortran
        real(kind=TYP), dimension(num_comps), intent(in) :: voltage
        real(kind=TYP), dimension(num_comps), intent(in) :: k_o_local
        real(kind=TYP), dimension(num_comps), intent(out) :: output

        !local variables
        real(kind=TYP), dimension(num_comps) :: K_R_t
        call K_R_t_func(k_o_local, k_R_t)

        output = (G_K * K_R_t**2)/(K_K + K_R_t**2)

        return
end subroutine g_hat_K_IR_t_func

!-----------------------------------------------------------------------
!
! Fraction of Kir channels open, i.e. Po (dimensionless)
!
!-----------------------------------------------------------------------
subroutine y_func(voltage,output)
        use constants
        implicit none

        real(kind=TYP), dimension(num_segments), intent(in) :: voltage
        real(kind=TYP), dimension(num_segments), intent(out) :: output

        output = 1 - 1/(1 + (K_s/((S_i**2) * exp(2 * (1 - delta) * voltage * F/(1000 * R *
T)))) * (1 + ((K_R)**2)/K_K))

        return
end subroutine y_func

subroutine y_t_func(voltage,k_o_local,output)
        use constants
        implicit none

        real(kind=TYP), dimension(num_comps), intent(in) :: voltage
        real(kind=TYP), dimension(num_comps), intent(in) :: k_o_local
        real(kind=TYP), dimension(num_comps), intent(out) :: output

        !Local variables
        real(kind=TYP), dimension(num_comps) :: K_R_tub
        call K_R_t_func(k_o_local, K_R_tub)

        output = 1 - 1/(1 + (K_s/((S_i**2) * exp(2 * (1 - delta) * voltage * F/(1000 * R *
T)))) * (1 + ((K_R_tub)**2)/K_K))

        return
end subroutine y_t_func

!-----------------------------------------------------------------------
!
! Concentration of potassium at the binding site (mM)
!
!-----------------------------------------------------------------------
subroutine K_R_t_func(K_o_local, output)
        use constants
        real(kind=TYP), dimension(num_comps), intent(in) :: K_o_local
        real(kind=TYP), dimension(num_comps), intent(out) :: output

        !Local variables
        real(kind=TYP), dimension(num_comps) :: E_K_local
        call E_K_t_func(K_o_local, E_K_local)

        output = K_o_local * exp((-1) * delta * E_K_local * F / (1000 * R * T))

        return
end subroutine K_R_t_func

----sodium.f90----
!-----------------------------------------------------------------------
!
! Surface membrane sodium channel conductance (uA/cm^2)
!
```

```fortran
!-----------------------------------------------------------------------
subroutine i_Na_func(voltage, y, output)
        use constants
        real(kind=TYP), dimension(num_segments), intent(in) :: voltage
        real(kind=TYP), dimension(num_mem_y), intent(in) :: y
        real(kind=TYP), dimension(num_segments), intent(out) ::output

        !Local variables
        real(kind=TYP), dimension(num_segments) :: g_Na

        call g_Na_func(y, g_Na)
        output = g_Na * (voltage - E_Na)

        return
end subroutine i_Na_func

!-----------------------------------------------------------------------
!
! T-tubule membrane sodium channel conductance (uA/cm^2)
!
!-----------------------------------------------------------------------
subroutine i_Na_t_func(voltage, y, output)
        use constants
        real(kind=TYP), dimension(num_comps), intent(in) :: voltage
        real(kind=TYP), dimension(num_comp_y), intent(in) :: y
        real(kind=TYP), dimension(num_comps), intent(out) :: output

        !Local variables
        real(kind=TYP), dimension(num_comps) :: g_Na_t

        call g_Na_t_func(y, g_Na_t)
        output = eta_Na * g_Na_t * (voltage - E_Na)
        return
end subroutine i_Na_t_func

!-----------------------------------------------------------------------
!
! Sodium channel conductance (uA/cm^2)
!
!-----------------------------------------------------------------------
subroutine g_Na_func(y, output)
        use constants
        real(kind=TYP), dimension(num_mem_y), intent(in) :: y
        real(kind=TYP), dimension(num_segments), intent(out) :: output

        output = g_hat_Na * y(3::5) * y(5::5) * y(1::5)**3

        return
end subroutine g_Na_func

subroutine g_Na_t_func(y, output)
        use constants
        real(kind=TYP), dimension(num_comp_y), intent(in) :: y
        real(kind=TYP), dimension(num_comps), intent(out) :: output

        output = g_hat_Na * y(3::5) * y(5::5) * y(1::5)**3

        return
end subroutine g_Na_t_func

----transporter.f90----
!-----------------------------------------------------------------------
!
! Surface membrane Na/K transporter current (uA/cm^2)
!
!-----------------------------------------------------------------------
subroutine i_NaK_func(voltage,output)
        use constants
        real(kind=TYP), dimension(num_segments), intent(in) :: voltage
        real(kind=TYP), dimension(num_segments), intent(inout) :: output

        !Local variables
        real(kind=TYP), dimension(num_segments) :: i_hat_NaK
```

210

```
        real(kind=TYP), dimension(num_segments) :: lower_f
        call i_hat_NaK_func(i_hat_NaK)
        call lower_f_func(voltage, lower_f)

        output = i_hat_NaK * lower_f

        return
end subroutine I_NaK_func

!-------------------------------------------------------------------------
!
! Tubular membrane Na/K transporter current (uA/cm^2)
!
!-------------------------------------------------------------------------
subroutine i_NaK_t_func(voltage, local_k_o, output)
        use constants
        real(kind=TYP), dimension(num_comps), intent(in) :: voltage
        real(kind=TYP), dimension(num_comps), intent(in) :: local_k_o
        real(kind=TYP), dimension(num_comps), intent(out) :: output

        !Local variables
        real(kind=TYP), dimension(num_comps) :: i_hat_NaK
        real(kind=TYP), dimension(num_comps) :: lower_f
        call i_hat_NaK_t_func(local_k_o, i_hat_NaK)
        call lower_f_t_func(voltage, lower_f)

        output = eta_NaK * i_hat_NaK * lower_f

        return
end subroutine i_NaK_t_func

!-------------------------------------------------------------------------
!
! Voltage-independent component of Na/K transporter current (uA/cm^2)
!
!-------------------------------------------------------------------------
subroutine i_hat_NaK_func(output)
        use constants

        implicit none
        real(kind=TYP), dimension(num_segments), intent(inout) :: output

        output = (F * J_hat_NaK)/(((1 + K_mK/K_o)**2) * ((1 + K_mNa/Na_i)**3))

        return
end subroutine i_hat_NaK_func

subroutine i_hat_NaK_t_func(K_o_local,output)
        use constants
        real(kind=TYP), dimension(num_comps), intent(in) :: K_o_local
        real(kind=TYP), dimension(num_comps), intent(inout) :: output

        output = (F * J_hat_NaK)/(((1 + K_mK/K_o_local)**2) * ((1 + K_mNa/Na_i)**3))

        return
end subroutine i_hat_NaK_t_func

!-------------------------------------------------------------------------
!
! Voltage-sensitive part of I_NaK current density (dimensionless)
!
!-------------------------------------------------------------------------
subroutine lower_f_func(voltage,output)
        use constants
        real(kind=TYP), dimension(num_segments), intent(in) :: voltage
        real(kind=TYP), dimension(num_segments), intent(out) :: output

        output = (1._TYP + 0.12_TYP * exp(-0.1_TYP * voltage * F / (1000 * R * T)) + &
                0.04_TYP * sigma * exp(-1 * voltage * F/(1000 * R * T)))**(-1)

        return
end subroutine lower_f_func
```

```fortran
subroutine lower_f_t_func(voltage, output)
        use constants
        real(kind=TYP), dimension(num_comps), intent(in) :: voltage
        real(kind=TYP), dimension(num_comps), intent(out) :: output

        output = (1._TYP + 0.12_TYP * exp(-0.1_TYP * voltage * F / (1000 * R * T)) + &
                0.04_TYP * sigma * exp(-1 * voltage * F/(1000 * R * T)))**(-1)

        return
end subroutine lower_f_t_func

----inter_segmental.f90----
!-----------------------------------------------------------------------
!
! Current density leaving T-tubule (uA/cm^2)
!
!-----------------------------------------------------------------------
subroutine i_tubular(voltage, output)
        use constants
        implicit none
        real(kind=TYP), dimension(num_segs), intent(in) :: voltage
        real(kind=TYP), dimension(num_segments), intent(out) :: output

        output = 1000 * (voltage(1:mem_v_end) - voltage(mem_v_end+1::num_compartments))/Ra

        return
end subroutine i_tubular

!-----------------------------------------------------------------------
!
! Calculate the inter-segmental current (uA/cm^2)
!
! ----------------------------------------------------------------------
subroutine inter_segmental_current_func(voltage, output)
        use constants

        implicit none
        real(kind=TYP), dimension(num_segments), intent(in) :: voltage
        real(kind=TYP), dimension(num_segments), intent(out) :: output

        !Local variables
        integer :: i

        do i=2, num_segments-1, 1
                output(i) = (voltage(i+1) + voltage(i-1) - 2*voltage(i)) * ISS_constant
        end do
        output(1) = (voltage(2) - voltage(1)) * ISS_constant
        output(num_segments)  =  (voltage(num_segments-1)  -  voltage(num_segments))  *
ISS_constant

        return
end subroutine inter_segmental_current_func

!-----------------------------------------------------------------------
!
! Calculate the inter-compartmental current (uA/cm^2)
!
!-----------------------------------------------------------------------
subroutine inter_compartmental_current_func(voltage, output)
        use constants

        implicit none
        real(kind=TYP), dimension(num_comps), intent(in) :: voltage
        real(kind=TYP), dimension(num_comps), intent(out) :: output

        !Local variables
        integer :: i
        i = 2

        do i=2, num_compartments-1, 1
                output(i::num_compartments) = (voltage(i+1::num_compartments) + voltage(i-
1::num_compartments) - &
                        2 * voltage(i::num_compartments)) * G_L(i)/t_area(i)
```

```
        end do

        !Compute for the outermost compartment
        output(1::num_compartments)        =        (voltage(2::num_compartments)        -
voltage(1::num_compartments)) * G_L(1)/t_area(1)

        !Compute for the innermost compartment
        output(num_compartments::num_compartments)    =    (voltage(num_compartments    -
1::num_compartments) - &
            voltage(num_compartments::num_compartments))                        *
G_L(num_compartments)/t_area(num_compartments)

        return
end subroutine inter_compartmental_current_func

----tubular_Ko.f90----
!----------------------------------------------------------------------
!
! Calculate what the tubular [K]o should be using runge-kutta.
!
!----------------------------------------------------------------------
subroutine change_tub_k(tubule_k_o, dKo, step)
        use constants

        implicit none
        real(kind=TYP), dimension(num_comps), intent(inout) :: tubule_k_o
        real(kind=TYP), dimension(num_comps), intent(in) :: dKo
        real(kind=TYP), intent(in) :: step

        !Local Variables
        real(kind=TYP), dimension(num_comps) :: k1, k2, k3, k4

        call tub_k_func(tubule_k_o, dKo, k1)
        call tub_k_func(tubule_k_o + 0.5_TYP * step*k1, dKo, k2)
        call tub_k_func(tubule_k_o + 0.5_TYP * step*k2, dKo, k3)
        call tub_k_func(tubule_k_o + step*k3, dKo, k4)
        tubule_k_o = tubule_k_o  + step* (k1 + 2*k2 + 2*k3 + k4)/6

        return
end subroutine change_tub_k

!----------------------------------------------------------------------
!
! The functions called by the runge-kutta routine
!
!----------------------------------------------------------------------
subroutine tub_k_func(tubule_k_o, dKo, output)
        use constants

        implicit none
        real(kind=TYP), dimension(num_comps), intent(in) :: tubule_k_o
        real(kind=TYP), dimension(num_comps), intent(in) :: dKo
        real(kind=TYP), dimension(num_comps), intent(out) :: output

        if(num_compartments > 2) then
            output = dKo - ((tubule_k_o - cshift(tubule_k_o, 1))/tau_K) - ((tubule_k_o
- cshift(tubule_k_o, -1))/tau_K)
        end if

        output(1::num_compartments)            =            dKo(1::num_compartments)            -
((tubule_k_o(1::num_compartments) - tubule_k_o(2::num_compartments))/tau_k) - &
            ((tubule_k_o(1::num_compartments) - K_o)/tau_k)
        output(num_compartments::num_compartments)                                =
dKo(num_compartments::num_compartments) - (tubule_k_o(num_compartments::num_compartments)
- tubule_k_o(1::num_compartments))/tau_k

        return
end subroutine tub_k_func

----voltage_dependent.f90----
!----------------------------------------------------------------------
!
! Surface & T-tubule membrane ionic current density (uA/cm^2)
```

213

```fortran
!
!-----------------------------------------------------------------------
subroutine i_ionic(voltage, y, output, tubule_k_o, dKo)
        use constants

        implicit none
        real(kind=TYP), dimension(num_segs), intent(in) :: voltage
        real(kind=TYP), dimension(num_y), intent(in) :: y
        real(kind=TYP), dimension(num_segs), intent(out) :: output
        real(kind=TYP), dimension(num_comps), intent(in) :: tubule_k_o
        real(kind=TYP), dimension(num_comps), intent(out) :: dKo

        !Local variables
        real(kind=TYP), dimension(num_segments) :: i_Cl
        real(kind=TYP), dimension(num_segments) :: i_K_DR
        real(kind=TYP), dimension(num_segments) :: i_Na
        real(kind=TYP), dimension(num_segments) :: i_K_IR
        real(kind=TYP), dimension(num_segments) :: i_NaK
        real(kind=TYP), dimension(num_comps) :: i_Cl_t
        real(kind=TYP), dimension(num_comps) :: i_K_DR_t
        real(kind=TYP), dimension(num_comps) :: i_Na_t
        real(kind=TYP), dimension(num_comps) :: i_K_IR_t
        real(kind=TYP), dimension(num_comps) :: i_NaK_t

        !Surface membrane
        call i_Cl_func(voltage(1:mem_v_end), i_Cl)
        call i_K_DR_func(voltage(1:mem_v_end), y(1:mem_y_end), i_K_DR)
        call i_Na_func(voltage(1:mem_v_end), y(1:mem_y_end), i_Na)
        call i_K_IR_func(voltage(1:mem_v_end), i_K_IR)
        call i_NaK_func(voltage(1:mem_v_end), i_NaK)
        output(1:mem_v_end) = i_Cl + i_K_DR + i_K_IR + i_Na + i_NaK

        !T-tubule membrane
        call i_Cl_t_func(voltage(mem_v_end+1:), i_Cl_t)
        call i_K_DR_t_func(voltage(mem_v_end+1:), y(mem_y_end+1:), tubule_k_o, i_K_DR_t)
        call i_Na_t_func(voltage(mem_v_end+1:), y(mem_y_end+1:), i_Na_t)
        call i_K_IR_t_func(voltage(mem_v_end+1:), tubule_k_o, i_K_IR_t)
        call i_NaK_t_func(voltage(mem_v_end+1:), tubule_k_o, i_NaK_t)
        output(mem_v_end+1:) = i_Cl_t + i_K_DR_t + i_K_IR_t + i_Na_t + i_NaK_t
        dKo = (i_K_DR_t + i_K_IR_t - 2 * i_NaK_t) / (1000 * F * zeta)

        return
end subroutine i_ionic

----iclamp.f90----
program main_prog
        use ISO_C_BINDING
        use constants
        implicit none

        integer(C_INT) :: total
        integer :: i = 1

        call get_total(total)
        write(*,'(A17,I4.4,A11)') 'Doing a total of ',total,' iterations'
        do i=1, total, 1
                call current_clamp()
        end do
end program main_prog

subroutine current_clamp()
        use constants
        use ISO_C_BINDING
        implicit none

        real(kind=TYP) :: position = 0._TYP                 !Time, in msec
        real(kind=TYP) :: position_old = 0._TYP             !Time, in msec
        real(kind=TYP), dimension(num_segs) :: voltage      !Voltage of the membrane and
the t-tubules
        real(kind=TYP), dimension(num_y) :: y               !Kinetic parameters
        real(kind=TYP), dimension(num_comps) :: tub_k_o     !array   of   tubular   K_out
concentrations
        real(kind=TYP), dimension(num_comps) :: dKo         !Change in tubular [K]o
```

214

```fortran
      real(kind=TYP), dimension(num_compartments+1) :: t_rad       !T-tubule radius
      character(len=11) :: V_string, Ko_string
      integer :: i
      TYPE, BIND(C) :: params
            INTEGER(C_INT) :: id
            real(C_DOUBLE) :: gNa, gKv, gKir, eta_Kir
      END TYPE params
      type(params) :: param

      !------------------------------------------------------------------------
      !
      ! Setupt initial values of the voltages and tubule compartmens [K]o
      !
      !------------------------------------------------------------------------
      voltage(1:mem_v_end) = -79.451000000000249_TYP
      voltage(mem_v_end+1:num_segs) = -79.476000000000241_TYP
      tub_k_o = 6.3391921372444022_TYP
      dKo = 0._TYP

      !------------------------------------------------------------------------
      !
      ! Set the initial values of the kinetics variables M(1), N(2), H(3),
      ! HK(4), S(5)
      !
      !------------------------------------------------------------------------
      y(1::5) = 3.77981807922042334E-002_TYP
      y(2::5) = 1.00632874093230015E-002_TYP
      y(3::5) = 0.47908258157333750_TYP
      y(4::5) = 0.99489649802208724_TYP
      y(5::5) = 1._TYP

      !------------------------------------------------------------------------
      !
      ! Precompute some values
      !
      !------------------------------------------------------------------------
      i = 1
      t_rad(num_compartments+1) = 0._TYP
      DO i=1, num_compartments, 1
            t_rad(i) = ((num_compartments + 1 - i) * lower_r)/num_compartments
      END DO
      DO i=1, num_compartments, 1
            G_L(i) = 2 * pi * (num_compartments - i + 1) * delta_x * rho * sigma_T *
GL
            t_area(i)   =   rho   *   pi   *   delta_x   *   (((t_rad(i))**2)   -
((t_rad(i+1))**2))/zeta
      END DO

      !------------------------------------------------------------------------
      !
      ! Get the new parameter values from the database
      !
      !------------------------------------------------------------------------
      call get_values(param)
      g_hat_Na = param%gNa
      g_hat_K_DR = param%gKv
      eta_K_IR = param%eta_Kir
      G_K = G_K_original * param%gKir
      g_hat_K_IR = (G_K * K_R**2) / (K_K + K_R**2)
      !If eta_Kir isn't 1 then we need to redistribute the channels to the surface (3:1
ratio)
      g_hat_K_IR = g_hat_K_IR * (1 + 3 * (1._TYP - param%eta_Kir))
      WRITE(V_string,'(A2,I4.4,A4)') 'V_',param%id,'.dat'
      WRITE(Ko_string,'(A3,I4.4,A4)') 'Ko_',param%id,'.dat'
      WRITE(*,'(A15,I3.3)') 'Started model #',param%id

      !------------------------------------------------------------------------
      !
      ! Open the output files for writing. "voltage.dat" contains voltages
      ! of the surface and T-tubule membranes. "Ko.dat" contains the [K]out
      ! of the T-tubule compartments.
      !
      !------------------------------------------------------------------------
```

```
        OPEN(UNIT=101,FILE=V_string,STATUS='REPLACE',ACCESS='STREAM',ACTION='WRITE',FORM='
UNFORMATTED')
        OPEN(UNIT=102,FILE=Ko_string,STATUS='REPLACE',ACCESS='STREAM',ACTION='WRITE',FORM=
'UNFORMATTED')

        !---------------------------------------------------------------------
        !
        ! Write the stimulation properties to file
        !
        !---------------------------------------------------------------------
        WRITE(UNIT=101)
stimulation_orig,Duration,num_segments,num_compartments,i_error,g_hat_Na,g_hat_K_DR,g_hat
_K_IR,eta_K_IR
        WRITE(UNIT=102)
stimulation_orig,Duration,num_segments,num_compartments,i_error,g_hat_Na,g_hat_K_DR,g_hat
_K_IR,eta_K_IR

        !---------------------------------------------------------------------
        !
        ! Write the initial values
        !
        !---------------------------------------------------------------------
        position = 0._TYP
        WRITE(*,*) position

        DO WHILE (position < Duration)
                position_old = position
                call membrane_voltage(voltage, y, tub_k_o, dKo, position)

                !---------------------------------------------------------------------
                !
                ! Alter the tubule [K]o
                !
                !---------------------------------------------------------------------
                call change_tub_k(tub_k_o, dKo, position - position_old)

                !Write the output
                WRITE(UNIT=101) position,voltage(3),voltage(7), &

        voltage(2*num_compartments+num_segments+1:3*num_compartments+num_segments), &

        voltage(6*num_compartments+num_segments+1:7*num_compartments+num_segments)
                WRITE(UNIT=102)  position,tub_K_o(2*num_compartments+1:3*num_compartments),
&
                        tub_K_o(6*num_compartments+1:7*num_compartments)
        END DO

        !Close the files
        CLOSE(UNIT=101)
        CLOSE(UNIT=102)
end subroutine current_clamp

subroutine membrane_voltage(voltage, y, tub_k_o, dKo, position)
        use constants

        real(kind=TYP), dimension(num_segs), intent(inout) :: voltage
        !Voltage output (also previous)
        real(kind=TYP), dimension(num_y), intent(inout) :: y
        !kinetic parameters output (also previous)
        real(kind=TYP), dimension(num_comps), intent(inout) :: tub_k_o
        !T-tubule K concentration (is this actually inout or just in?)
        real(kind=TYP), dimension(num_comps), intent(out) :: dKo                !Change
in potassium concentration
        real(kind=TYP), intent(inout) :: position
        !Position (both previous and next)

        !Local variables
        real(kind=TYP), dimension(num_segs) :: prev_voltage
        real(kind=TYP), dimension(num_y) :: prev_y
        real(kind=TYP), dimension(num_segs) :: membrane_current
        real(kind=TYP), dimension(num_segs) :: ionic_current
        real(kind=TYP), dimension(num_segs) :: cap_current
        real(kind=TYP), dimension(num_segs) :: voltage_change
```

216

```
      real(kind=TYP), dimension(num_segments) :: trans_tubular_current
      real(kind=TYP), dimension(num_segments) :: inter_segmental_current
      real(kind=TYP), dimension(num_comps) :: inter_compartmental_current
      real(kind=TYP) :: stimulation
      real(kind=TYP) :: stim
      real(kind=TYP) :: position_old
      logical :: CHANGED
      logical, dimension(num_segs) :: completions
      integer, dimension(num_segs) :: last          !1:  Hyperpolarizing   current,  2:
Depolarizing current
      real(kind=TYP) :: htry
      integer(kind=ITYP) :: i,k                      !i: generic counter
      k: iteration counter
      integer, dimension(num_segs) :: j, l          !j:  count  for  decreasing  voltage
change l: count for increasing voltage change
      real(kind=TYP) :: original_stim
      real(kind=TYP), dimension(2) :: stim_positions
      integer :: iterations_about_stim, last_stim_position
      integer :: looped                       !0: we need to return to the do loop even if
all(completions) == .TRUE.
                                              !1: we can finish with the whole looping bit

      prev_voltage = voltage
      prev_y = y
      last = 0
      i = 1
      j = 0
      k = 0
      l = 0
      iterations_about_stim = 0
      looped = 0
      htry = step_size
      inter_compartmental_current = 0._TYP
      inter_segmental_current = 0._TYP
      trans_tubular_current = 0._TYP
      position_old=position
      CHANGED = .FALSE.
      stim_positions = 0._TYP
      last_stim_position = 1

      !-----------------------------------------------------------------------
      !
      ! Do the runge-kutta to get the kinetic parameters
      !
      !-----------------------------------------------------------------------
      call odeint(y, position, htry, epsilon(htry), voltage)

      !-----------------------------------------------------------------------
      !
      ! Determine the ionic current
      !
      !-----------------------------------------------------------------------
      call i_ionic(voltage, y, ionic_current, tub_k_o, dKo)
      membrane_current = ionic_current

      !-----------------------------------------------------------------------
      !
      ! Calculate the inter-segmental current
      !
      !-----------------------------------------------------------------------
      call inter_segmental_current_func(voltage(1:mem_v_end), inter_segmental_current)
      membrane_current(1:mem_v_end)       =       membrane_current(1:mem_v_end)       -
inter_segmental_current

      !-----------------------------------------------------------------------
      !
      ! Calculate the inter-compartmental current
      !
      !-----------------------------------------------------------------------
      call
inter_compartmental_current_func(voltage(mem_v_end+1:),inter_compartmental_current)
      membrane_current(mem_v_end+1:num_segs) = membrane_current(mem_v_end+1:num_segs) -
inter_compartmental_current
```

```
!-----------------------------------------------------------------
!
! Determine the trans-tubular current
!
!-----------------------------------------------------------------
      call i_tubular(voltage, trans_tubular_current)
      membrane_current(1:mem_v_end)      =      membrane_current(1:mem_v_end)      +
trans_tubular_current
      membrane_current(mem_v_end+1::num_compartments)                           =
membrane_current(mem_v_end+1::num_compartments) - &
            (area/t_area(1)) * trans_tubular_current


!-----------------------------------------------------------------
!
! Get the Capacitive current
!
!-----------------------------------------------------------------
      call cap(voltage, prev_voltage, position - position_old, cap_current)
      membrane_current = membrane_current + cap_current


!-----------------------------------------------------------------
!
! Tack on the stimulation to the 1st segments
!
!-----------------------------------------------------------------
stim = stimulation(position)
membrane_current(1) = membrane_current(1) + stim
original_stim = stim


!-----------------------------------------------------------------
!
! Figure out what voltage_change should be
!
!-----------------------------------------------------------------
voltage_change = 0.1_TYP
if(stim .NE. 0._TYP) then
        if(voltage(1) < -70._TYP) then
                voltage = -70._TYP
                CHANGED = .TRUE.
        else if(voltage(1) < -50._TYP) then
                voltage = -30._TYP
                CHANGED = .TRUE.
        end if
else
        if(voltage(1) > 0._TYP) then
                voltage = 0._TYP
                CHANGED = .TRUE.
        else if(voltage(1) > -20._TYP) then
                voltage = -20._TYP
                CHANGED = .TRUE.
        end if
end if

if(CHANGED .NEQV. .TRUE.) then
        !-----------------------------------------------------------------
        !
        ! Calculate the voltage change required for each of the segments
        !
        !-----------------------------------------------------------------
        do while(i<=size(voltage))
                if(membrane_current(i) > i_error) then
                        !Hyperpolarizing current, lower Vm
                        voltage(i) = voltage(i) - voltage_change(i)
                        last(i) = 1
                elseif(membrane_current(i) < -1 * i_error) then
                        !Depolarizing current, raise Vm
                        voltage(i) = voltage(i) + voltage_change(i)
                end if
                i = i + 1
        end do
end if
```

```
!----------------------------------------------------------------------
!
! This is the main loop. "looped" determines if we've looped through
! enough times to continue (1 more time than required for the various
! segmental voltages to stablize).
!
!----------------------------------------------------------------------
main:   do
                !----------------------------------------------------------------------
                !
                ! Do the runge-kutta to get the kinetic parameters
                !
                !----------------------------------------------------------------------
                y = prev_y
                position = position_old
                if(iterations_about_stim == 100) then
                        write(*,*) 'Changed runge-kutta methods'
                        !so we don't keep printing this:
                        iterations_about_stim = 101
                end if
                if(iterations_about_stim < 100) then
                        call odeint(y, position, htry, epsilon(htry), voltage)
                else
                        position = minval(stim_positions)
                        call RK4int(y, position-position_old, voltage)
                end if

                !----------------------------------------------------------------------
                !
                ! Determine the ionic current
                !
                !----------------------------------------------------------------------
                call i_ionic(voltage, y, ionic_current, tub_k_o, dKo)
                membrane_current = ionic_current

                !----------------------------------------------------------------------
                !
                ! Calculate the inter-segmental current
                !
                !----------------------------------------------------------------------
                call                      inter_segmental_current_func(voltage(1:mem_v_end),
inter_segmental_current)
                membrane_current(1:mem_v_end)     =     membrane_current(1:mem_v_end)     -
inter_segmental_current

                !----------------------------------------------------------------------
                !
                ! Calculate the inter-compartmental current
                !
                !----------------------------------------------------------------------
                call
inter_compartmental_current_func(voltage(mem_v_end+1:),inter_compartmental_current)
                membrane_current(mem_v_end+1:)     =     membrane_current(mem_v_end+1:)     -
inter_compartmental_current

                !----------------------------------------------------------------------
                !
                ! Determine the trans-tubular current
                !
                !----------------------------------------------------------------------
                call i_tubular(voltage, trans_tubular_current)
                membrane_current(1:mem_v_end)     =     membrane_current(1:mem_v_end)     +
trans_tubular_current
                membrane_current(mem_v_end+1::num_compartments)                         =
membrane_current(mem_v_end+1::num_compartments) - &
                        (area/t_area(1)) * trans_tubular_current

                !----------------------------------------------------------------------
                !
                ! Get the Capacitive current
                !
                !----------------------------------------------------------------------
                call cap(voltage, prev_voltage, position - position_old, cap_current)
```

219

```
                membrane_current = membrane_current + cap_current

                !------------------------------------------------------------------------
                !
                ! Tack on the stimulation to the 1st segments
                !
                !------------------------------------------------------------------------
                stim = stimulation(position)
                membrane_current(1) = membrane_current(1) + stim
                if(stim .NE. original_stim) then
                        iterations_about_stim = iterations_about_stim + 1
                        original_stim = stim
                        stim_positions(last_stim_position) = position
                        if(last_stim_position == 1) then
                                last_stim_position = 2
                        else
                                last_stim_position = 1
                        end if
                end if

                !------------------------------------------------------------------------
                !
                ! Determine which of the membrane segments needs further changes
                !
                !------------------------------------------------------------------------
                completions = .FALSE.
                forall(i=1:num_segs, abs(membrane_current(i)) <= i_error)
                        completions(i) = .TRUE.
                end forall

                if(all(completions) .EQV. .TRUE.) then
                        if(looped == 1) then
                                exit main
                        else
                                looped = 1
                        end if
                end if

                i = 1
                !------------------------------------------------------------------------
                !
                ! Calculate the voltage change required for each of the segments
                !
                !------------------------------------------------------------------------
                do while(i<=num_segs)
                        if(membrane_current(i) > i_error) then
                                !Hyperpolarizing current, lower Vm
                                if (last(i) == 2) then
                                        if(j(i) > 5) then
                                                j(i) = 0
                                                voltage_change(i)       =       0.1_TYP      *
voltage_change(i)
                                                if(voltage_change(i)    <    epsilon(1._TYP))
voltage_change(i) = epsilon(1._TYP)
                                        end if
                                        j(i) = j(i) + 1
                                        l(i) = 0
                                else
                                        if(l(i) > 6) then
                                                l(i) = 0
                                                voltage_change(i)       =       10._TYP      *
voltage_change(i)
                                        end if
                                        l(i) = l(i) + 1
                                end if
                                voltage(i) = voltage(i) - voltage_change(i)
                                last(i) = 1
                        elseif(membrane_current(i) < -1 * i_error) then
                                !Depolarizing current, raise Vm
                                if (last(i) == 1) then
                                        if(j(i) > 5) then
                                                j(i) = 0
```

```fortran
                                                 voltage_change(i)        =        0.1_TYP        *
voltage_change(i)
                                                 if(voltage_change(i)    <     epsilon(1._TYP))
voltage_change(i) = epsilon(1._TYP)
                                 end if
                                 j(i) = j(i) + 1
                                 l(i) = 0
                        else
                                 if(l(i) > 6) then
                                         l(i) = 0
                                         voltage_change(i)        =        10._TYP        *
voltage_change(i)
                                 end if
                                 l(i) = l(i) + 1
                                 end if
                                 voltage(i) = voltage(i) + voltage_change(i)
                                 last(i) = 2
                        end if
                        i = i + 1
                end do

                !-------------------------------------------------------------------
                !
                ! If we've iterated through excessively then we should quite (can't
                ! get any more stable)
                !
                !-------------------------------------------------------------------
                k = k+1
                if(k>MAXITER) then
                        write(*,*) 'Hit the maximum number of iterations',position
                        exit main
                end if
        end do main

        return
end subroutine membrane_voltage
```

Publishing Agreement

It is the policy of the University to encourage the distribution of all theses, dissertations, and manuscripts. Copies of all UCSF theses, dissertations, and manuscripts will be routed to the library via the Graduate Division. The library will make all theses, dissertations, and manuscripts accessible to the public and will preserve these to the best of their abilities, in perpetuity.

Please sign the following statement:

I hereby grant permission to the Graduate Division of the University of California, San Francisco to release copies of my thesis, dissertation, or manuscript to the Campus Library to provide access and preservation, in whole or in part, in perpetuity.

_____   3/17/10

Author Signature   Date